AN INVESTIGATION INTO THE EFFECTS OF INJECTION BEHAVIOUR ON PERFORMANCE AND EMISSIONS CHARACTERISTICS OF A COMPRESSION IGNITION ENGINE FUELLED WITH DIESEL AND DIMETHYL ETHER

Anton F. Meiring

A research report submitted to the Faculty of Engineering and the Built Environment, University of the Witwatersrand, Johannesburg, in partial fulfilment of the requirements for the degree of Master of Science in Engineering.

Johannesburg, 2010

DECLARATION

I declare that this research report is my own, unaided work. It is being submitted for the Degree of Master of Science in Engineering in the University of the Witwatersrand, Johannesburg. It has not been submitted before for any degree or examination in any other University.

____

Anton F Meiring

this _______________ day of _______________ 2010

ABSTRACT

The injection behaviour of diesel and dimethyl ether was investigated by means of advanced visualisation techniques and conventional performance and emissions engine testing. The results of these investigations were analysed collectively, with specific attention being paid the correlation between the injection characteristics of the two fuels, and the emissions of oxides of nitrogen. Analysis of the footage obtained clearly illustrates the differences between the injection characteristics, and analysis of the engine testing results revealed similar performance characteristics of diesel and dimethyl ether. The emissions of oxides of nitrogen are higher than those produced by diesel at low speeds, are similar at high engine speeds, and reduce with engine load. These characteristics can be attributed to the properties of the fuel and the physical geometry of the fuel injection system. Recommendations are made as to how to further this research into dimethyl ether as a viable alternative fuel.

ACKNOWLEDGEMENTS

I would like to express my thanks to Dr Daniele Cipolat, Mr Nandu Menon and Mr Anton Andreis from the University of the Witwatersrand, for their assistance with this project.

I would also like to thank the Mining Visualisation Laboratory at DeBeers-GTS Technology for the use of their high speed digital camera, without which this work would not have been possible.

CONTENTS

LIST OF FIGURES

LIST OF TABLES

LIST OF SYMBOLS

Power	P
Engine Speed (rpm)	N
Torque	T
Spray Angle	θ
Gas Density	ρ_g
Liquid Density	ρ_l
Injector Nozzle Length	L_n
Injector Nozzle Diameter	d_n
Penetration Depth	S
Pressure Differential	ΔP
Gas Temperature	T_g
Time	t
Mechanical Efficiency	η_m
Indicated Power	P_i
Brake Power	P_b
Stroke Length	L
Piston Area	A
Power Strokes/revolution	e
Equivalence Ratio	$\varnothing$
Stoichiometric Air/Fuel Ratio	A/F_S
Actual Air/Fuel Ratio	A/F_A
Fuel Conversion Efficiency	η_f
Specific Fuel Consumption	sfc
Lower Heating Value	Q_{HV}

1 INTRODUCTION

Although alternative fuels research has been taking place since the invention of the internal combustion engine itself, the necessity for a viable alternative to fossil fuels has never been more urgent than it is today. Simply put, the world's fossil fuel reserves are rapidly being depleted, and the effects on the environment of burning them are well known and undeniable.

The search for a viable alternative fuel is one that is fraught with difficulties, but the implications of failure could well be globally catastrophic. Modern society is so reliant on internal combustion engines, and the fuels that run them, that if the current fossil fuels were to run out without a substitute readily available, the resulting political, economic, social and environmental turmoil is unimaginable. The political uncertainty in the Middle East, and the current volatility in the crude oil price are perhaps indications that this scenario might well already have been set into motion.

There are a number of alternative means of propulsion being investigated at the moment, including battery power and hydrogen power, but none have the infrastructure and existing technology that the internal combustion engine has developed over more than a century of continued development.

The logical step in the evolution of the internal combustion engine is to find a fuel that would at least supplement, but ideally replace fossil fuels, with minimal modification to existing equipment and infrastructure. If the lessons of the past have been learnt, this fuel will be renewable, cost effective, and environmentally friendly.

One such fuel is dimethyl ether. Dimethyl ether has properties similar to diesel, and the technology exists to produce it in large quantities, from fossil fuels but more importantly from renewable biomass. With relatively minor modifications, dimethyl ether can be used to fuel existing compression ignition engines, with comparable performance and emissions results.

The objective of this project is to investigate the injection characteristics of both diesel and dimethyl ether, and what impact they have on engine performance and emissions, specifically oxides of nitrogen. This investigation consists of two means of analysis: advanced visualisation techniques and engine testing. These methods will be analysed in isolation to one another and collectively in order to facilitate a meaningful analysis of the injection characteristics of diesel and dimethyl ether, and their influence on engine performance and emissions.

2 ALTERNATIVE FUELS

The internal combustion engine is the only means of propulsion in widespread use in the global automotive transportation system. The fuels these engines burn, petrol and diesel, are both highly refined products, both almost entirely derived from petroleum, or crude oil. In the face of decreasing availability of these fuels, and other social, economic and international political pressures, the potential and viability of alternative fuels is obviously of great importance. It is generally accepted that the future of the automotive transportation is greatly dependent on a means of propulsion other than the use of the fossil fuels in use today.

The necessity for alternative fuels first came to the fore during the fuel crisis of early seventies. The subsequent uncertainty surrounding fuel availability resulted in substantial research being carried out into the future of fossil fuels, the internal combustion engine and transportation in general. These efforts were also fuelled by concerns around the political instability in the Middle East, which was and still is the major global supplier of crude oil.

The introduction of a feasible alternative fuel is not a simple matter of realising the need for change and implementing it accordingly. A viable and comparable alternative has to be found. Added to the massive technical obstacles that need to be overcome, there are many social, economic and political issues, often with different agendas, that need to be taken into account.

2.1 The Necessity for Alternative Fuels

The necessity of alternative fuels is due to two main factors: environmental concerns and the finite nature of crude oil reserves. Other factors include the political instability in the Middle East, and the desire for non-reliance on this region.

2.1.1 Environmental Issues

The causes, severity and effects of environmental issues are widely debated and viewed with different degrees of severity by different parties. What is acknowledged however, is the fact that the sustainability of transportation in its current guise, depends entirely on our future ability to adapt to a lifestyle that takes these environmental issues into account. As far as the internal combustion engine is concerned, the environmental issue of main concern is global warming.

As the name implies, global warming is the increase in the atmospheric temperature of the earth, mainly due to the enhancement of the greenhouse effect. The greenhouse effect, as depicted in Figure 2.1, is one of the earth's natural processes and is essential for life on this planet. It is the result of heat absorption by certain gases in the atmosphere. Energy from the sun drives the earth's weather and climate, and heats up the earth's surface. The earth in turn radiates energy back into the atmosphere. Atmospheric greenhouse gases trap some of the outgoing heat, retaining it in the earth's atmosphere and regulating the temperature. Without the greenhouse effect, the earth's temperature would be well below zero degrees Celsius [1].

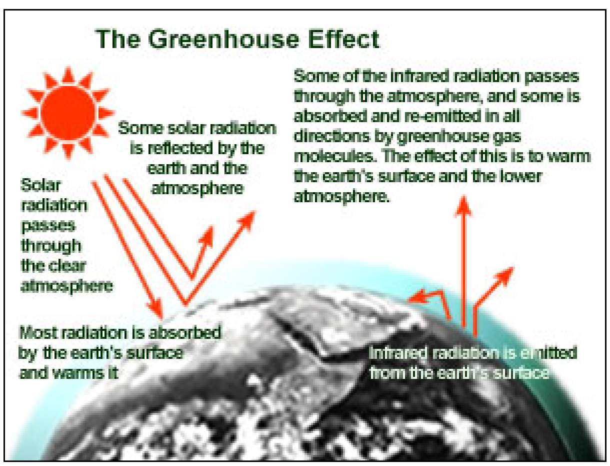

Figure 2.1 - Summary of Greenhouse Effect [1]

Water vapour and carbon dioxide are the two most abundant greenhouse gases, and their concentrations effectively control the temperature of the earth's atmosphere. Other greenhouse gases include methane and nitrous oxide [2].

The increase in concentration of carbon dioxide in the earth's atmosphere is of particular concern. Pre-industrial (late 19th century) levels of carbon dioxide were about 280ppmv, whereas in 2001 they were 370ppmv. Predictions of future carbon dioxide concentrations in the earth's atmosphere range from 500 to 1250ppmv by the end of the 21st century [3].

The mean global temperature has increased by as much as 0.9ºC since the nineteenth century as illustrated in Figure 2.2, and it is predicted that this increase could be as much as 5.8 ºC over the next century [4].

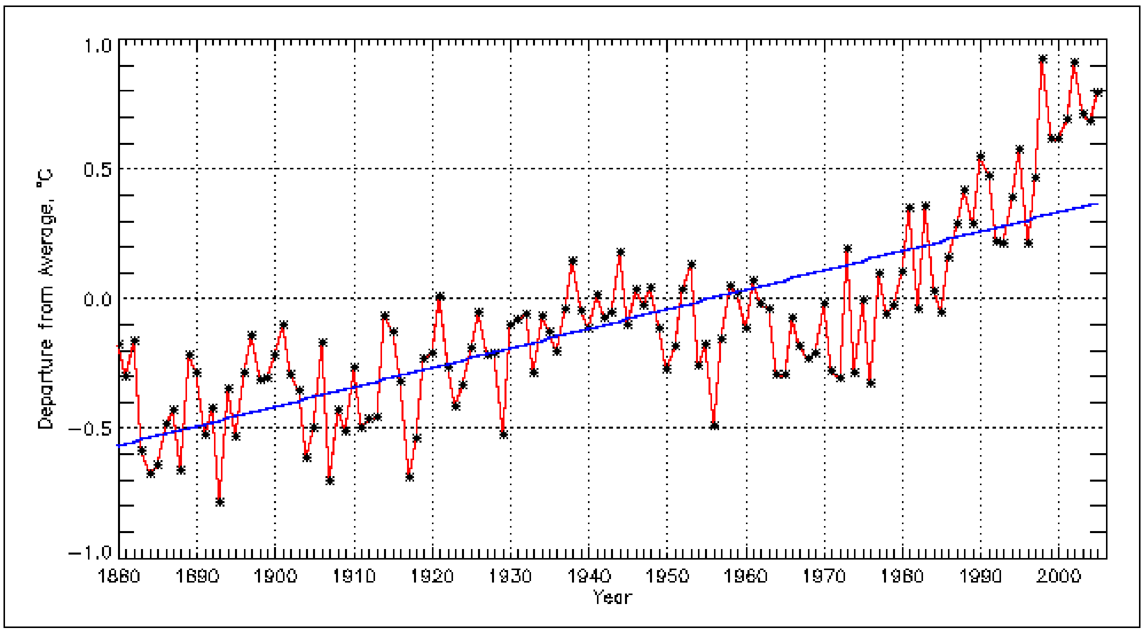

Figure 2.2 - Global Temperature Variations – 1880 to 2007 [4]

It is generally accepted that the global average temperature increase in the recent past and that anticipated for the foreseeable future is dangerously high, and that these increases can be attributed to global warming [2].

Although the internal combustion engine is not the only culprit in contributing to excessive carbon dioxide, and other greenhouse gases, it is undeniably a major contributor. For instance, in the United States cars, sport utility vehicles and light trucks emit over 20% of the carbon dioxide pollution [5].

2.1.2 Sustainability

The second challenge threatening the internal combustion engine is it's sustainability due to finite fuel reserves, and the fact that the majority of oil reserves are located in politically unstable regions.

Research has shown that in 2004, six barrels of oil are consumed for every barrel discovered, with discoveries of major oil reserves (over 500 million barrels) having peaked in 1964. This is made evident by the fact that in 2000 there were 13 discoveries of reserves that could be classified as major, in 2001 there were 6, in 2002 there were 2, and none in 2003 [6].

Proven world oil reserves as at the end of 1995 stood at 1 011 574 million barrels, of which 785 066 million barrels (77.6%) were found in the 11 OPEC (Organisation of Petroleum Exporting Countries) member countries. Proven world oil reserves as at the end of 2007 stood at 1 204 182 million barrels, of which 939 016 million barrels (77.9%) were found in the 11 OPEC member countries. In 2005, 79% of the OPEC reserves were in the Middle East [7].

OPEC is formed by: Saudi Arabia, United Arab Emirates, Qatar, Iran, Iraq, Kuwait, Venezuela, Indonesia, Libya, Nigeria, Algeria, Angola and Ecuador. The majority of these countries are in unstable regions. Figure 2.3 shows a plot of the projected crude oil reserves and an indicative illustration of the current production rates of the major oil producing countries.

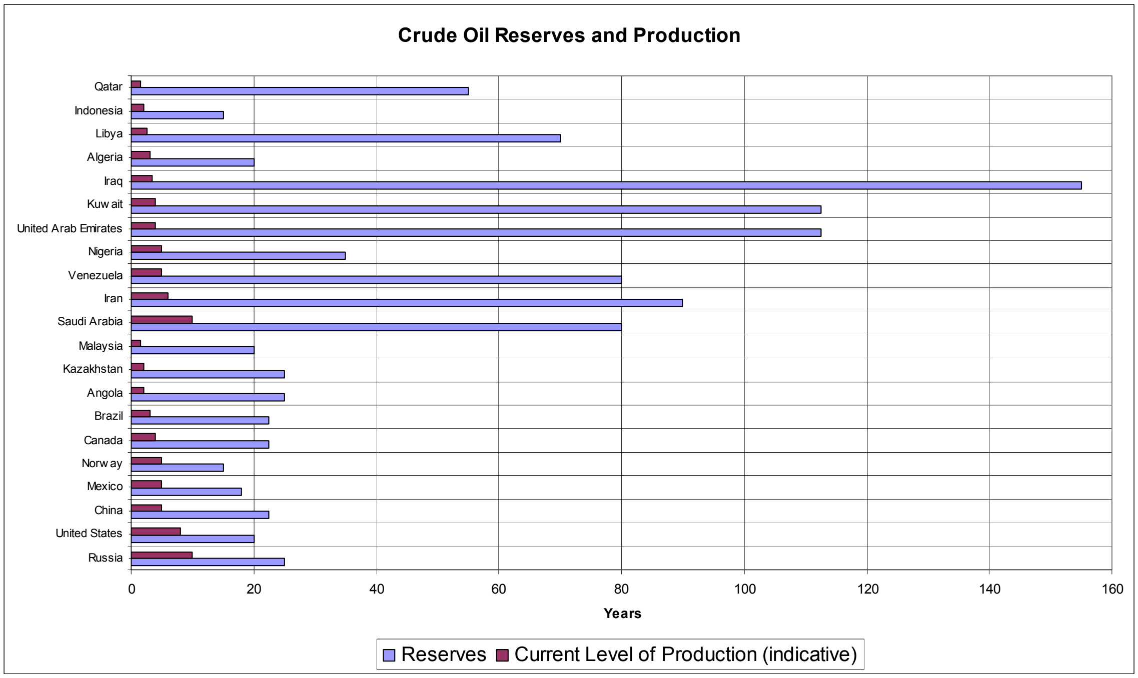

Figure 2.3 - Crude Oil Reserves and Current Production [8]

The finite nature of fossil fuels, and the world's dependency on the OPEC nations is clearly illustrated by Figure 2.3.

The largest consumer of fossil fuels is the United States, consuming approximately 25% of the worlds oil production, while having approximately 4.5% of it's population [9]. Of the over 250 million light duty vehicles in the United States and Canada, only 1% can be considered fuel efficient, having a fuel consumption of under 8.0 litre/100km [10].

Also to be considered is the massive growth in the automotive industry in emerging markets, especially China, where the vehicle population is expected to increase from 17 million vehicles in 2000, to over 65 million vehicles in 2010 [11]. This clearly illustrates a need for more efficient vehicles for the short to medium term, and a comparable alternative fuel to replace the current fossil fuels in the long term.

Figure 2.4 follows the crude oil price over the last 20 years and clearly illustrates both the continued increase in price up until mid-2008, and the volatility of the market.

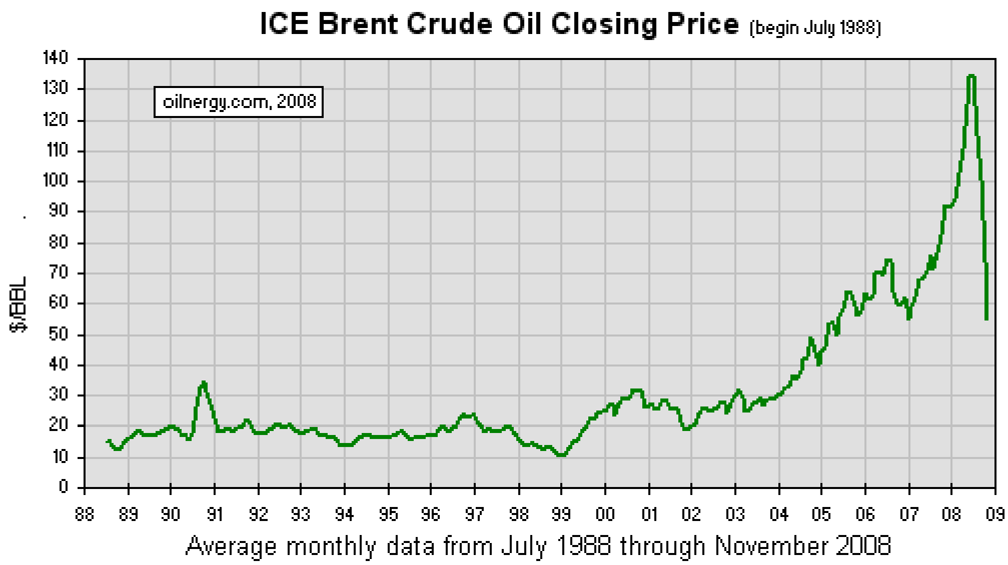

Figure 2.4 - Crude Oil Price from July 1988 to November 2008 [12]

2.2 Dimethyl Ether as an Alternative Fuel

Dimethyl ether is a colourless compressed gas or liquid, and is generally used as a refrigerant, solvent, propellant for aerosol sprays, and in making certain plastics [13]. Dimethyl ether is classified a Group II Hazardous Substance, in accordance with the Hazardous Substance Act, 1973, due to its flammability [14]. Dimethyl ether's high energy content and clean burning characteristics make it an appealing fuel. It can be used as a fuel additive and in a mixture with methanol, but more significant is its potential as an ultra clean alternative fuel. What makes the use of dimethyl ether as an alternative fuel even more appealing is that as well as being environmentally friendly in terms of emissions, it can be produced from a wide spectrum of raw materials such as coal, natural gas and biomass. This means that it can be produced almost anywhere in the world, which eradicates the dependence on specific regions, as is created by the location specific nature of crude oil from which existing fuels are produced. The production of dimethyl ether from biomass is of particular relevance when considering long term sustainability.

Dimethyl ether is a stable gas with the chemical composition: CH_3-O-CH_3, as illustrated in Figure 2.5. Due its low vapour pressure, it can be easily liquefied, and stored and transported in ordinary gas cylinders.

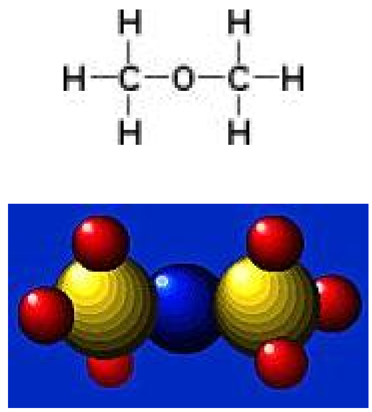

Figure 2.5 - Dimethyl Ether

Table 2.1 summarises the main physical and chemical properties of both diesel and dimethyl ether.

Table 2.1 - Physical Properties – Diesel and Dimethyl Ether [15],[16],[17]

Property	Diesel	Dimethyl Ether
Chemical Formula	$C_{16}H_{34}$	CH_3OCH_3
Molecular Weight (g/mol)	190-220	46.07
Density of Liquid @ 293K (kg/m^3)	840	668
Boiling Point (K)	453-633	248.1
Vapour Pressure (MPa)	-	0.51
Heat of Vapourisation at 293K (kJ/kg)	270	410
Heat of Combustion (MJ/kg)	43.5	28.8
Critical Pressure (MPa)	-	5.37
Critical Temperature (K)		400
Stoiciometric Air/Fuel Ratio	14.6	9
Auto-ignition Temperature (K)	523	508
Cetane No.	38-53	>55
Viscosity (Liquid) (cP)	4.4-5.4	0.15

In comparing dimethyl ether with diesel, a number of points are worth noting from Table 2.1. Dimethyl ether has better ignition characteristics due to its higher cetane number and lower auto-ignition temperature. The lower boiling point also implies that it will have better atomisation qualities. The lower boiling point and vapour pressure of dimethyl ether means that it evaporates more easily than diesel, and therefore requires lower injection pressures. These are obviously important considerations when analysing the injection characteristics.

The fact that dimethyl ether has a lower heat of combustion than diesel means that a larger mass of fuel is required for a given amount of work to be done. The lower viscosity and density of dimethyl ether has a negative effect on current injection systems in that leakage and wear are more pronounced than when diesel is used [1].

Recent research into the applicability of dimethyl ether as an alternative fuel has shown that it has efficiency and performance characteristics comparable to those of diesel, produces significantly lower levels of most emissions, and can be sustainably produced from natural, renewable resources. The limitations that have come to light do not seem to be insurmountable, but require substantial research and development if dimethyl ether is going to compete with, and potentially replace the current fossil fuels [1].

From a performance, efficiency and emissions point of view, the key problems encountered when testing a diesel engine fuelled with dimethyl ether are as a result of fuel leakage and lubrication limitations within the fuel injection system. Cavitation can also occur due to dimethyl ether's relatively high vapour pressure, and its high compressibility has shown to limit the injection systems' ability to inject the optimum fuel quantity during full load operation [1].

The fuel leakage and lubrication problems compromise the efficiency and durability of the components of the fuel injection system that rely on fine clearances. Dimethyl ether also chemically attacks seals and other plastic parts in the fuel injection system [1].

The different physical and chemical properties of diesel and dimethyl ether mean that simply using a standard diesel fuel injection system when fuelling an engine with dimethyl ether is not optimal. These fuel injection systems have been optimised for the use of diesel and its physical characteristics, and need to be optimised for the use of dimethyl ether.

2.3 Literature Survey - Alternative fuels

A survey of literature on the subject of alternative fuels was carried out, and the outcomes of which are as follows:

2.3.1 Automotive Engines and Fuels: A Review of Future Options, [18]

An overview of future engine technologies is presented with emphasis being placed on where future research and development resources should be allocated. The status and development potential of automotive heat engines is reviewed, including various types of internal combustion engines, gas turbines, Stirling and Rankine cycle engines, and compound engine systems. The anticipated future alternative fuels are introduced and discussed. The expected changes in transportation fuels, and the impact of alternative fuels, are reviewed. Anticipated timeframes for the lifecycles of different propulsion systems are discussed.

2.3.2 Societal Lifecycle Costs of Cars with Alternative Fuels/Engines, [19]

The success of any alternative fuel and propulsion system will be based on the criteria set out on which they are judged. A means of effective, objective and relevant comparison is proposed. The “societal lifecycle cost” of transportation includes a full analysis of the cost of vehicle first purchase, fuel costs, damage costs of emissions and greenhouse gases and the environment and health, and externality costs associated with oil supply security, over the full lifecycle of the vehicle. A number of different fuels and propulsion systems were considered including: current fuels, alternative fuels, hybrids and fuel cell vehicles. The large uncertainties associated with an investigation into future technologies were taken into account by anticipating a range of possible future conditions. The hydrogen fuel cell car was shown to have the lowest lifecycle cost.

2.3.3 Energy Policies and their Consequences after 25 years, [20]

Following the energy crisis of the early to mid 1970's, a number of research teams investigated the future of energy policies. The conclusions, policy recommendations, and energy supply, demand and price forecasts, of two of these studies (Landsberg and Schurr, 1979), are reviewed and analysed, and compared which actual realisations. The nature, magnitude and reasons for differences in these studies and what actually happened in the following 25 years, are discussed. Considering the large number of unknowns and unforeseen circumstances at the time of the studies themselves, they have proven to be remarkably accurate and insightful. These studies are both centred around the US market, but are relevant to the global energy market as a whole. The two major shortfalls of both the studies are the underestimation of the increase in the consumption of petroleum for personal transport, and the increased dependency of the West on foreign oil produced in politically unstable parts of the world.

2.3.4 Evaluating Automobile Fuel/Propulsion System Technologies, [21]

The lifecycle implications over the next three decades, of a number of existing and alternative fuels, and propulsion systems, are investigated. The environmental, cost and performance characteristics of these fuels and propulsion technologies are reviewed. The fuel/propulsion characteristics of importance to consumers and regulators are investigated and compared with those of the conventional petrol fuelled spark ignition engine. The contradictions in past and existing vehicle legislation with respect to weight, performance, safety, fuel consumption, emissions and cost are illustrated and recommendations made. The comprehensive, qualitative, lifecycle approach to fuels and propulsion system comparisons is addressed. It is concluded that, without any major technological breakthroughs, a drastic increase in the price of petroleum, or stringent regulation of fuel economy and emissions, personal transport in the year 2030 will be powered by a petrol fuelled spark ignition engine. With the continuing progress being made in increasing engine efficiencies, decreasing emissions and the supply of relatively inexpensive fuel, it is extremely unlikely that any of the foreseen alternative fuels or propulsion systems will be a viable replacement for the internal combustion engine.

2.3.5 OPEC Annual Statistical Bulletin – 2008, [7]

The OPEC Annual Statistical Bulletin serves as a valuable and reliable source of statistical data on the oil and gas industries of the 11 OPEC Member Countries, as well as the industry as a whole. This document provides an abundance of information relating to the oil industry including detailed statistics of OPEC countries, global crude oil imports and exports, production and reserves.

2.4 Literature Survey - Dimethyl Ether

A survey of literature on the subject of dimethyl ether as an alternative fuel was carried out, and the outcomes of which are as follows:

2.4.1 Dimethyl Ether as Fuel for CI Engines – A New Technology and its Environmental Potential, [1]

Dimethyl ether is compared to other oxygenated synthetic fuels, and a brief overview of the available resources, production and distribution, of dimethyl ether is given. An overview is presented of the new technologies that are required for the successful implementation of dimethyl ether as an alternative automotive fuel - specifically the fuel injection system. The limitations of existing diesel fuel injection systems are illustrated, and the improvements and alterations detailed. Fuel injection tests are carried out and results presented. Dimethyl ether as an alternative automotive fuel is assessed from an environmental and sustainability point of view, and compared with other proposed alternative fuels.

2.4.2 Dimethyl Ether in Diesel Fuel Injection Systems, [22]

General characteristics of dimethyl ether as an alternative automotive fuel are discussed. The characteristics of dimethyl ether under high pressure injection in a diesel injection system with a single hole are investigated. The effects of the fuel compressibility were analysed and compared to typical hydrocarbon fuels. Dimethyl ether was shown to have a higher compressibility than typical hydrocarbon fuels under the same conditions. High speed photography, and Schlieren photography, were used to analyse the physical jet characteristics under different operating conditions. The jet characteristics of dimethyl ether were shown to be similar to those of diesel in general shape and penetration, by these photographic techniques, although higher evaporation rates were observed.

2.4.3 An Experimental Investigation on the Spray Characteristics of Dimethyl Ether, [23]

Scattered laser light photography is used to study the spray characteristics of dimethyl ether and diesel fuel. Although the spray characteristics were shown to be similar, dimethyl ether displayed a slower penetration speed, faster evaporation and a wider spray angle than diesel. Shadow photography was also used to study the spray characteristics of dimethyl ether, which showed the break up time of dimethyl ether to be shorter than that of diesel. Needle valve opening pressure, and ambient test temperature were shown to have little effect on the spray characteristics. The test results were verified with the use of the James Model.

2.4.4 An Experimental Study on DME Spray Characteristics and Evaporation Processes in a High Pressure Chamber, [24]

An optical investigation into the spray characteristics of dimethyl ether was carried out in relation to those of diesel, using a double pass Schlieren photography setup. Single hole injectors were used in a constant volume chamber at room temperature. This analysis was carried out at different chamber pressures, injection pressures, injector orifice diameters and injection quantities. As with diesel, the spray tip penetration and spray angle increase with chamber pressure, but the spray tip penetration of dimethyl ether is slower than that of diesel, and the spray angle wider. Dimethyl ether showed a faster evaporation time than that of diesel. The spray tip penetration of dimethyl ether was about half that of diesel at the time of ignition start.

2.4.5 Effects of Fuel Injection Characteristics on Heat Release and Emissions in a DI Diesel Engine Operated on DME, [9]

An investigation into the injection characteristics, and their effects on engine heat release and exhaust emissions, was carried out using a direct injection, single cylinder engine, with a common rail fuel injection system. Tests were run using a 5-hole x 0.55mm diameter jet nozzle, and one with 3 x 0.7mm diameter holes (same total area). The physical characteristics of the jet sprays assessed using a high pressure injection chamber, and the emissions and heat release characteristics they produced were investigated using the single cylinder engine. The spray penetration of the 3-hole jet was longer, the spray angle wider, the spray volume greater and the atomisation speed slower at the beginning, than the 5-hole jet. An increase in unburned emissions from the 3-hole jet results from the delay in fuel atomisation.

2.4.6 Performance of a Controllable Premixed Combustion Engine Fuelled with Dimethyl Ether, [11]

The concept of a compression ignition engine fuelled by dimethyl ether, and making use of a premix chamber, is investigated. The dimethyl ether is injected into the premix chamber, which is separated from the combustion chamber by a electronic control valve. In the premix chamber, the dimethyl ether mixes with the residual gases from the previous cycle. Ignition takes place in the premix chamber, and the control valve is opened just before top dead centre. The high temperature, high pressure, gas then rushes into the main combustion chamber.

Ultra low NO_x emissions have been achieved in preliminary studies, while emissions of unburned hydrocarbons and carbon monoxide were higher than an equivalent diesel engine.

3 VISUAL ANALYSIS

The value of flow visualisation techniques is often underestimated in scientific and engineering experimentation and research. Most liquids and gases under analysis are transparent to the human eye, and require specialized visualisation techniques for valuable assessment of flow characteristics or thermodynamic behaviour. Flow visualisation techniques not only provide visual evidence of flow characteristics, but many of these techniques provide a means of deriving quantitative data from the footage obtained. As important is the fact that these analyses can be carried out in a non-obtrusive way. This means that the results of the analysis are not influenced in any way by the analysis itself, as is the case with most physical flow measuring devices [25].

3.1 Flow Visualisation Techniques

Flow visualisation can be achieved in a number of ways:

A relatively simple, but very useful, means of flow visualisation is high speed photography. This footage can be viewed at a much slower playback speed, with the flow characteristics of the particles/tracers being thoroughly analysed.

There are numerous flow visualisation techniques that make use of tracer particles. The fluid can be traced with visible foreign particles, and the flow characteristics of these particles can be analysed, giving a relatively accurate indication of the actual flow characteristics of the fluid itself. This method is obviously limited and compromised by the differences is the physical properties of the fluid under assessment, and the foreign particles. These experimental discrepancies can be minimised, but never eliminated, by matching the properties of the respective fluids and tracers as closely as possible.

Another method of flow visualisation takes advantage of the fact that the refractive index of a fluid is a function of its density. This makes it possible to visualise compressible flows by means of optical techniques that are influenced by the refractive index. The light being transmitted through the fluid is affected by the variations in density caused by the flow of the fluid. These visualisation techniques are sensitive to the variations in the resulting light quality, allowing for the analysis of the flow characteristics themselves.

The use of these flow visualisation techniques is not limited to the analysis of flow characteristics in single-phase mediums. They can be as effective for the analysis of multi-phase flow characteristics, such as injection behaviour, where the particles themselves act as tracers. On the other hand, the obvious density differences between the injected fluid, and the atmosphere into which it is expelled, are sufficient for effective analysis of flow characteristics by means of the density variations between the two mediums.

For the purpose of this investigation, the following flow visualisation techniques, which rely on the above principles, will be considered:

3.1.1 Particle Image Velocimetry

Particle Image Velocimetry (PIV) is a flow visualisation technique that applies the principle of following tracer particles, or individual particles in a two-phase medium. PIV is a non-intrusive, instantaneous means of analysis of the flow characteristics, and in the proposed application of two-medium jet analysis, it would not require tracers, as the individual jet particles act as the tracers themselves.

Current PIV techniques are the result of the development of a number of principles and technologies, starting with the obtaining of quantitative velocity data from particle streak photographs in the 1930's. The technique today takes advantage of advances in digital technology, including high speed digital photography, and advanced computer hardware and software [26].

The basic principle of PIV is the tracking of particles by means of capturing successive images of the flow. Statistical methods are then employed to assess the motion of each particle, from which valuable flow characteristic information can be obtained [26].

The typical optical configuration of a PIV set-up as illustrated in Figure 3.1, includes a light source (usually a double-pulse laser), light-sheet optics (beam combining optics, beam delivery, and light-sheet formation optics), tracer particles, and a camera (imaging lens and recording media) [27].

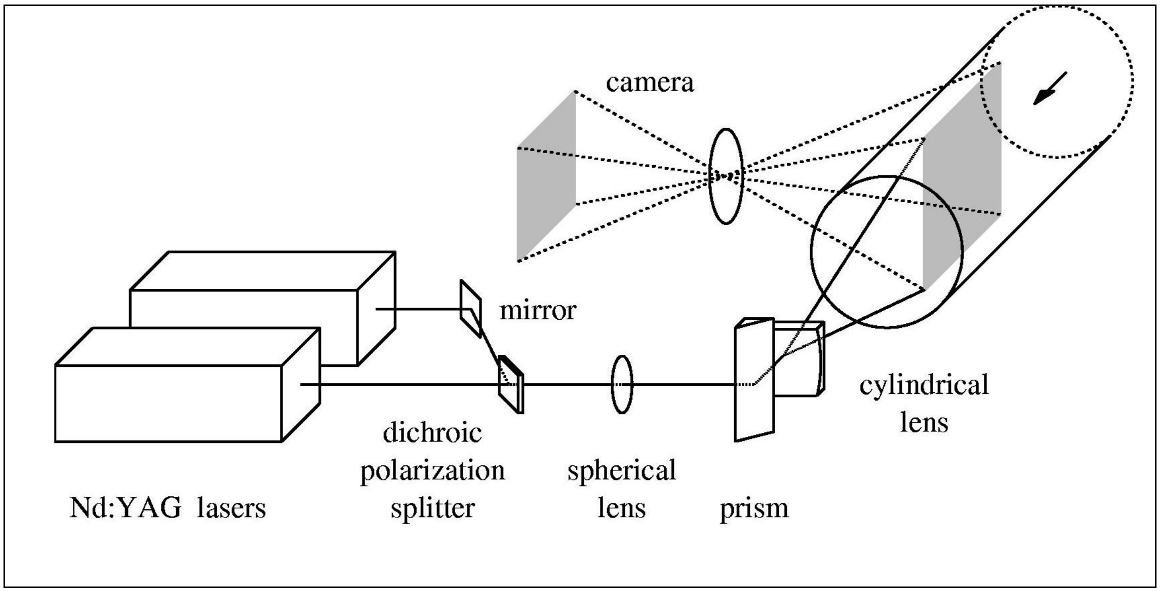

Figure 3.1 - Typical optical configuration of a PIV set-up [27]

The images of the tracer particles are recorded at least twice, with a small (known) time delay. The particle displacement between images represents the particle’s motion. Because the time delay between successive images is known, velocity vectors for each particle can be calculated.

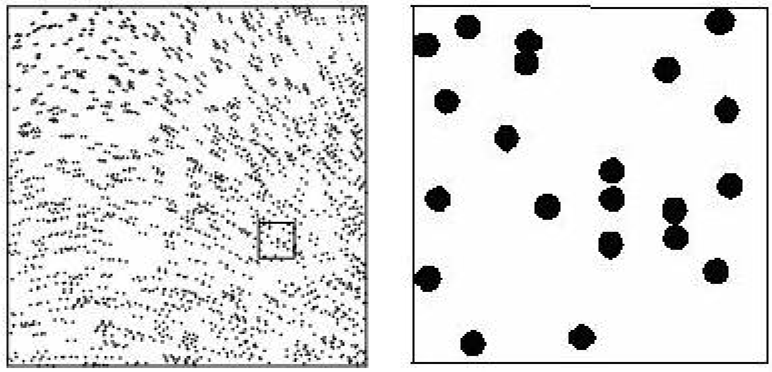

Figure 3.2 – Double exposure image and interrogation region [27]

PIV images are analyzed by subdividing the image into small interrogation regions. Each interrogation region contains many particle-image pairs, and the interrogation region size is dictated by the requirement that the velocities of all the particles within the region are in the same order of magnitude. Statistical methods of image analysis are used to ensure that the path of each particle is correctly traced, in order to obtain each particle's velocity vector.

Consider a single particle image, and determine the distance histogram of all possible match candidates. Each match has an equal probability, but only one match will be correct. When this is done for all particle images, only the matching particle-image pairs will be cumulative, whereas the random unrelated particles are not, and a sharp peak will appear that reflects the displacement of the particle-image vector. The statistical analysis of spatial correlation is based on this histogram approach as illustrated in Figure 3.3 [26] [27].

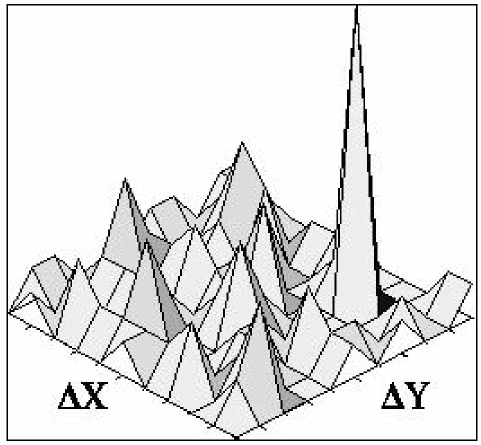

Figure 3.3 – Distribution of matching possibilities from spatial correlation [27]

One of the outputs of a PIV analysis is an illustration of the flow velocity vectors at a given point in time. The individual particle flow characteristics, magnitude and direction of velocity, are illustrated by arrows as in Figure 3.4. This is a very useful technique for the analysis of the instantaneous flow characteristics.

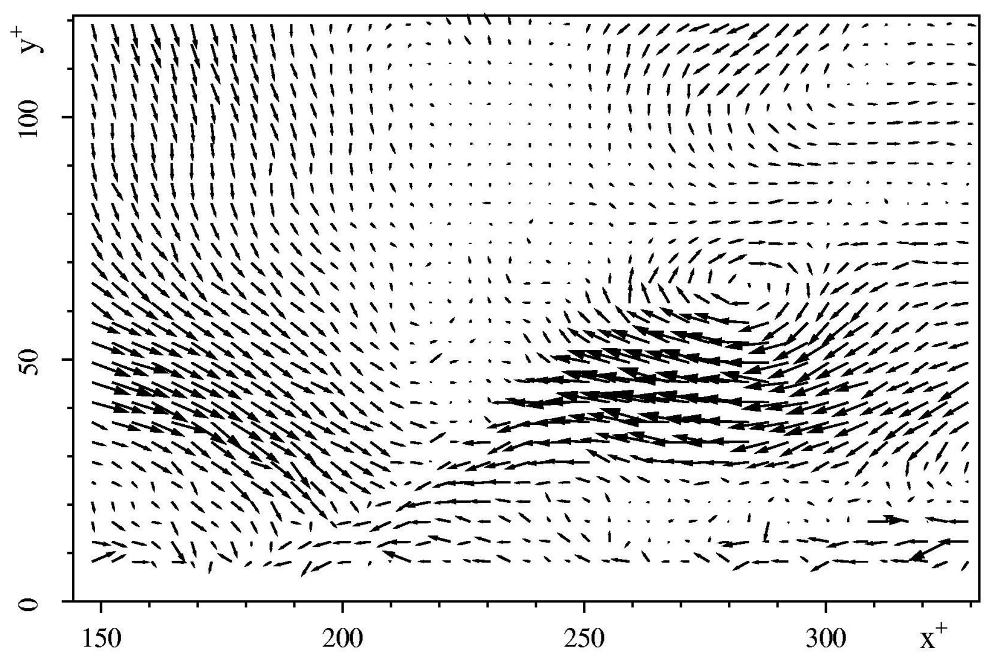

Figure 3.4 – Flow velocity vector diagram of “Hairpin Vortex” [27]

3.1.2 Schlieren photography

Schlieren photography is an optical visualisation technique that takes advantage of the influence of fluid density on refractive index. Rays of light are deviated differently depending on the density variations of the medium through which they travel (see Figure 3.5). This phenomenon is known by its German name – the Schlieren effect. This in turn means that the resulting variations in the quality of light that is captured correspond to the density variations of the fluid under analysis – hence Schlieren photography [28].

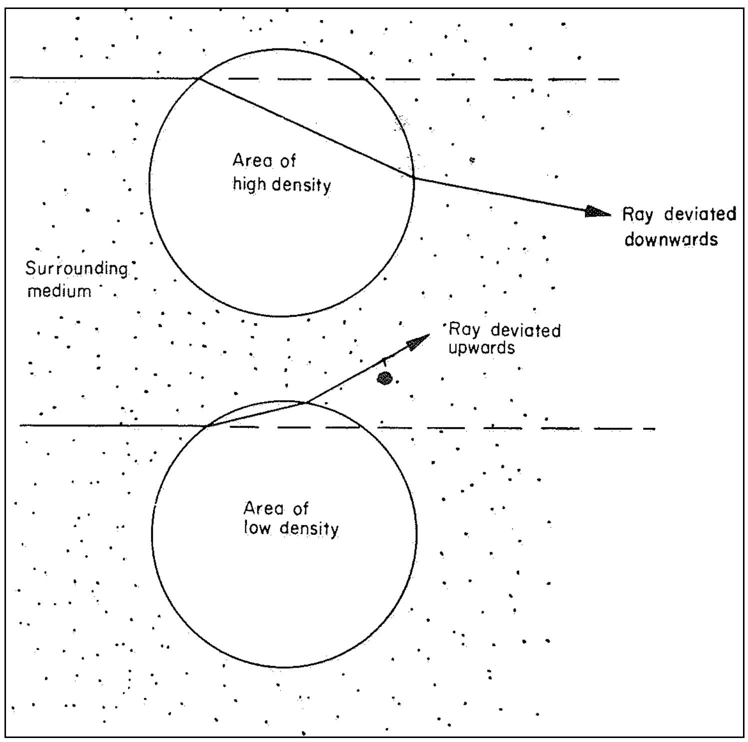

Figure 3.5 – Refraction of light due to density gradient [28]

The density and refractive index of a gas or liquid varies with the temperature and pressure of the medium, and any local variations can be captured by a Schlieren Optical System, as illustrated in Figure 3.5.

Figure 3.6 is a schematic of a typical Schlieren optical set-up. The light from the slit S is focused in the plane of the knife edge K by the condenser C and passes into the camera lens L which focuses an image of the object O onto the emulsion.

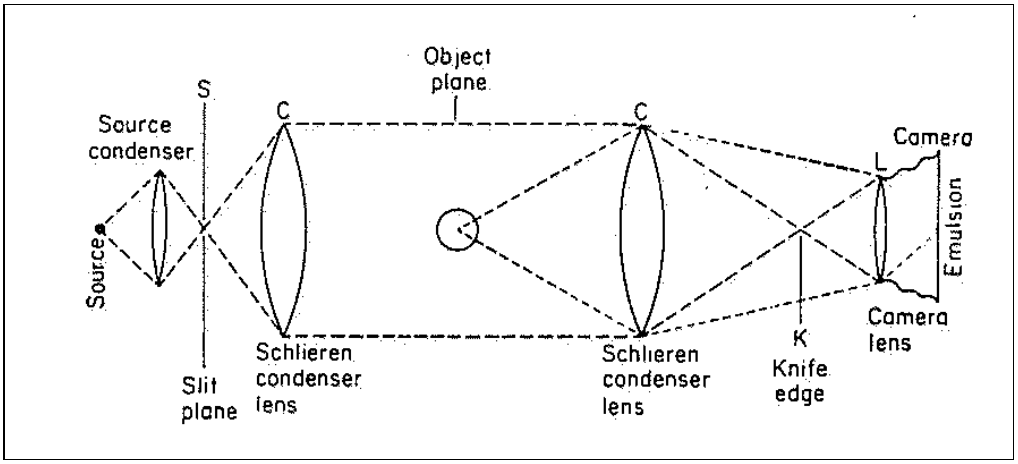

Figure 3.6 – Typical optical configuration of a Schlieren photography set-up [28]

The way in which the variations of density are captured for analysis by the Schlieren technique is best illustrated by Figure 3.7. In Figure 3.7 (a), there is no disturbance in the optical system and the image of the source is adjusted so that half of the beam passes over the knife edge. In Figure 3.7 (b), an increase in density in the medium being analysed causes a greater refraction of the light, so that it is obstructed by the knife edge, resulting in less light being captured on the emulsion, and a dark area representing greater density being recorded. In Figure 3.7 (c), a decrease in density in the medium being analysed causes less refraction of the light, so that it misses the knife edge. This results in more light being captured by the emulsion, and a bright area representing the lower density being recorded [28].

Light rays from the high and low density areas in the medium, pass below and above the knife edge respectively, resulting in an illustration of the density variations in terms of shadow and highlight. The position of the image captured by the emulsion is not altered by the deviation of the source image at the knife edge, only the brightness.

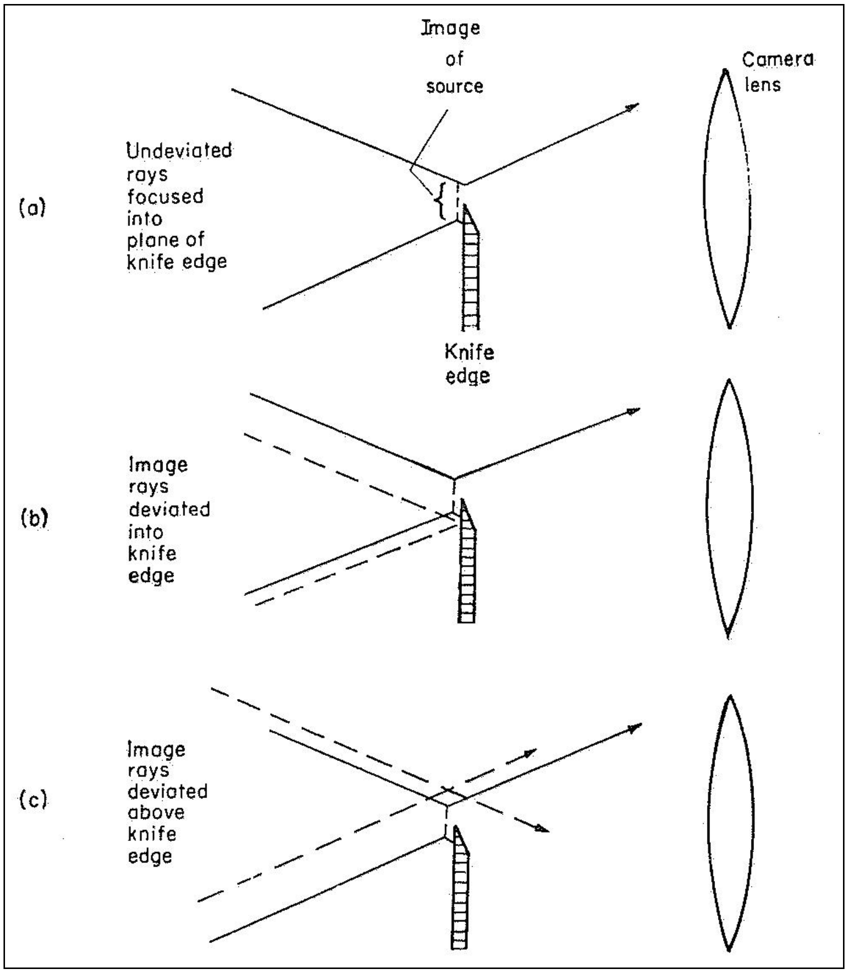

Figure 3.7 – Illustration of the role of the knife edge in the Schlieren Visualisation Technique [28]

The set-up represented in Figure 3.6 has a limitation on field size (limited by the diameter of the optical field elements) which compromises its usefulness in experimental visualisations. This can be overcome by the use of mirror lenses, which allow for a larger optical field, as illustrated in Figure 3.8. It is however, essential that all lenses should be of very high quality as any defects in the mirrors are revealed with greater sensitivity.

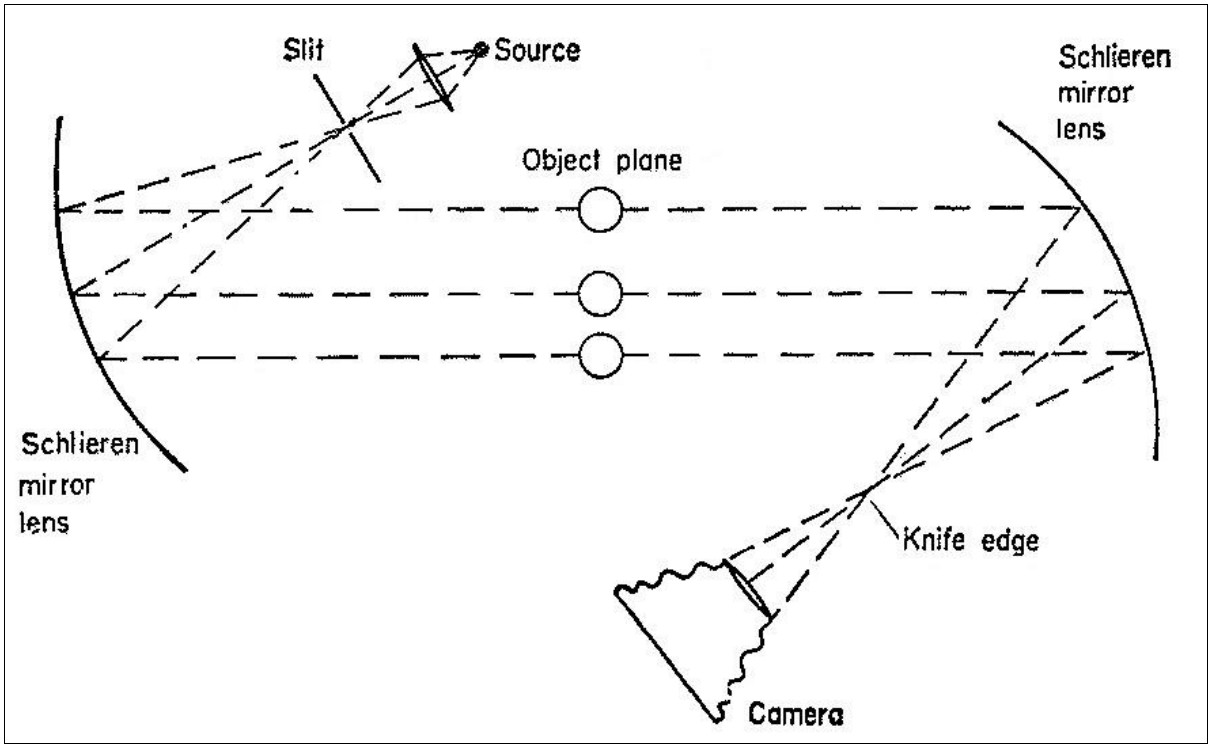

Figure 3.8 – Typical optical configuration of a Schlieren photography set-up using mirror lenses to increase the field size [28]

The variations in density of the different mediums in a two medium system such as the analysis of injection behaviour, can be visualised using the Schlieren method due to the obvious density variations between the jet particles and the atmosphere into which they are injected.

3.1.3 High Speed Digital Videography

Recent technological advances in video equipment, and computer hardware and software, have resulted in video equipment capable of filming at frame rates in excess of 120 000 frames per second. This has three distinct advantages over conventional still photography from a visual analysis point of view:

Firstly, the footage can be viewed at a slow playback speed for detailed analysis. A sequence that takes between 0.003 and 0.015 seconds, such as the injection of diesel or dimethyl ether from an injector, can be filmed at 4000 frames per second, and viewed at 4 frames per second, where 1/1000s becomes 1 second for complete and thorough analysis.

Secondly, uncertainty associated with unreliable trigger timing is negated, i.e. if the trigger timing is a fraction of a second too late (or early) in still photography, the applicability of the resulting image being analysed is compromised and very difficult to identify as such, whereas review of a sequence of images from video allows for more reliable selection of valid footage for analysis, relative to a reference point. By analysing individual images of a video sequence, from a reliable and repeatable reference point, the footage (and individual images) can be analysed and compared with more confidence than analysis of a single image captured by conventional still photography.

Thirdly, due to the fact that one is analysing a complete sequence of images, there is a high level of confidence in the repeatability and progression of the sequence of images of the test. In conventional still Schlieren photography, only one image can be captured at a time. The test therefore has to be repeated for the next image in the sequence to be captured, and analysis is therefore highly dependent on the repeatability of the trigger timing, and of the test itself.

These factors are compounded in analysis of still Schlieren photography, but negated in digital videography allowing for more reliable comparative image analysis.

The intricacy of the conventional still photography Schlieren set-up was simplified by the ability to view the image in real time during the optical set-up. This meant that minute changes in knife-edge height, or lens angle, could be made and the results viewed in real time as the image changed. With a traditional still photography Schlieren set-up, these results would only be known after sample photographs had been taken and developed, only to reveal the necessity for another minute adjustment to obtain a clear and effective Schlieren image. The relative ease of this real-time set-up allowed for a very clear, accurate and repeatable, Schlieren image, and sequence of images, to be attained.

3.2 Selection of Visual Analysis Technique

After consideration of the visualisation techniques, it was decided that a combination of Schlieren photography and high speed digital videography was best suited to this investigation. High speed digital Schlieren videography, as the name implies, takes advantage of the optical techniques optimised in high speed videography and Schlieren photography as discussed above. The optical set-up is identical to that of normal Schlieren photography, but instead of the image being focused onto the emulsion of a still camera, it is focused onto the CCD (Charged Couple Device) sensor of a high speed digital video camera. This results in a sequence of digital Schlieren images being captured for analysis, as opposed to as single hardcopy image that would be the result from still Schlieren photography.

3.3 Literature Survey - Visualisation Techniques

A survey of literature on the subject of advanced visualisation techniques was carried out, and the outcomes of which are as follows:

3.3.1 Flow Visualisation, [25]

The general principles and characteristics of a number of flow visualisation and optical testing techniques are introduced. Flow visualisation techniques that rely on the addition of foreign materials into the flow, and carrying these experiments out in such a way as to optimise the results, are described. Non-intrusive flow visualisation techniques, and ways of optimising their results are also described and explained. Fluid flow as a refractive index field, and visualisation by means of the resulting light deflection, are described and illustrated in detail. Flow visualisation techniques of interest that are detailed are: laser-doppler anemometry, shadowgraphs, interferometry, laser speckle photography, Schlieren photography, smoke screening and high speed photography amongst others.

3.3.2 High Speed Video for Flow Visualisation, [29]

This document describes the design and implementation of a high-speed digital video capture system for the use in a flow visualisation laboratory. The system design included a digital high-speed camera, lenses, lighting and a data acquisition and storage system.

3.3.3 Photography for the Scientist, [30]

A wide variety of photographic techniques are described and illustrated. High-speed, and Schlieren photography, are described in detail, and the optimisation of their use detailed for the scientific user.

3.3.4 Flow Visualisation with Laser Light Sheet Techniques in Automotive Research, [31]

This paper presents a number of techniques for the visualisation of flow fields for automotive research in both aerodynamics and internal combustion engines. These techniques are used in the quantative analysis of the flow fields. Several current techniques and applications are introduced, and the theory and set-up outlined. The applications introduced include aerodynamic wind tunnel testing (using smoke screening) and in cylinder flow and swirl analysis (using particle seeding and particle image velocimetry).

3.3.5 The Amateur Scientist – An air flash lamp advances colour Schlieren photography, [32]

The theoretical principles of Schlieren photography are detailed, and set-up and system optimisation are presented.

3.3.6 Schlieren photography, [33]

This is a technical guide to Schlieren photography. General principles of the Schlieren optical method, and the details and arrangement of the equipment required, are introduced and detailed. The applications and attributes of

Schlieren photography are compared with those of comparable optical visualisation techniques. Optimisation of the method is presented, including the application of colour Schlieren photography, and examples given.

3.3.7 Particle Image Velocimetry, [34]

General principles and theory behind Particle Image Velocimetry (PIV) are detailed. The theory behind PIV, the equipment and optimising the use of this technique are explained and illustrated. Guidelines for good PIV application are presented, and the equipment required and methods of analysis of the information obtained, are explained in detail.

3.3.8 Photoelectric Schlieren Method used to study the properties of diesel engine injection, [35]

The Schlieren optical technique is used to analyse the delivery rate of a diesel injection system. A Schlieren optical system is set-up in such a way that intensity of the luminous flux of a light ray, which is intersected by the flow of the fuel jet, is measured by a photoelectric sensor placed immediately beyond the Schlieren knife edge. This instantaneous, non-intrusive method of delivery rate measurement is detailed, the method and theory explained and the results presented.

4 EXPERIMENTAL APPARATUS AND PROCEDURES

This research project consists of an advanced visual analysis and engine testing analysis, each of which has its own experimental apparatus and procedure as summarised below:

4.1 Visual Analysis

The visual analysis requires the simulation of injection characteristics of both diesel and dimethyl ether injection, and effective video capture to allow for meaningful review and analysis.

4.1.1 Experimental Apparatus

The choice of high speed digital Schlieren photography as a means of injector behaviour analysis influenced the design of the experimental apparatus. A requirement for Schlieren photography is that parallel light to be passed through the object plane, as illustrated in Figure 3.6. For this reason, the injector chamber had to have parallel windows perpendicular to the light source. This limited the shape of the visualisation chamber to cubic or rectangular. Schlieren photography also required glass, mirrors and lenses of a very high quality, as any irregularities would be magnified in the resulting images.

Although the simulation of the cylinder of an internal combustion engine was compromised by the non-cylindrical shape of the visualisation chamber, it is believed that it was justified, in order to facilitate the use of Schlieren photography. It was also decided that the swirl effects, and the movement of the piston in the cylinder, and its effects on the injection characteristics, would be neglected for this preliminary study.

Two means of injection simulation were considered for this investigation – a pressurised and a non-pressurised analysis:

In order to simulate the cylinder pressures at the point of injection, the injector was to be mounted in a pressurised visualisation chamber. Typical cylinder pressures at the point of injection are in the order of 2.5MPa. A pressure vessel, 200 x 200 x 200mm, with high quality glass windows making up two of the sides, was designed to withstand this pressure. The injector would be mounted to the top, with a drain plug at the bottom. In order to ensure that the diesel and dimethyl ether did not combust spontaneously on injection, it would be filled with nitrogen, and would require nitrogen/air exchange ports. The vessel pressure would be monitored and logged via a pressure transducer.

The final design of this pressure vessel is shown in Figure 4.1, while the detailed design and finite element analysis of the structure can be found in Appendix A1.

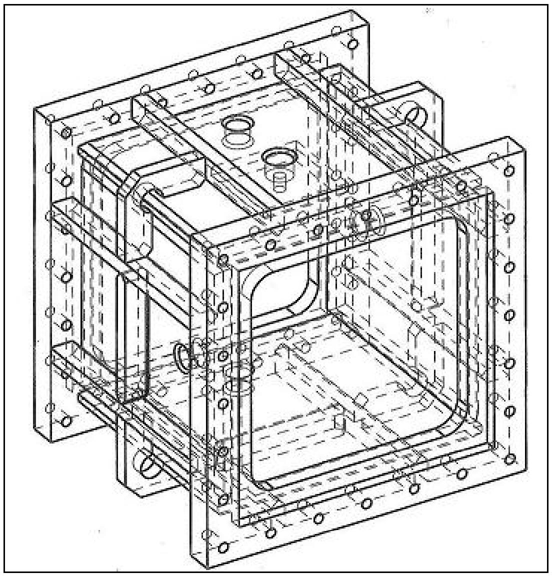

Figure 4.1 – Pressurised Visualisation Chamber

This design revealed a complex structure required to withstand the necessary pressures, to be manufactured and certified by pressure vessel industry specialists. The expense of the high quality glass, of the thickness required to withstand the simulation pressures (approximately 35mm), also had to be taken into account.

Alternatively, the cylinder pressure was to be neglected, and a non-pressurised visualisation chamber would be used to simulate and analyse the injection characteristics - see Figure 4.2. The injector is mounted on a simple 120mm x 90mm x 90mm structure with two parallel, removable, high quality windows (BK70 quality glass), making up two sides, and a drain plug at the bottom. Because the chamber is not pressurised, thinner panes of glass were specified, and the actual structure was not required to withstand the high pressure. The chamber was therefore simpler and was not required to be manufactured by specialists and certified. No finite element analysis was required, and the complete design is shown in Appendix A2.

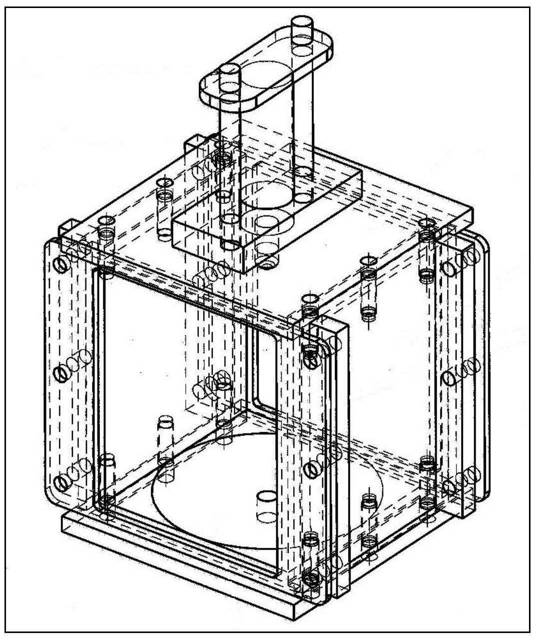

Figure 4.2 – Non-pressurised Visualisation Chamber

Although the lack a cylinder pressure would compromise injector spray behaviour, the simplicity and cost effectiveness of the apparatus had obvious practical and financial advantages, especially for a preliminary, exploratory investigation such as this.

On reviewing the proposed designs, experimental implications, and resulting compromises, with regard to the project scope and financial limitations, and in view of the fact that this is a comparative analysis, it was decided to carry out the investigation using the non-pressurised visualisation chamber as shown in Figure 4.2.

4.1.2 Experimental Set-up - Optical and Video Arrangement

The nature of the visual analysis dictated that the experimental procedure be carried out in complete darkness, and the apparatus was therefore set-up in a light free room. The Schlieren set-up is extremely sensitive, requiring precise alignment of the optical equipment to obtain as clear an image as possible.

The optical arrangement is illustrated in Figure 3.6, with the major components being:

~ source light

~ slit

~ pair of parabolic mirrors

~ two bi-convex lenses

~ image capturing device.

The light source was a 300W projector lamp, the source lens had focal length of 300mm and the slit was made up of two parallel razor blades arranged in such a way that the separation between the cutting edges was approximately 0.5mm. The two parabolic mirrors were 150mm in diameter and had a focal length of approximately 300mm. The capture lens was 75mm in diameter with a focal length of 150mm, the knife edge was a standard optical knife edge, and the capturing device was a Photron Fastcam Ultima ApX high speed digital video camera.

The advantage of this camera, other than its ability to record digitally at up to 120 000 frames per second, is its 0.75“ CCD (Charged Couple Device) sensor. Current industry standard is a CCD sensor size of 0.37”, which requires digital enlargement for effective analysis. The Photron camera’s large CCD sensor allowed the image to be focused directly onto the CCD sensor, with resulting clear images which do not require enlarging and the associated loss in image quality.

Figure 4.3 is a snapshot of the real time functionality of the Photron Fastcam software. A live picture of the object plane can be viewed during set-up for a precise Schlieren image.

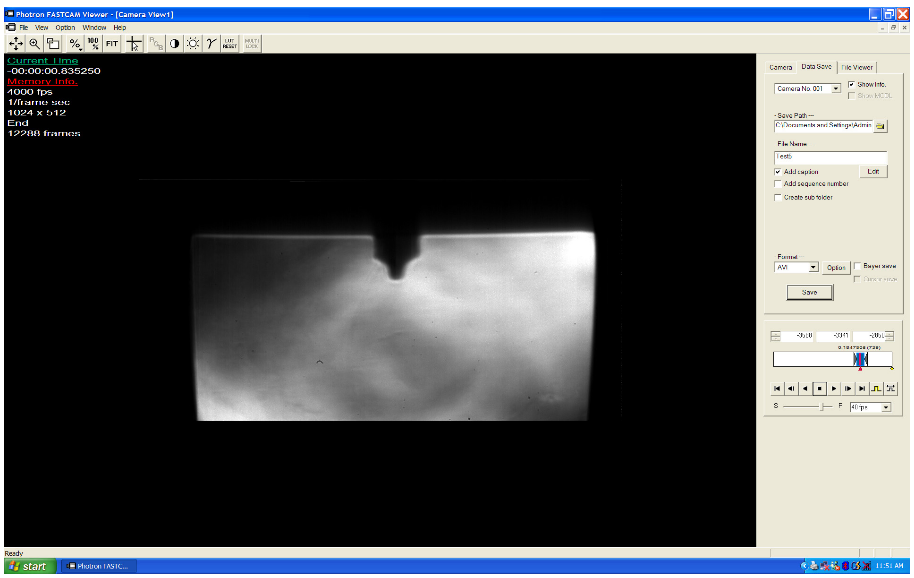

Figure 4.3 – Real time Schlieren image

The apparatus was arranged on the same horizontal plane, on an optical table with the visualisation chamber situated in the middle of the object plane. Refer to Figures 4.4 to Figure 4.6.

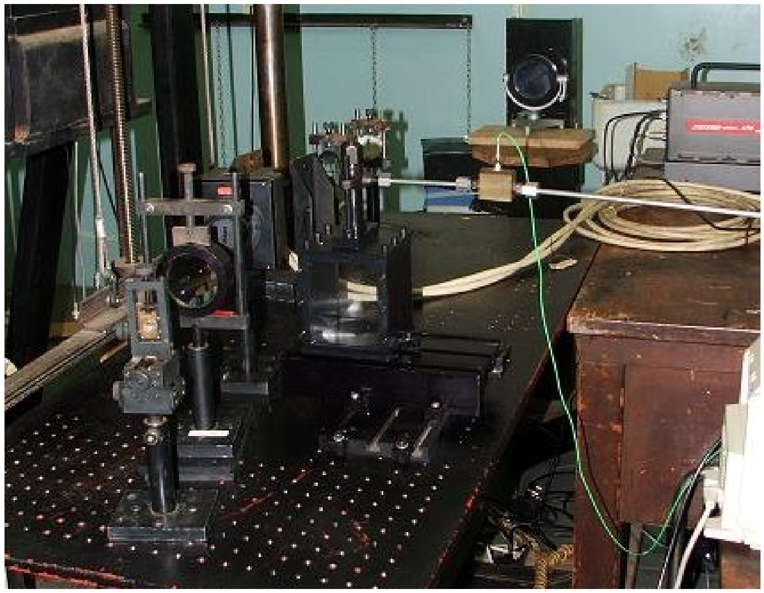

Figure 4.4 – Optical Configuration

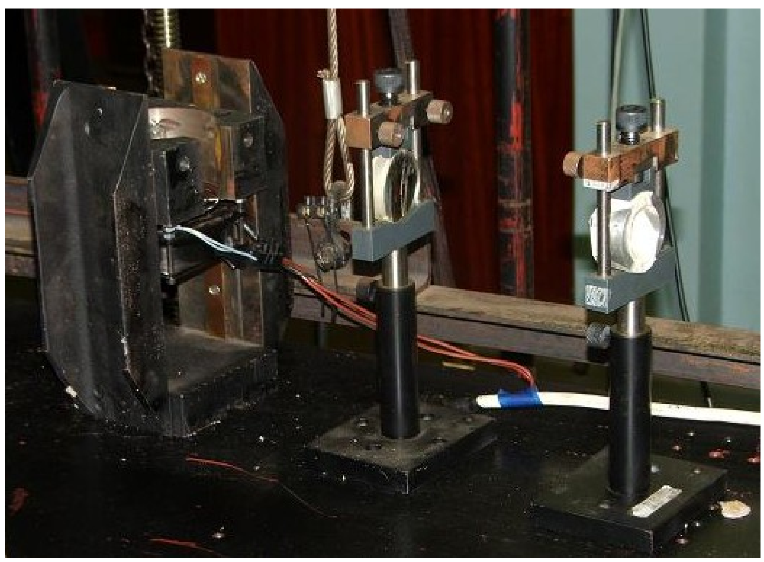

Figure 4.5 – Optical Source Configuration

Figure 4.6 – Optical Capture Configuration

4.1.3 Experimental Set-up - Fuel System Configuration

The fuel delivery system consisted of an injector test pump. This pump supplied a Lucas-Bryce three, or four hole injector with fuel through a pressure line fitted with a pressure transducer. The injection pressure was displayed on a pressure gauge on the pump itself, and the line pressure logged via the transducer by a digital oscilloscope, as shown in Figure 4.7.

Figure 4.7 – Fuel Set-up with Diesel Reservoir

For the diesel tests, the fuel was supplied from a reservoir mounted to the pump, while the dimethyl ether tests required the dimethyl ether to be fed directly from the pressurised bottle, as shown in Figure 4.8. The bottle is pressurised to 4 bar, at which pressure the dimethyl ether is in the liquid form. Because this is a closed system, the dimethyl ether remains a liquid until the point of injection.

Figure 4.8 – Fuel Set-up with Dimethyl Ether Bottle Attached

4.1.4 Experimental Procedure – Visual Analysis

In order to ensure reliable and repeatable results, a number of tests were conducted for each scenario. These are listed in Appendix B.

High speed video footage of the jet behaviour was captured for a standard three hole injector, injecting both diesel and dimethyl ether. The apparatus was set up to simulate the injection characteristics of the Lister Petter test engine used for the engine testing investigation run concurrently to this visual analysis, and discussed in Section 5. This required an injection pressure of 210 bar, which was achieved for the diesel tests, but proved to be impossible for the tests conducted with dimethyl ether. The injector pump, having been designed for the use of diesel, was unable to pressurise dimethyl ether to the required 210 bar due to leakage. For this reason the tests were conducted at an injection pressure of 150 bar which was attainable for both fuels, and allows for direct comparison of injection characteristics. Tests were conducted at 210 bar injection pressure for diesel for reference purposes. A number of video sequences were captured and analysed, showing a high level of repeatability.

The footage was captured at 1000 times the playback speed, i.e. the film speed was 4000fps and playback 4fps. The footage analysed is for the duration of the injection itself.

The experimental procedure can be summarised as follows:

Fuel system preparation:

- For the diesel tests, the reservoir on the injection tester was filled with the test fuel
- For the dimethyl ether tests, the pressurised dimethyl ether bottle was attached to the injection tester.

Optical set-up preparation:

- The optical set-up was checked for misalignment, or interference

Pressure transducer signal capture preparation:

- The digital oscilloscope was zeroed and its trigger activated.

Video capture preparation:

- The video capture software was prepared, ensuring that all the settings were correct and that the image was as required.

Room sealed and lights off:

- The laboratory door was sealed, and the lights switched off, ensuring that there was no external light to compromise the footage.

Start digital video recording:

- The video capture was activated.

Pump fuel until injection pressure reached:

- The injection test pump was pumped until the specified pressure (150 bar) was reached, resulting in the injection of fuel into the visualisation chamber.

Stop digital video recording:

- De-activate video capture.

Review footage and trim:

- The footage was then reviewed and trimmed relative to datum point.

Although this visual analysis is best conducted using the digital videos accompanying this report, the actual analysis was conducted using 'snapshots' taken from the video footage. These snapshots were extracted every 5th frame giving a time between images of 0.00125 seconds. This analysis is illustrated and discussed in Section 5.

4.2 Engine Testing

The engine testing analysis entails the simulation of engine operating conditions when fuelled with diesel and dimethyl ether, and the effective capture of key operating parameters for analysis.

4.2.1 Experimental Apparatus

A series of engine tests were carried out with a twin cylinder Lister Petter engine coupled to a Borghi & Saveri eddy current dynamometer. Refer to Table 4.1 and Table 4.2 for technical specifications of the test engine and dynamometer respectively. This engine was equipped with a piezo-electric pressure transducer in the cylinder head for cylinder pressure measurement.

Table 4.1 – Test Engine Specifications

Manufacturer	Lister Petter
Model	PH2
Capacity (litre)	1.3
Number of Cylinders	2
Bore (mm)	87.7
Stroke (mm)	110
Compression Ratio	16.5:1
Maximum Power (kW @ rpm)	13.4 @ 2200
Maximum Torque (Nm @ rpm)	59.4 @ 2200
Fuel Injection Pressure: 900 – 1099 rpm	137/152bar
Fuel Injection Pressure: 1100 – 2000 rpm	197/217bar
Inlet Valve Opening	13.5º BTDC
Inlet Valve Closing	38.5º ABDC
Exhaust Valve Opening	38.5 º BBDC
Exhaust Valve Closing	13.5 º ATDC
Fuel Injection Timing: 0 – 1650 rpm	24º BTDC
Fuel Injection Timing: 1651 – 2000 rpm	28º BTDC

Table 4.2 – Dynamometer Specifications

Manufacturer	Borghi & Saveri
Model	FE150S
Maximum Speed (rpm)	13000
Maximum Power (kW)	110
Maximum Torque (Nm)	280
Accuracy	0.1rpm and 0.1 Nm

Figure 4.9 – Test engine with dynamometer

The Borghi-Saveri dynamometer simulates load conditions by keeping either the torque or speed constant, by acting as a generator in converting the electrical energy created by the rotation into a mechanical resistive force on the crankshaft of the engine. The resulting torque produced at the lever arm is measured by a load cell, while the engine speed in registered by a shaft encoder on the crankshaft.

During these tests a sample of exhaust gas was diverted through the gas analyser, and the emissions characteristics logged for analysis.

The gas analyser was made up of an oven filter unit, and an analyser for each emissions gas:

~ Signal 4000VM NO_x Analyser

~ Signal 7000 GFIR CO_2 Analyser

~ Signal 7000 GFIR CO Analyser

~ Signal HM THC Analyser

4.2.2 Experimental Procedure

The tests were carried out at loadings of 25Nm, 35Nm and 45Nm, using both diesel and dimethyl ether. These tests were run under constant speed conditions at speeds between 1100 and 1800rpm, at 100rpm increments.

The relevant information was then logged and previously developed software was then used to assimilate and output the required information for each test. The results of all the tests conducted can be found in Appendix C and D.

Analysis of the results of these tests at the various speeds and loadings gives valuable insight into the performance of the engine when fuelled with both diesel and dimethyl ether. These results, and a detailed discussion thereof, can be found in Section 5.

5 RESULTS

5.1 Visual Analysis

On completion of the visual analysis procedure as discussed in Section 4, the results were assimilated, and edited for analysis.

A total of thirty nine tests were conducted. Of these, nine were simply to finalise the Schlieren and video set-up, whilst the remaining thirty were for formal evaluation. A log of tests can be found in Appendix B.

A number of different camera speeds were tested ranging from 500 to 10 000 frames per second, with 4000 frames per second proving to illustrate the injection characteristics best for thorough analysis. In order to ensure directly comparable footage and images, the footage was edited to start at the exact point of beginning of injection.

Both a three, and a four hole injector was tested, however the video footage captured from the four hole injector tests proved to be more applicable to visual analysis due to the orientation of the holes. Comparative analysis of the footage of these two injectors illustrated that they showed similar injection characteristics and sensitivity to changes in operating conditions, and therefore for the purposes of this investigation the four hole injector is analysed further.

Although the intention was to simulate injection operating conditions as closely as possible at the diesel injection pressure of 21 MPa, this proved impossible when injecting dimethyl ether, due to excessive leakage past the injector sealing surfaces. This can be attributed to the fact that the tolerances required to limit leakage of diesel are lower than those required to seal the injector from leakage of dimethyl ether due to diesel’s higher viscosity and density. For this reason the test pressure was dropped to 15 MPa for the purposes of this investigation. Although this needs to be kept in mind when reviewing the results, the injection characteristics of diesel at 15 MPa are almost identical to those at 21 MPa, as illustrated by the comparative snapshots presented in Figure 5.1 for four hole injection of diesel at 15 MPa and 21MPa respectively. The frames depicted are 0.0025 seconds apart in real time, i.e. at the film speed of 4000 frames per second, a snapshot was taken of every 10^{th} frame.

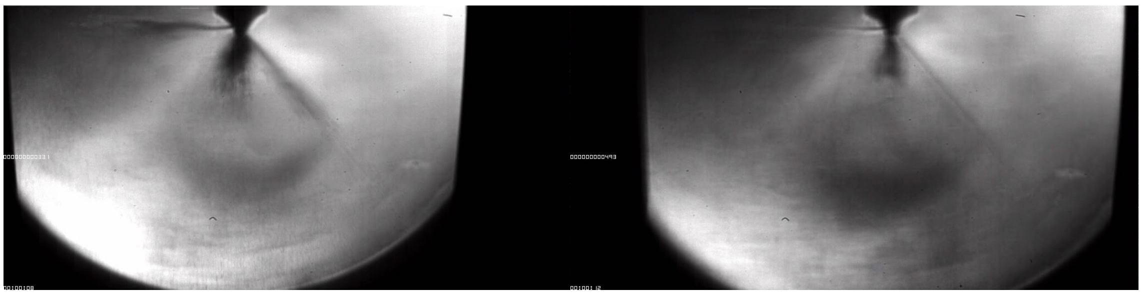

t = 0.0ms

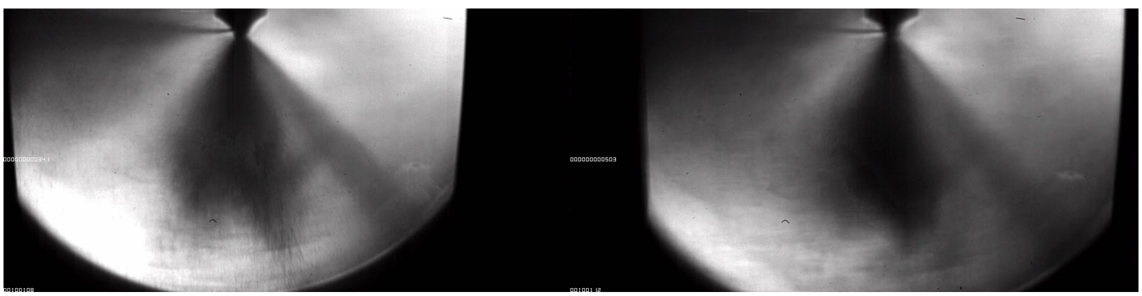

t = 2.5ms

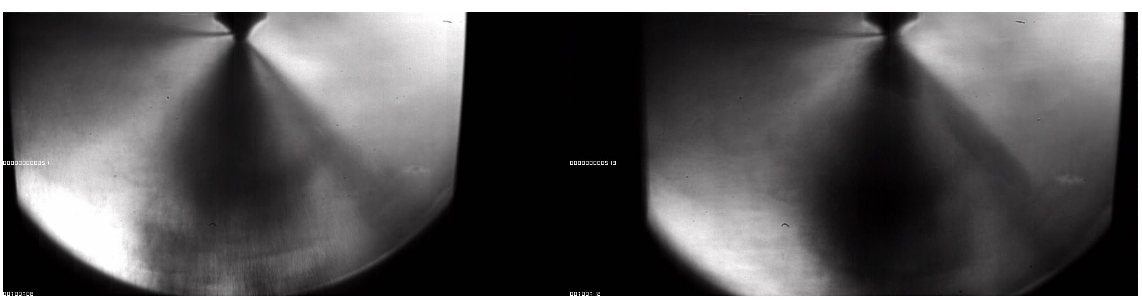

t = 5.0ms

Figure 5.1 – Snapshots of video footage sequence – 4 hole diesel injection 15 MPa (L) and 21MPa (R)

5.1.1 Results of Visual Analysis

Figure 5.2 illustrates a sequence of snapshots from the high speed footage of the injection of both diesel (on the left) and dimethyl ether (on the right). The frames depicted are 0.00125 seconds apart in real time, i.e. at the film speed of 4000 frames per second, a snapshot was taken of every 5th frame.

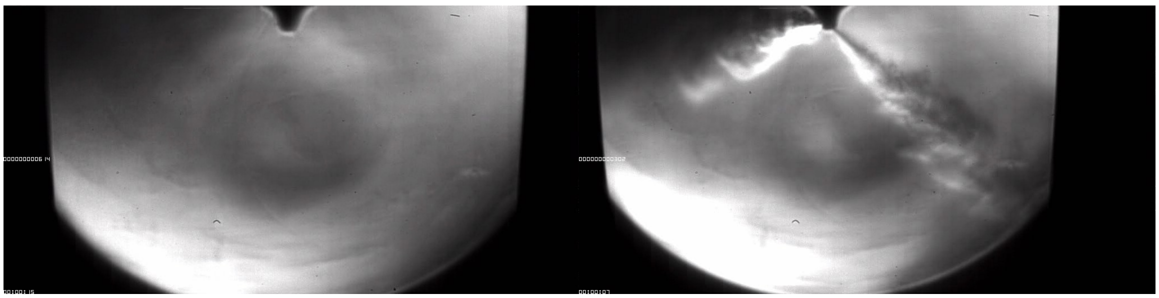

t = 0.0ms

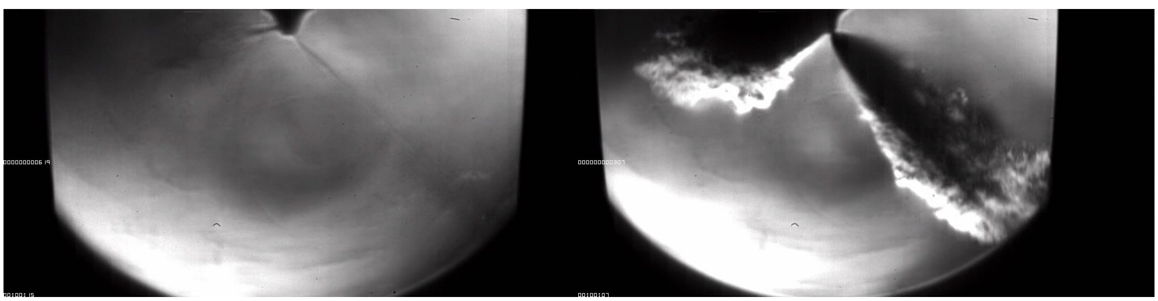

t = 1.25ms

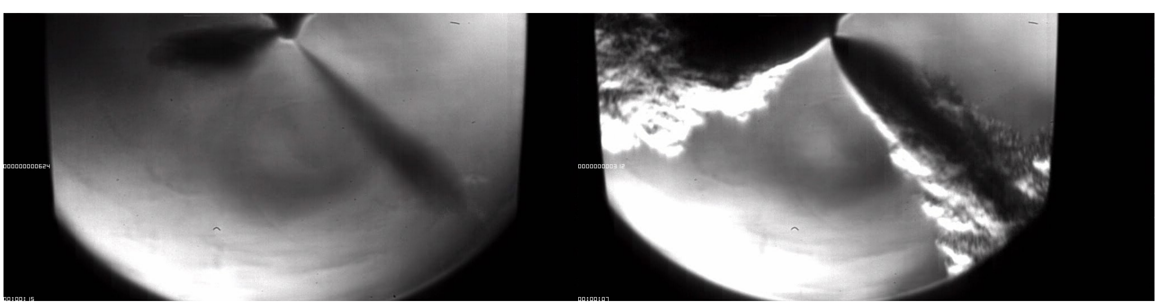

t = 2.5ms

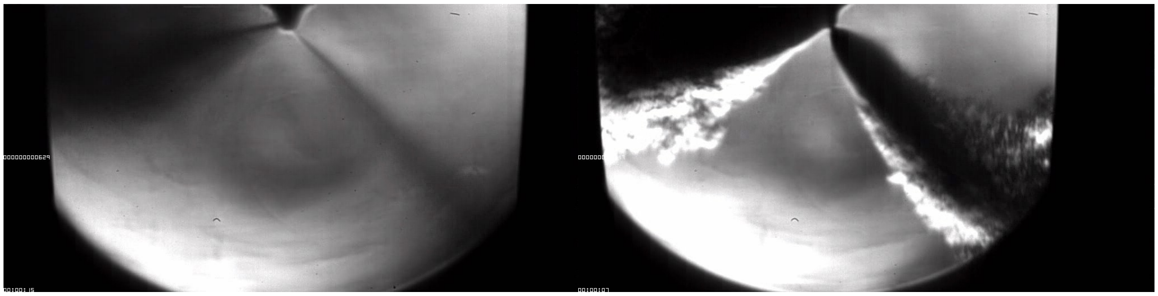

t = 3.75ms

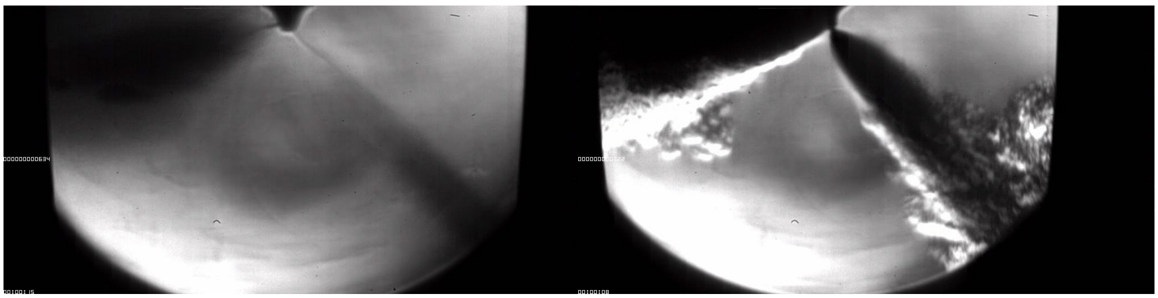

t = 5ms

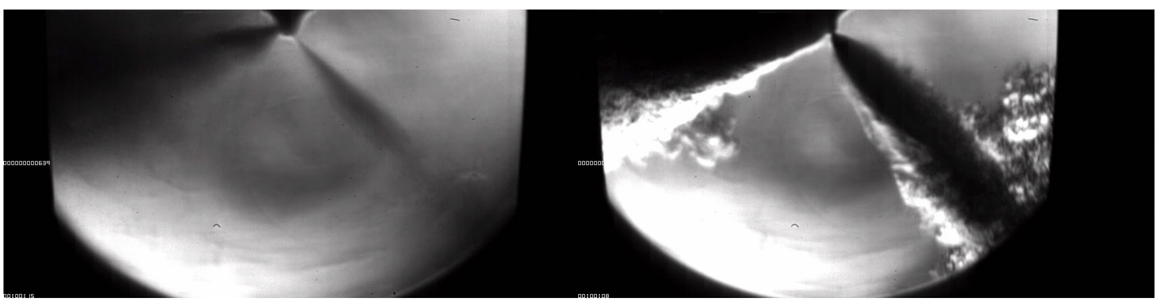

t = 6.25ms

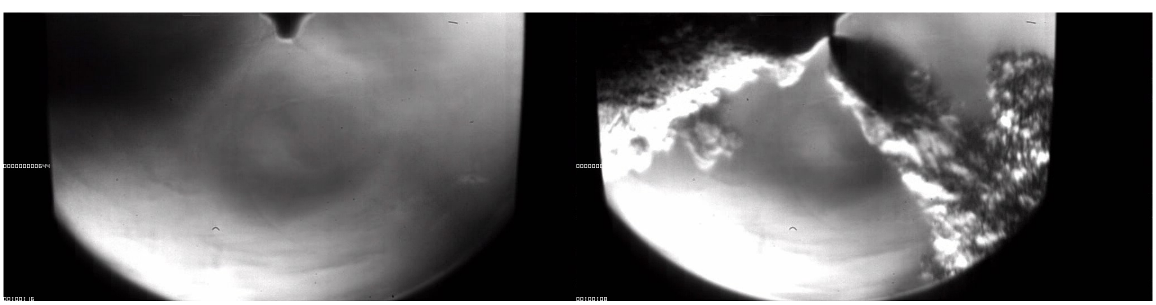

t = 7.5ms

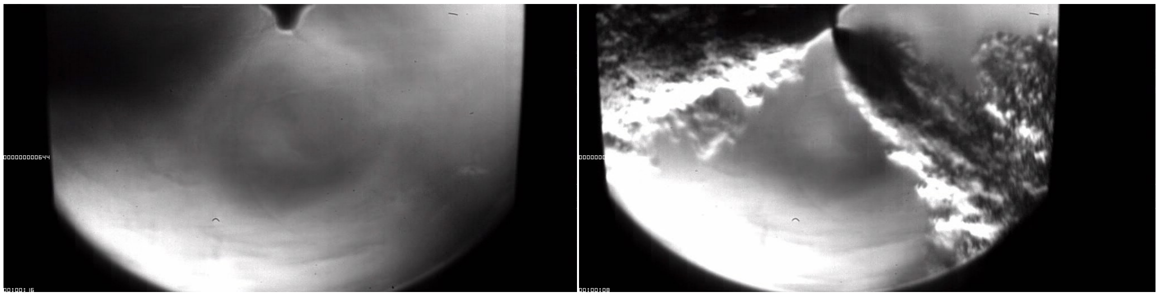

t = 8.75ms

Figure 5.2 – Snapshots of video footage sequence – diesel (L) and dimethyl ether (R), 15 MPa

Immediately evident is the pre-injection leakage of the dimethyl ether test, the comparative violence of the dimethyl ether injection, with greater penetration and longer injection duration

The footage presented in Figure 5.2 is of the four hole injector with both diesel and dimethyl ether at 15 MPa, and is indicative of the injection characteristics of all the successful tests, illustrating the differences between the injection characteristics of the two fuels.

5.1.2 Pre-injection Fuel Leakage

At the test pressure of 15 MPa, all tests conducted with dimethyl ether showed pre-injection leakage from the injector nozzle. This leakage is due to the injectors being specifically designed for diesel fuel, which does not require as high sealing tolerances because of its higher density and viscosity.

5.1.3 Spray Characteristics and Fluid Atomisation

Standard diesel injectors operate between 20 MPa and 170 MPa, injecting into a cylinder at a pressure between 2 to 10 MPa, and a temperature of 1000K [15]. This large pressure differential is required to ensure that the liquid fuel is sufficiently atomised to facilitate rapid evaporation, and that the air fuel mixture has sufficient time to fill the combustion chamber. This injection is illustrated in Figure 5.3 (adapted from reference [15]), with the main attributes highlighted.

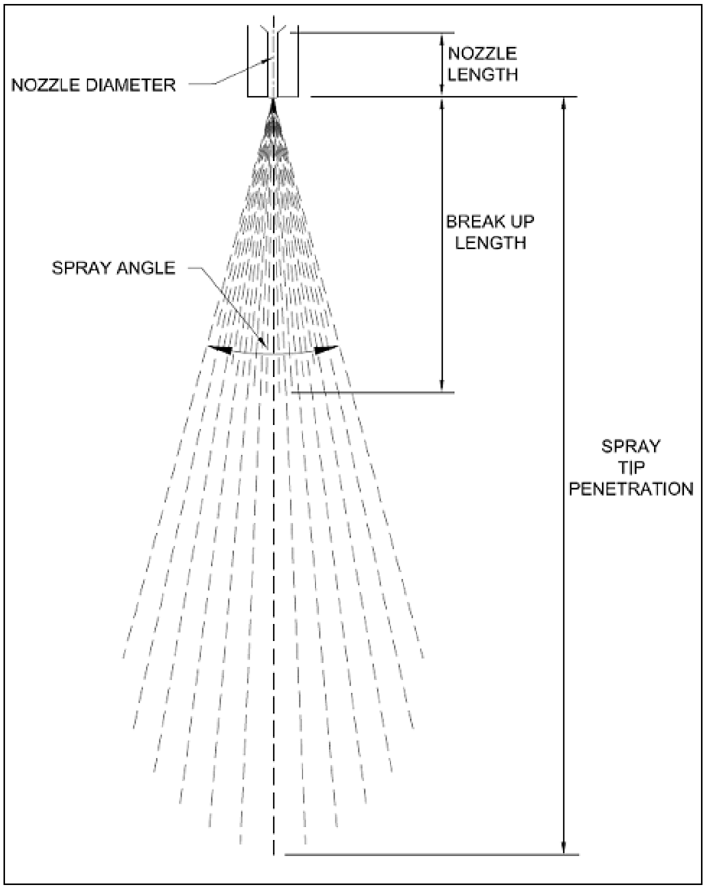

Figure 5.3 – Diesel injection spray characteristics [15]

The initial injection velocity is of the order of 100m/s, with the outer surface of the jet atomising into drops approximately 10μm in diameter. The area in which this atomisation takes place is known as the break up area, with its physical length being the break up length. The atomisation is primarily a result of aerodynamic interactions at the liquid gas interface at the nozzle exit, and results in droplet sizes very much smaller than those at nozzle exit. The extent to which these aerodynamic interactions effect the atomisation of the injected fluid is greatly dependent on the fluid density, viscosity and jet configuration [15].

As the spray travels further from the nozzle, entraining cylinder gases, its velocity decreases and width increases. The degree to which the spray diverges is defined in terms of the spray angle, and the extent of spray reach in terms of the spray tip penetration, or penetration depth. The spray velocity is largest on the centreline of the jet, while the spray on the outer limits evaporate first, meaning that the equivalence ratio is greatest in the centre of the spray, decreasing to zero on the spray boundary [15].

As can be seen in Figure 5.2, these spray characteristics are well illustrated in the footage of the diesel injection. However, the footage of the dimethyl ether injection demonstrates that this injection is not as uniform and ordered.

5.1.4 Spray Angle

In the break up area, the spray angle can be calculated as follows [15]:

$$\tan\frac{\theta}{2} = \frac{1}{A}.4.\pi.\left(\frac{\rho_g}{\rho_l}\right)^{1/2}.\frac{\sqrt{3}}{6}$$

where $A = 3 + 0.28.(\frac{L_n}{d_n})$

θ ~ spray angle

ρ_g ~ density of the in-cylinder gases

ρ_l ~ density of the liquid fuel being injected

L_n/d_n ~ length/diameter ratio of the injector nozzle.

Both A (being a function of the nozzle geometry), and ρ_g (being dependent on the in-cylinder gas conditions), are independent of fuel properties. Therefore, the above relationship can be simplified as follows for the purposes of direct comparison:

$$\theta = C.\tan^{-1}\left(\frac{1}{\rho_l}\right)$$

with C being a constant dependent on nozzle geometry and in-cylinder gas characteristics. Figure 5.4 is an illustrative trend plot of the relationship between fuel density and spray angle.

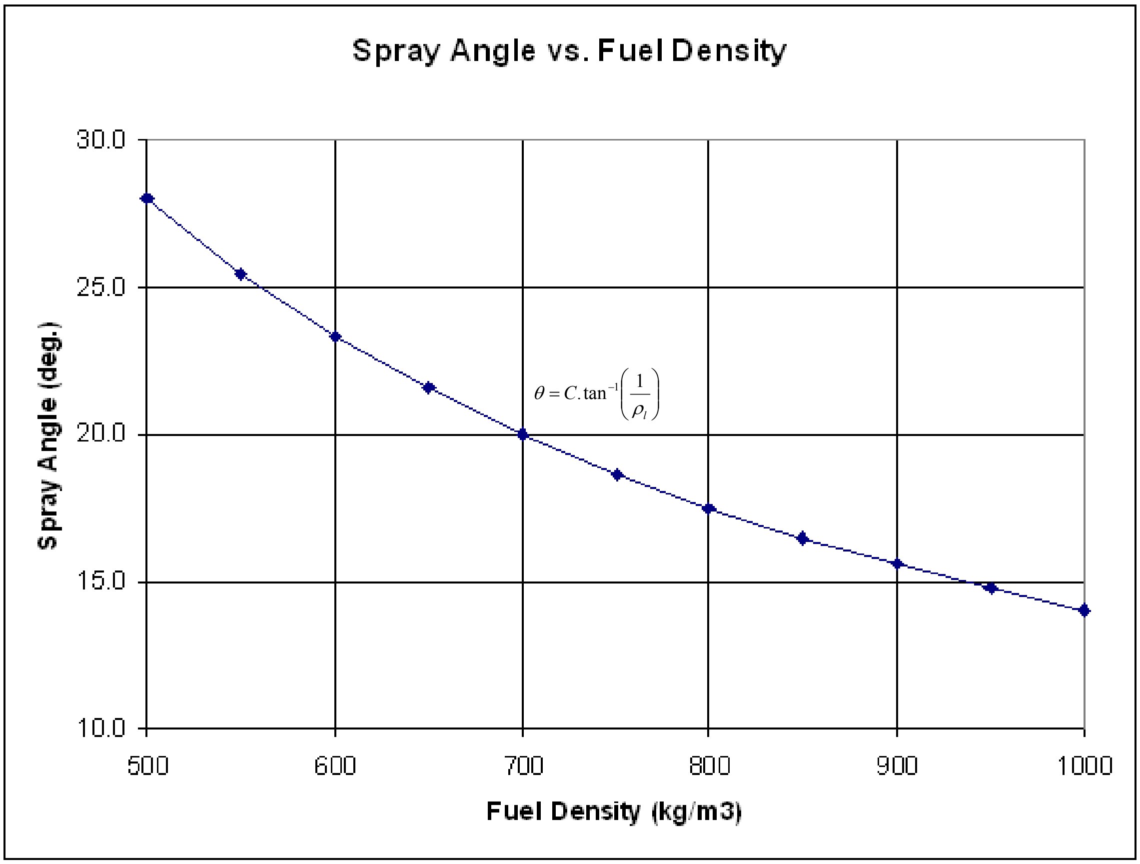

Figure 5.4 – Indicative graph of spray angle vs. fuel density

With dimethyl ether having a lower density than diesel, it therefore follows that when injected under the same operating conditions, through the same injector into the same cylinder conditions, the spray angle of the dimethyl ether injection will be wider than that of the diesel injection. This injection characteristic is verified by the visual analysis as illustrated in Figure 5.2, with the spray angle being noticeably wider than that of the diesel injection.

The approximate maximum spray angles in the visual analysis tests as illustrated in Figure 5.2 were 18º and 41º for diesel and dimethyl ether respectively. These angles are shown in Figure 5.5.

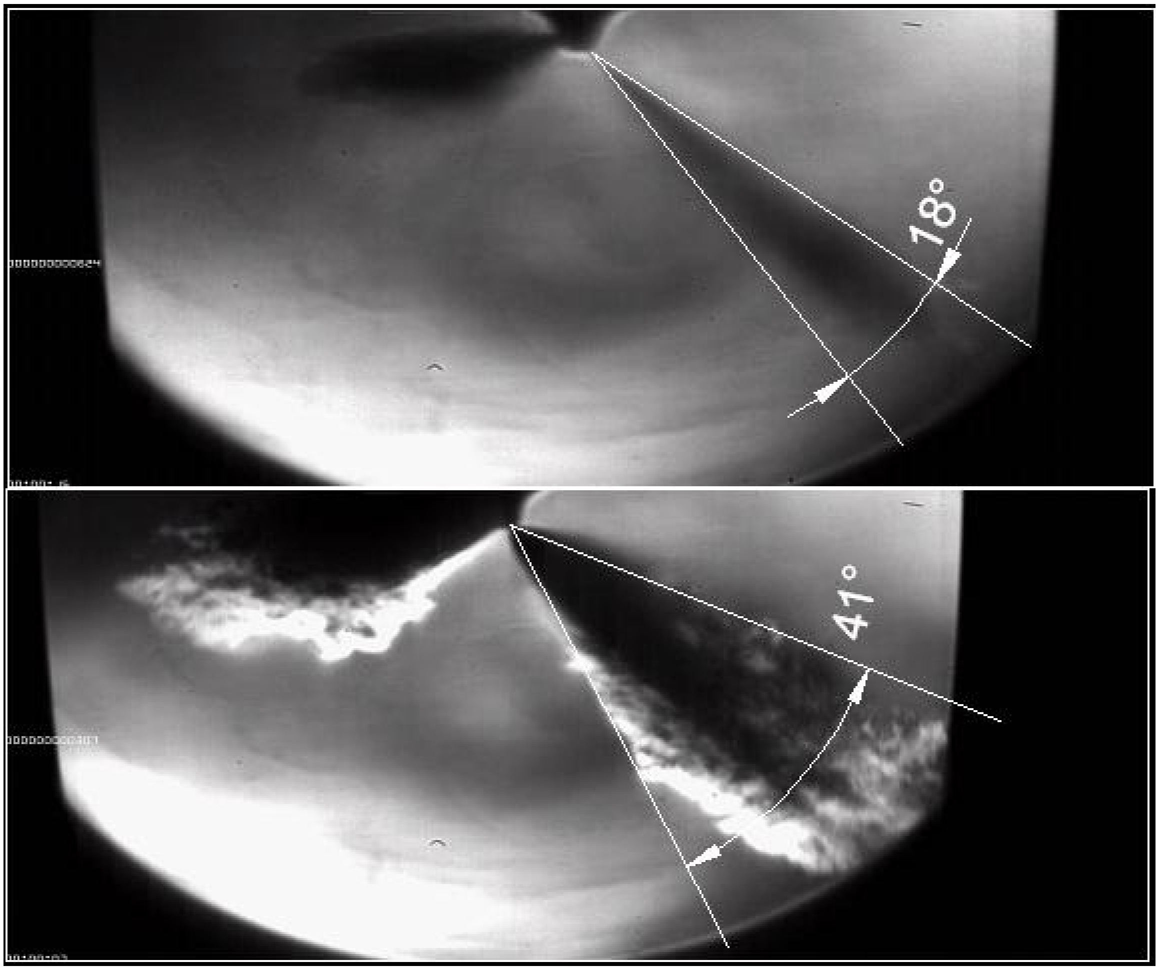

Figure 5.5 – Spray angle of diesel and dimethyl ether injection

5.1.5 Penetration Depth

The penetration depth and speed have an important effect on air utilisation and fuel-air mixing rates. Overpenetration results in fuel interacting with the cylinder walls, generally resulting in reduced mixing rates and increased emissions of unburned hydrocarbons. On the other hand underpenetration results in poor air utilisation and reduced fuel-air mixing rates, due to underutilisation of cylinder volume [15].

Injection penetration depth with respect to pressure differential (Δp), liquid density (ρ_l), in-cylinder gas density (ρ_l), time (t) and nozzle diameter (d_n) can be approximated as follows [15]:

$$S = 0.39.\sqrt{\frac{2.\Delta p}{\rho_l}}.t \qquad \text{for } t < t_{break}$$

and $$S = 2.95.\sqrt{\frac{\Delta p}{\rho_g}}.\sqrt{d_n.t} \qquad \text{for } t < t_{break}$$

with t_{break} being the break up length as defined in Section 5.1.3, and illustrated in Figure 5.3.

The diesel and dimethyl ether injection tests were conducted at atmospheric pressure, at the same injection pressure and with the same injection equipment, i.e. nozzle, therefore the penetration depth pre-breakup can be simplified as follows for the purposes of direct comparison:

$$S = C.\sqrt{\frac{1}{\rho_l}}.t \qquad \text{for } t < t_{break}$$

with C being a constant dependent on injection pressure characteristics.

Figure 5.6 is an illustrative trend plot of the pre-breakup penetration depth as a function of time for diesel and dimethyl ether.

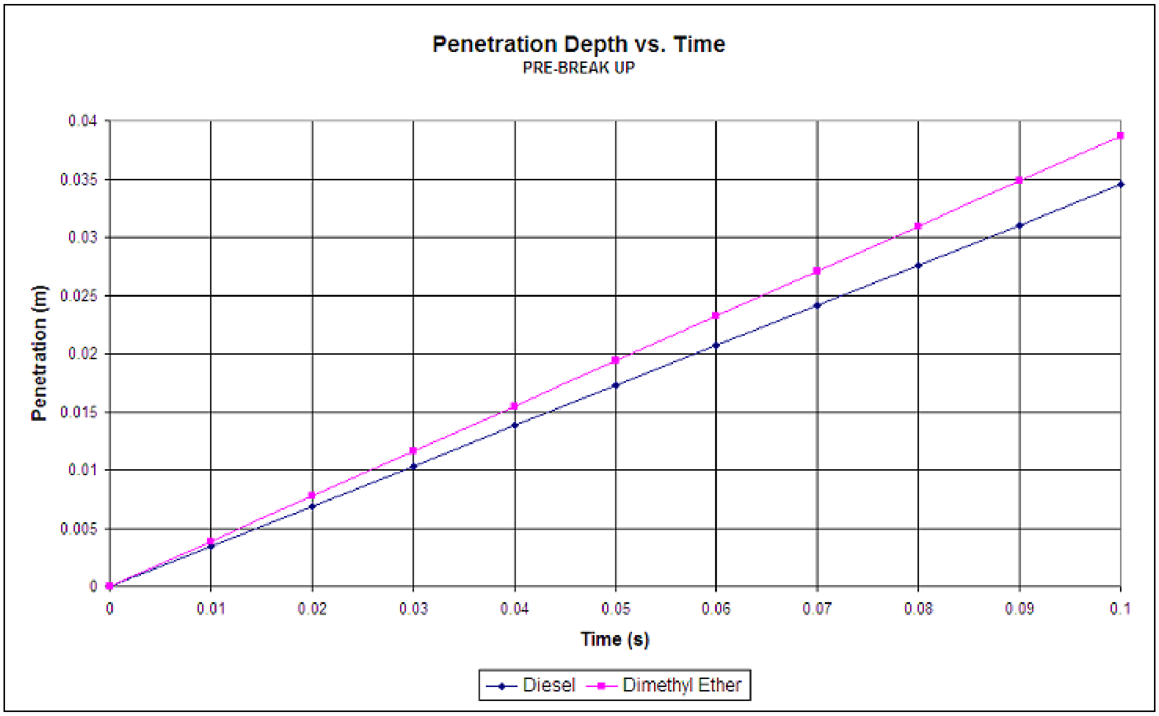

Figure 5.6 – Indicative graph of pre-breakup penetration depth vs. injection time

As illustrated in Figure 5.6, the penetration depth as a function of time of dimethyl ether is consistently larger for dimethyl ether than for diesel injection. This is supported by the observations from the visual analysis presented in Figure 5.2.

The post-breakup penetration depth is dependent on injection pressure characteristics, nozzle geometry and in-cylinder gas density, and not a function of fuel characteristics.

5.1.6 Injection duration

The optimal injection duration is dictated by the operating conditions and physical characteristics of the engine being tested, as well as the properties of the fuel being used. Ideally the fuel is injected at the correct flow rate for the correct duration to facilitate complete and efficient combustion.

The visual analysis illustrated in Figure 5.2 shows the following injection characteristics:

Diesel ~ injection starts at t=0 with a simple thin stream, which develops into a uniform, linear jet that reaches maximum intensity at approximately t=1.25ms. The injection intensity tapers down linearly to termination at approximately t=6.25ms.

Dimethyl Ether ~ injection starts with a violent and non-uniform stream from the jet nozzle, that continues to completion at approximately t=8.75ms.

Injection duration ~ the injection time of dimethyl ether is approximately 0.00875 seconds, 40% longer than that of diesel at 0.00625 seconds.

The extended injection duration, and the pre-injection leakage, of dimethyl ether when injected using the standard diesel injection system, indicates that this injection system does not facilitate optimal injection of dimethyl ether, and will result in inefficient combustion and poor fuel efficiency.

5.2 Engine Testing

The engine testing was carried out as discussed in Section 4.2, and in accordance with the specifications presented in Table 4.1 and Table 4.2.

Engine performance, efficiency and suitability to an application, are generally judged by performance and emissions attributes, but there are a number of engine characteristics that are key in dictating what these attributes will be. These characteristics range from the in-cylinder pressure and temperature, to the delay between the injection of the fuel and the point of ignition, to the ratio of air and fuel entering the combustion chamber.

5.2.1 Brake and Indicated Power

The figure commonly quoted as an engine's power is more specifically its peak brake power at a specific engine speed, which is the power output of the engine at the output shaft.

The indicated power on the other hand, is the theoretical power resulting from the work done on the pistons of an engine, by the burning of fuel and air, and is obtained by calculating the area enclosed by the pressure vs. volume diagram as illustrated in Figure 5.7 below.

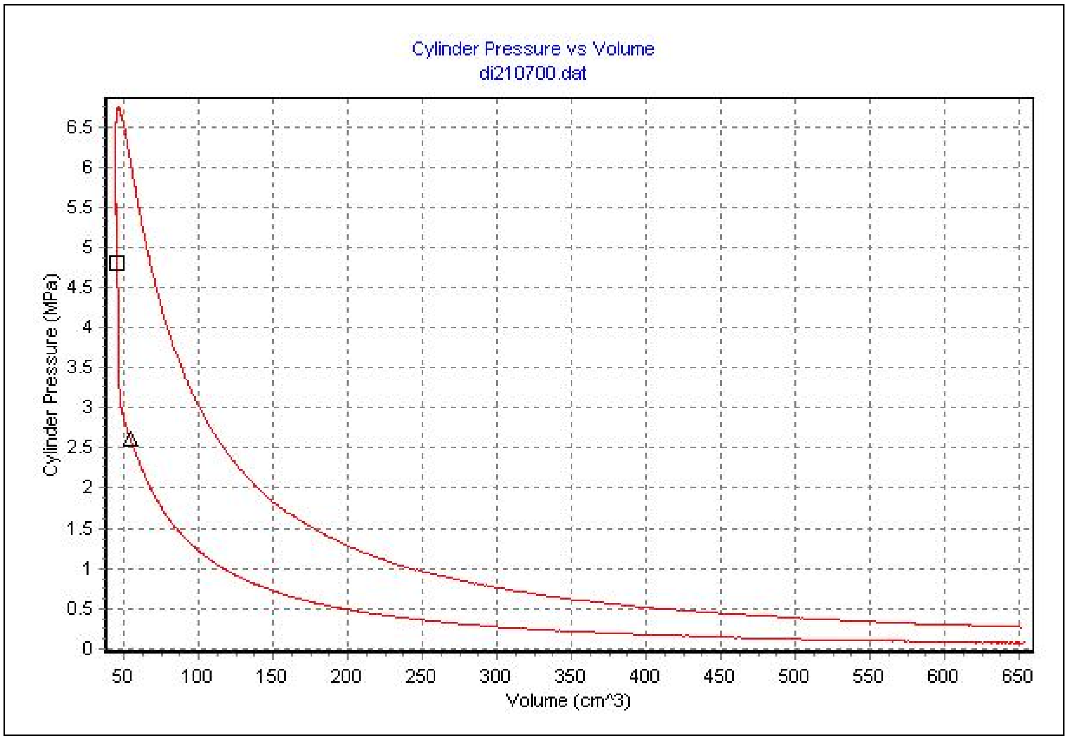

Figure 5.7 – Cylinder pressure vs. crank angle for diesel fuelling at 35Nm and 1300rpm

The difference between these two characteristics can be attributed to the mechanical friction losses within the engine, and are well illustrated in Figure 5.8 and Figure 5.9 where the brake power is consistently lower than the indicated power.

Figure 5.8 is a plot of brake power, over a range of engine speeds, when fuelled diesel and dimethyl ether.

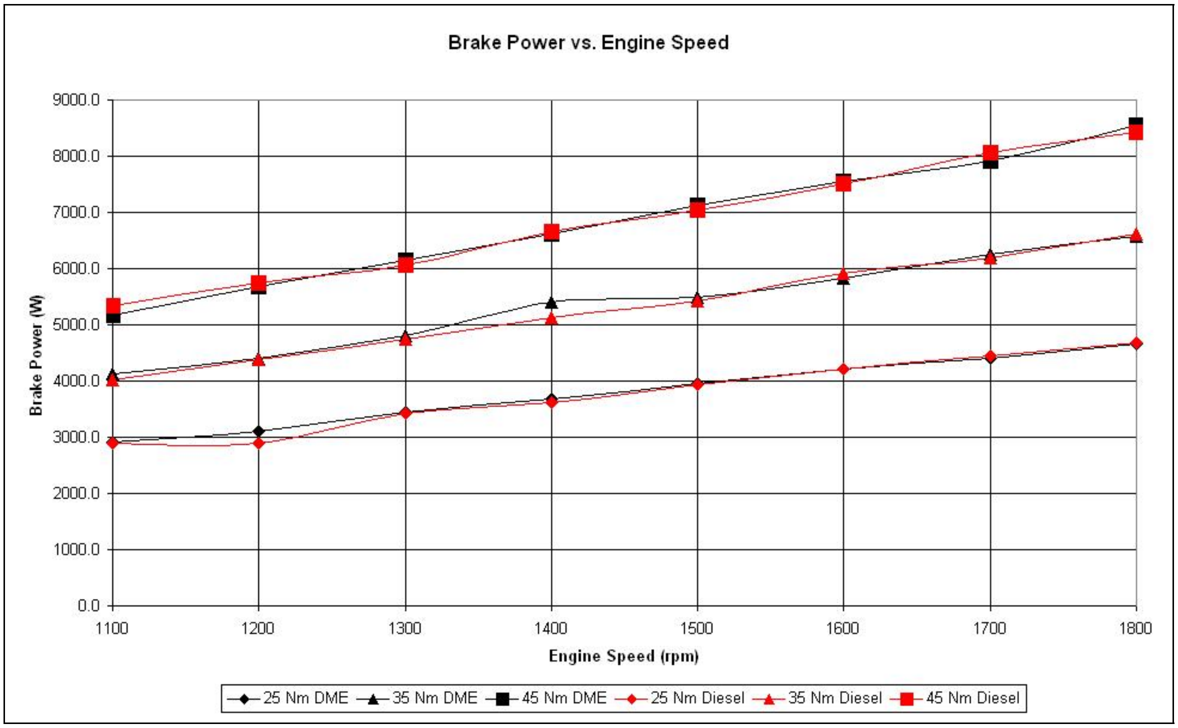

Figure 5.8 - Brake power vs. engine speed

The brake power of the test engine fuelled on diesel and dimethyl ether is very similar throughout the range of engine speeds, with the power increasing uniformly with load.

Figure 5.9 is a plot of the indicated power, over a range of engine speeds, when fuelled by both diesel and dimethyl ether.

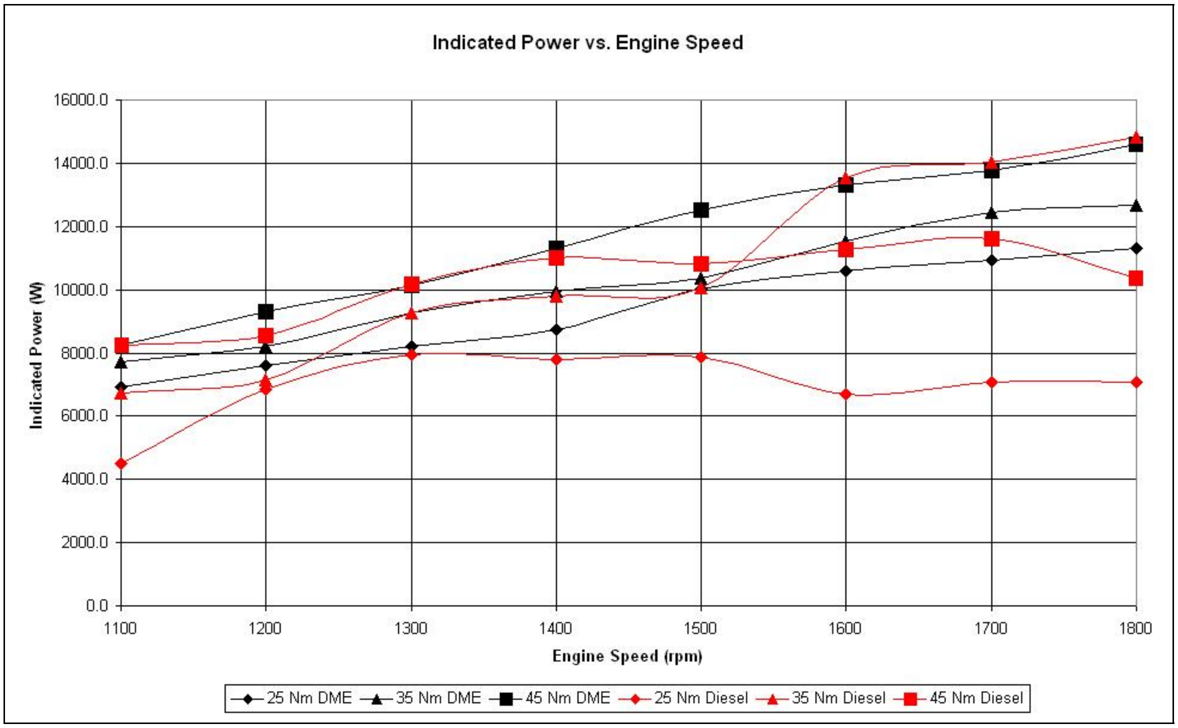

Figure 5.9 – Indicated power vs. engine speed

Although the general trend of indicated power is similar to that of brake power, the results are less uniform, with the diesel and dimethyl ether results deviating from each other.

When the test engine is fuelled with dimethyl ether the indicated power increases constantly with engine load and speed in the same way as the brake power.

The indicated power when the engine is fuelled with diesel on the other hand, is inconsistent, increasing with loading and engine speed until an engine speed of approximately 1500rpm, after which the 25Nm and 45Nm loading results in a plateau, while the 35Nm results continue increasing.

5.2.2 Mechanical Efficiency

An engine's mechanical efficiency is defined as the ratio of the brake power to indicated power:

$$\eta_m = \frac{P_b}{P_i}$$

Figure 5.10 is a plot of the mechanical efficiency of the test engine when fuelled with both diesel and dimethyl ether, at engine speeds of 1100rpm to 1800rpm.

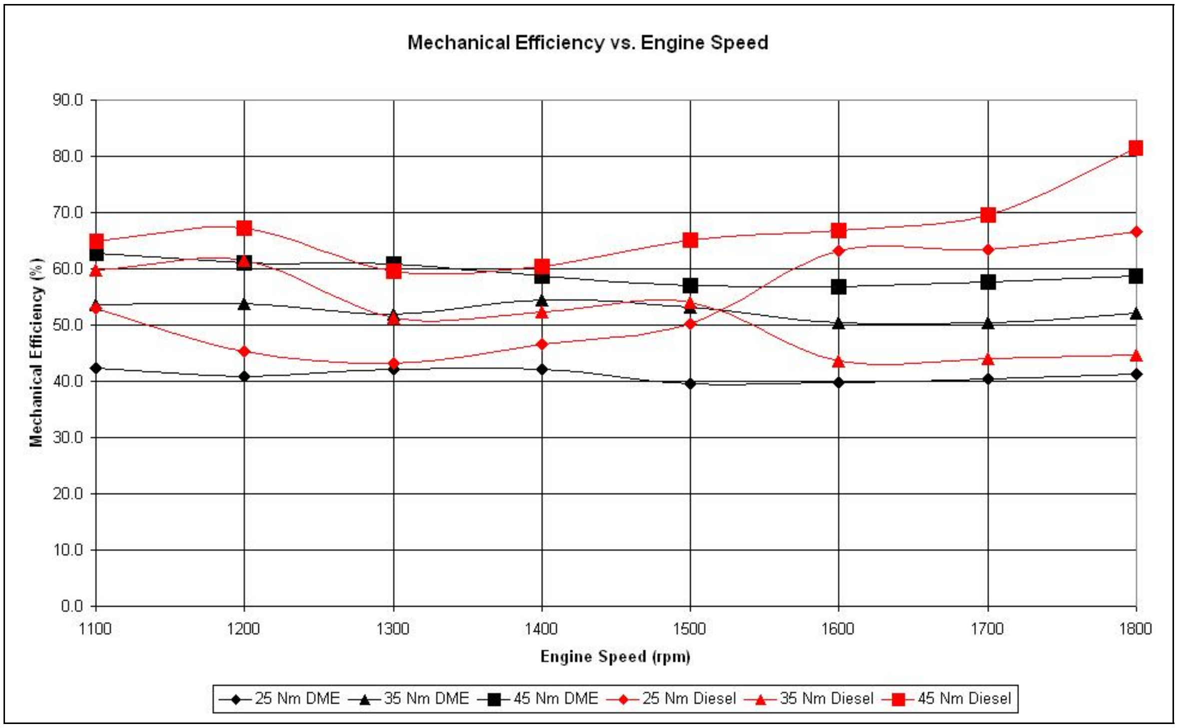

Figure 5.10 – Mechanical efficiency vs. engine speed

The mechanical efficiency when the engine is fuelled with dimethyl ether is relatively constant with respect to engine speed, increasing with engine loading. When fuelled with diesel, the mechanical efficiency is relatively constant until an engine speed of 1500rpm, after which the engine is more efficient when running under a load of 25Nm than 35Nm.

Mechanical efficiency is directly proportional to the relationship between brake and indicated power. It therefore follows that the mechanical efficiency will follow the same trend as the indicated power results as seen in Figure 5.9, due to the consistency in the brake power results.

5.2.3 Mean Effective Pressure

While power and torque are a valuable measure of engine performance and efficiency, because they are dependent on engine size, direct comparisons cannot be made between engines of different sizes and configurations. A relative comparison can be made by dividing the work done by the cylinder volume, per cycle. The resulting engine characteristic is termed the mean effective pressure.

The brake mean effective pressure is a theoretical pressure exerted during the power stroke, to produce the engine brake power:

$$bmep = \frac{2.\pi.P_b}{L.A.N.e}$$

with $bmep$ ~ Brake mean effective pressure (N/m^2)

P_b ~ Brake power (W)

L ~ Stroke (m)

A ~ Piston area (m^2)

N ~ Engine speed (rad/s)

e ~ Power strokes/revolution

Similarly, the indicated mean effective pressure is that theoretical pressure exerted to produce the indicated power:

$$imep = \frac{bmep}{\eta_m}$$

where $imep$ is the indicated mean effective pressure.

Figure 5.11 and Figure 5.12 show the brake mean effective pressure and the indicated mean effective pressure respectively, over the range of engine speeds, for both fuels.

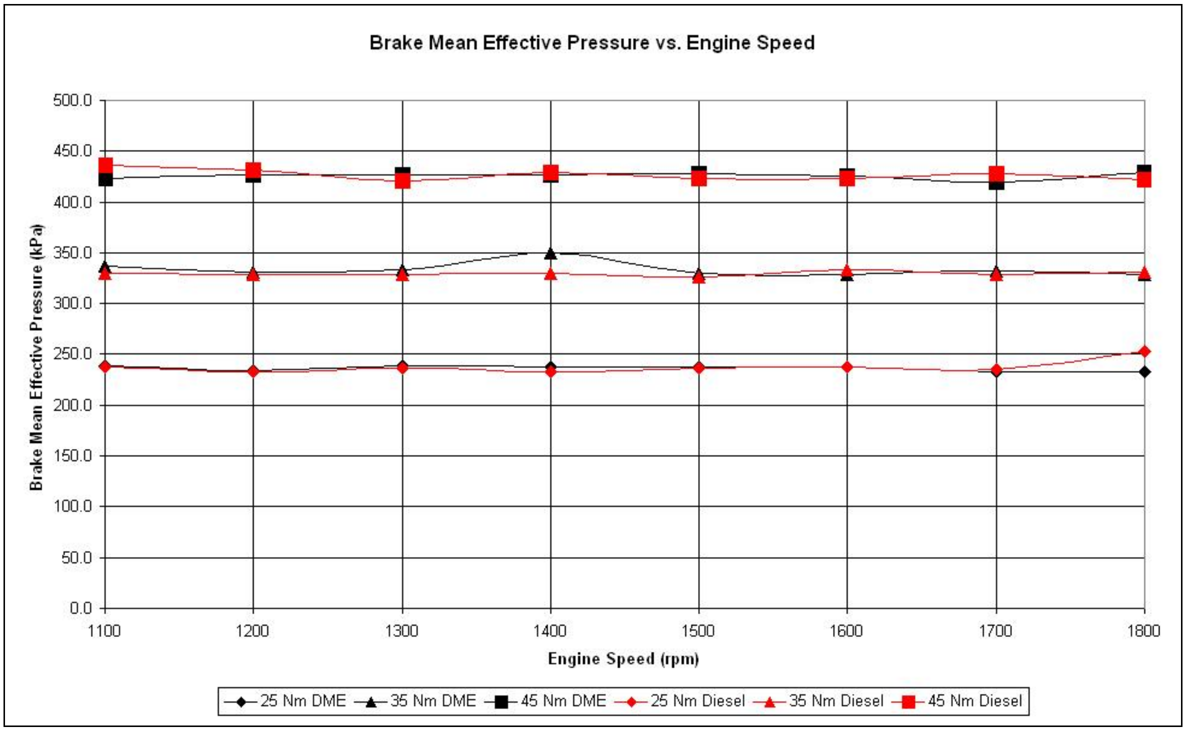

Figure 5.11 – Brake mean effective pressure vs. engine speed

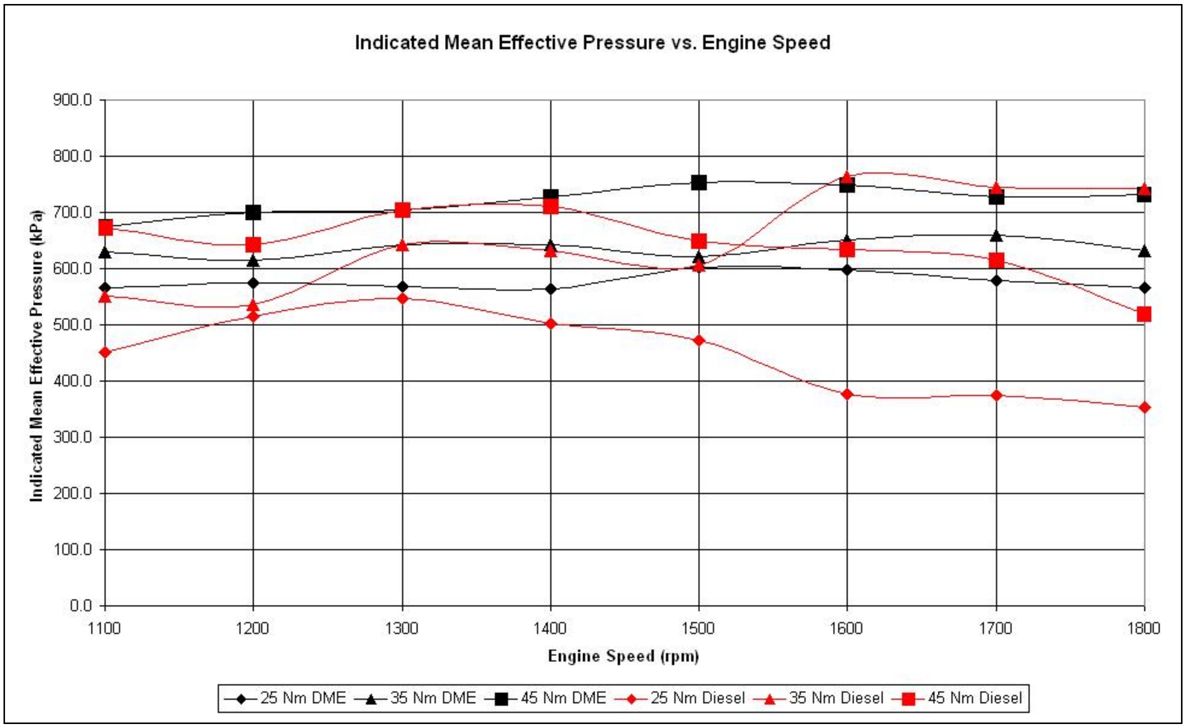

Figure 5.12 – Indicated mean effective pressure vs. engine speed

As would be expected, due to the fact that mean effective pressure is directly proportional to power, the trends of mean effective pressure follow those of power as illustrated in Figure 5.8 and Figure 5.9.

As with brake power, the test engine's brake mean effective pressure is largely unaffected by the fuel used, increasing uniformly as the load increases. The indicated mean effective pressure also follows a very similar trend to that of the indicated power, with the dimethyl ether results increasing uniformly with an increase in loading, while the diesel results are not consistent with respect to engine speed or load.

5.2.4 Equivalence Ratio

The power output of an engine is directly proportional to the mass flow rate of air/fuel mixture entering the cylinder. In theory the optimal air/fuel ratio is that which allows for complete combustion of reactants (fuel/air mixture), and is referred to as stoichiometric. In reality a slightly lean mixture is ideal from a fuel economy point of view, while a slightly rich mixture gives maximum power output [15].

The equivalence ratio is the ratio of stoichiometric to actual air/fuel ratio:

$$\phi = \frac{(A/F)_s}{(A/F)_a}$$

where $(A/F)_s$ is the stoichiometric air/fuel ratio, which is approximately 14.6 and 9 for diesel and dimethyl ether respectively, and $(A/F)_a$ is the actual air/fuel ratio

Figure 5.13, is a plot of the equivalence ratio versus engine speed, fuelled with both diesel and dimethyl ether fuelling.

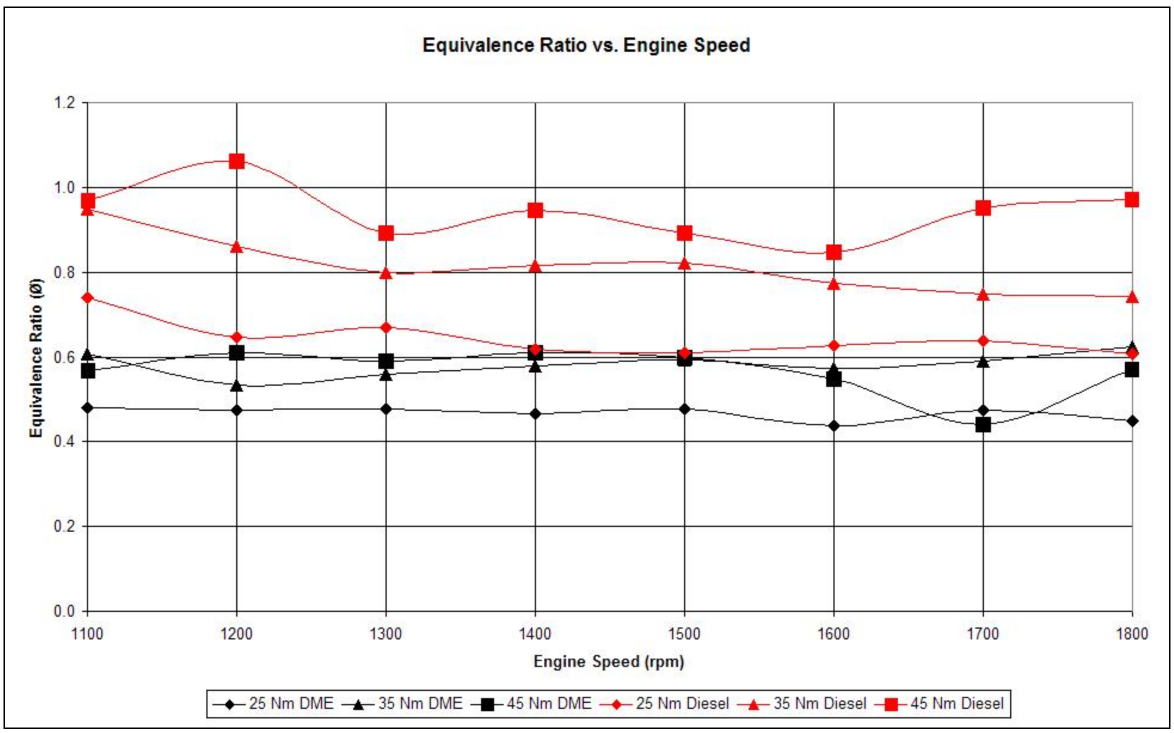

Figure 5.13 – Equivalence ratio vs. engine speed

Immediately obvious is the fact that both the diesel and dimethyl ether tests are being fuelled lean, i.e. the actual air/fuel ratio is higher than the optimal stoichiometric air/fuel ratio. When fuelled with diesel, the mixture is richer (closer to stoichiometric), with an equivalence ratio ranging between 0.61 and 1.06, while when dimethyl ether is used this ranges from 0.44 to 0.62.

The equivalence ratios for each loading and fuel are relatively constant, with the tests conducted with diesel fuel consistently running at a higher equivalence ratio than those run with dimethyl ether. The equivalence ratio increases consistently with engine loading for both fuels.

Figure 5.14 is a plot of the air and fuel flow versus engine speed, and indicates that the fuel and air flow characteristics do not differ substantially between the diesel and dimethyl ether tests.

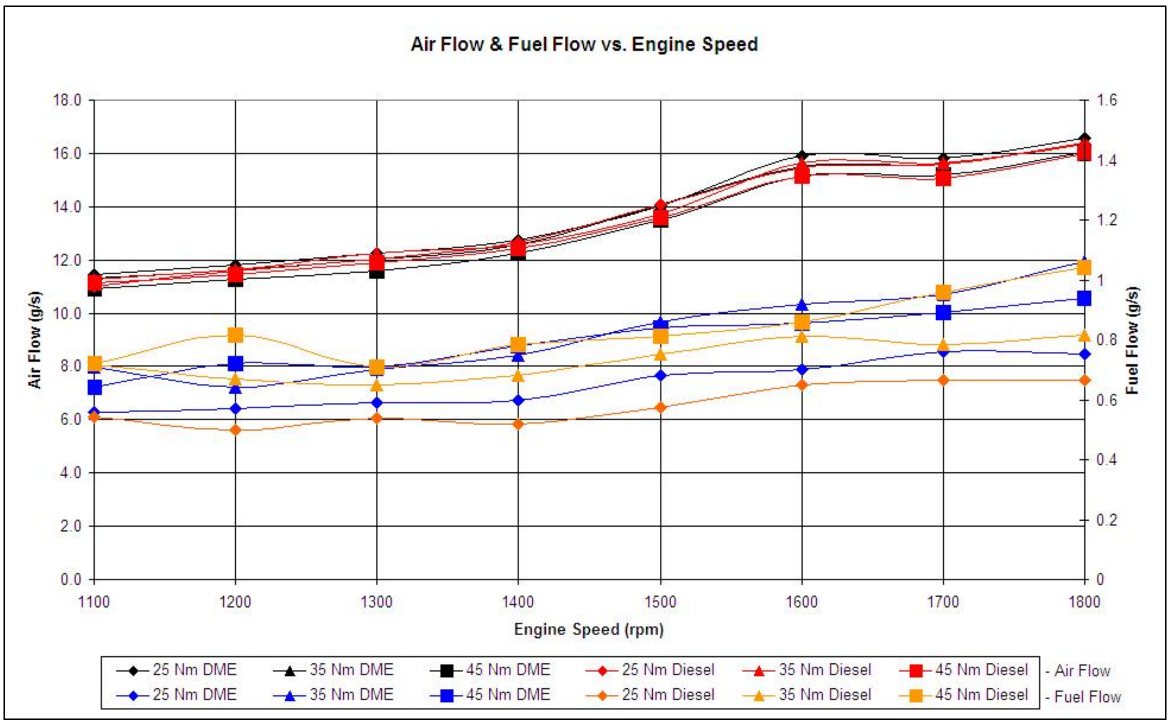

Figure 5.14 – Air flow and fuel flow vs. engine speed

The consistently higher equivalence ratios experienced when fuelled with diesel versus dimethyl ether are therefore a result of their respective chemical properties, i.e. stoichiometric air/fuel ratio, and not due to physical injection characteristics.

These properties need to be taken into account in optimising the fuel system for dimethyl ether, which would improve both engine performance and emissions characteristics.

5.2.5 Fuel Conversion Efficiency

The fuel conversion efficiency is the ratio of work produced, to the amount of fuel energy available per cycle, and is a function of the specific fuel consumption (fuel flow per unit power) and the heating value of the fuel in question [15].

$$\eta_f = \frac{1}{sfc.Q_{HV}}$$

where η_f is the fuel conversion efficiency

sfc is the fuel specific fuel consumption (mg/J),

Q_{HV} is the Lower heating value of the fuel (MJ/kg)

Figure 5.15 is a plot for the fuel conversion efficiency for the diesel and dimethyl ether tests.

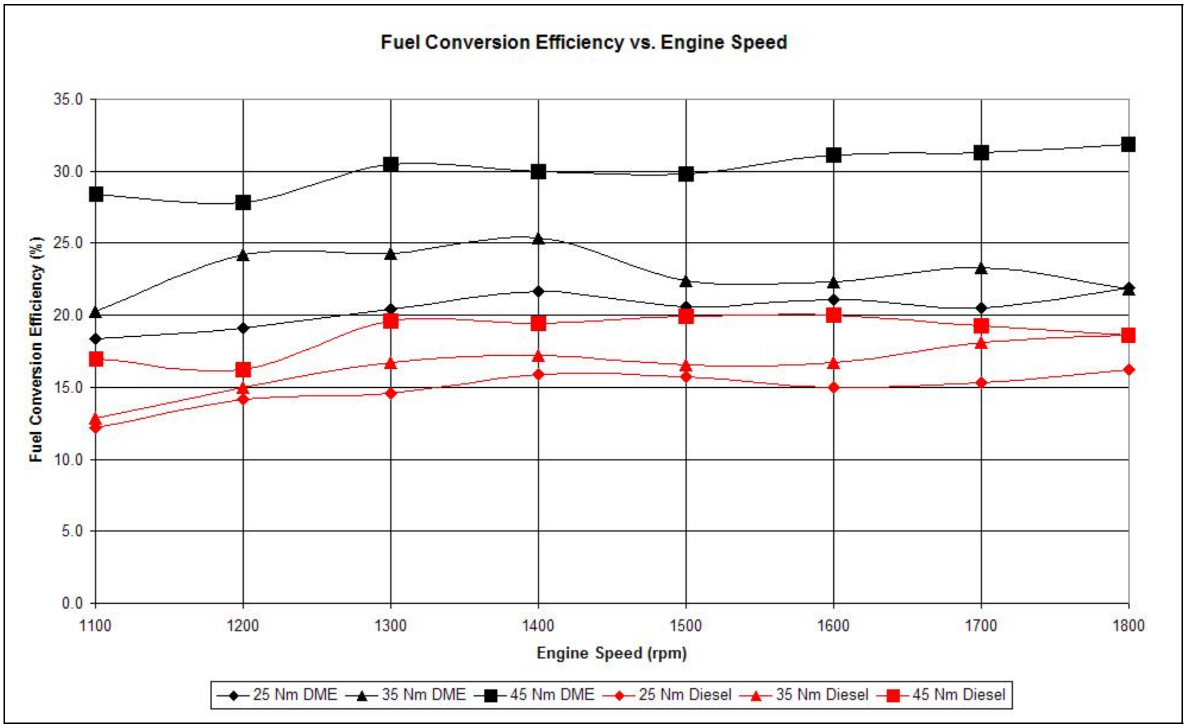

Figure 5.15 – Fuel conversion efficiency vs. engine speed

As can be seen from Figure 5.15 the fuel conversion efficiency of dimethyl ether is constantly higher than that of diesel, due to the higher heat of combustion of diesel of 43.5MJ/kg compared to 28.8MJ/kg of dimethyl ether. The fuel conversion efficiency of both fuels follow similar trends, increasing with load while remaining relatively constant as the engine speed increases.

5.2.6 Ignition Delay

In a compression ignition engine the ignition delay is the time between the injection of the fuel and the beginning of combustion and flame propagation.

Engine performance and efficiency rely on ignition delay, with respect to injection timing, to ensure that the in-cylinder pressure and temperature characteristics are optimal for effective combustion. The fuel system is therefore designed to ensure injection takes place to allow for optimal ignition timing with regard to in-cylinder pressure and temperature characteristics and engine heat release characteristics, taking ignition delay into consideration.

Ignition delay is dependent on the following engine characteristics and operating parameters [15]:

- Fuel properties, i.e. ignition quality and autoignition properties, primarily related to cetane number. Ignition delay is inversely proportional to the cetane number of the fuel being used, with a shorter ignition delay being a characteristic of a fuel with a higher cetane number.

- Injection timing with respect to top dead centre, which is dependent on fuel system design. Injection both further and closer to TDC will cause ignition delay, due to the resulting sub-optimal in cylinder pressure and temperature environment.

- Engine load demands and resulting injection quantity. As the engine load increases, the in-cylinder pressures and temperatures increase, resulting in improved conditions for combustion, and therefore reduced ignition delay.

- Engine speed. As with engine load, in-cylinder pressures and temperatures increase with increased engine speed, resulting in reduced ignition delay.

- Combustion chamber design. Cylinder wall effects and in-cylinder swirl characteristics impact the fuel evaporation and mixing processes, which effect ignition delay.

Investigations have shown that injection pressure, and injector design characteristics such nozzle geometry and type have little effect on ignition delay [15].

Figure 5.16 is a plot of the ignition delay, over the range of engine speeds, when fuelled with both diesel and dimethyl ether.

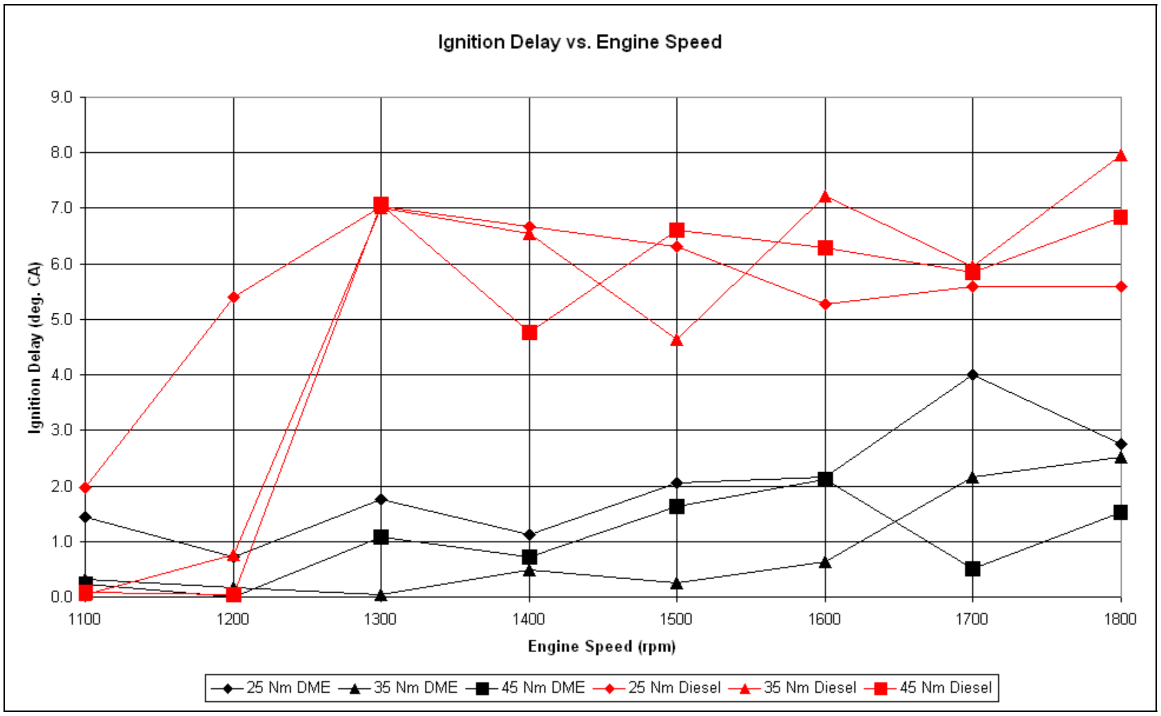

Figure 5.16 – Ignition delay vs. engine speed

The ignition delay experienced when the engine is fuelled with diesel is notably longer than when fuelled with dimethyl ether. When diesel is used ignition delay climbs sharply to approximately 7° at 1300rpm, after which the ignition delay is between 5° to 7° crank angle. When fuelled with dimethyl ether, ignition delay is between 0° and 4° crank angle after injection.

This longer ignition delay experienced when the engine is fuelled with diesel is a result of its lower cetane number – diesel has a cetane number between 38 and 53, while dimethyl ether's cetane number is generally greater than 55.

The ignition delay for a particular engine is dependent on the fuel being tested, and the fuel system itself, and dictates many of the engine's performance, emissions and heat release characteristics. As the fuel system is set up on the test engine, the ignition timing has been optimised for the use of diesel fuel, and is effectively advanced when fuelled with dimethyl ether.

The sharp increase in ignition delay between 1200rpm and 1300rpm when the engine is fuelled with diesel can be attributed the variations in both fuel injection pressure and timing set points with respect to engine speed. Due to the physical properties of dimethyl ether, it is not sensitive to these injection parameters under the test conditions. There is therefore no sharp increase when the engine is fuelled with dimethyl ether, with ignition delay increasing constantly as engine speed increases

5.2.7 Maximum Cylinder Pressure and Temperature

Analysis of an engine's in-cylinder pressure and temperature gives a valuable insight into its operating characteristics. These include peak pressure position, energy release, volumetric and thermal efficiencies, fraction of fuel burnt and combustion chamber gas temperature, as well as the work done.

Figure 5.17 is the plot of maximum cylinder pressure over the range of engine speeds, when fuelled with both diesel and dimethyl ether.

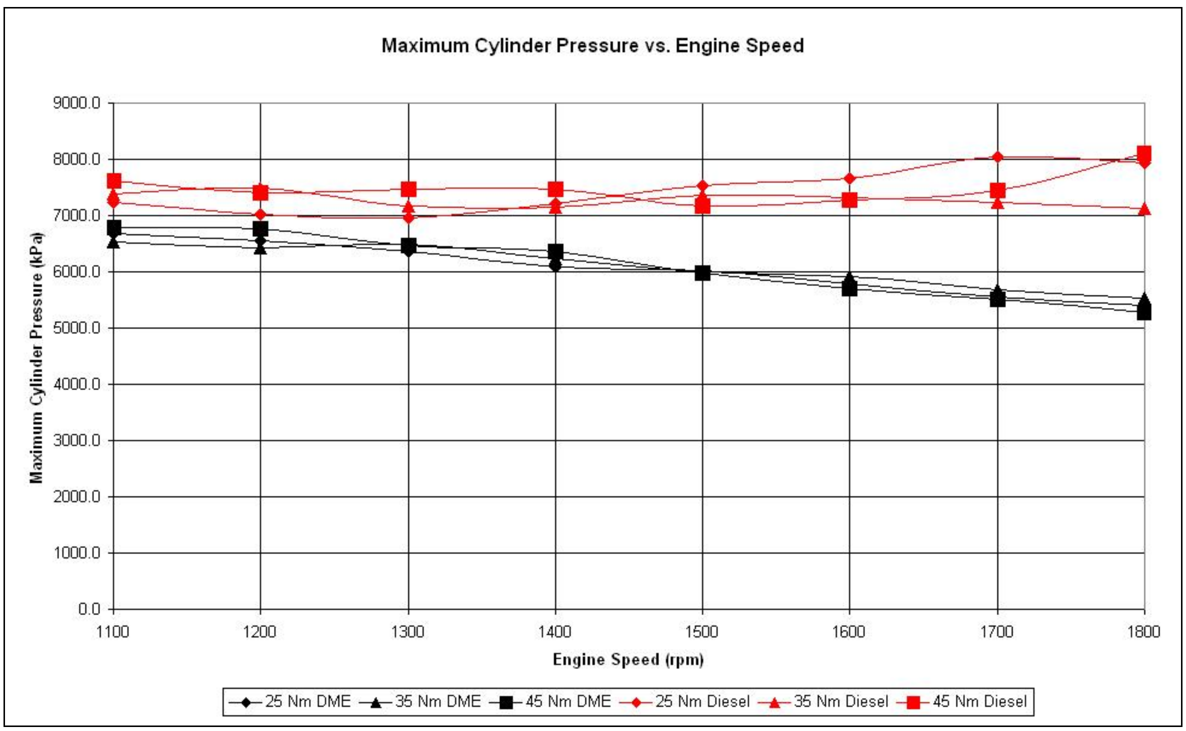

Figure 5.17 – Maximum cylinder pressure vs. engine speed

As can be seen from Figure 5.17, the maximum cylinder pressure when the engine is fuelled with diesel is consistently higher than when fuelled with dimethyl ether, and both vary little with variations in engine load. This can be attributed to dimethyl ether's lower heat of combustion value of 28.8MJ/kg, compared to that of diesel of 43.5MJ/kg. As the engine speed increases, the maximum cylinder pressure when fuelled by dimethyl ether decreases constantly, to such an extent that the maximum cylinder pressure at 1800rpm is approximately 26% less than that at 1100rpm. In contrast, when fuelled with diesel the maximum cylinder pressure remains relatively constant.

Figure 5.18 is a plot of maximum cylinder temperature over the range of engine speeds, when fuelled with both diesel and dimethyl ether.

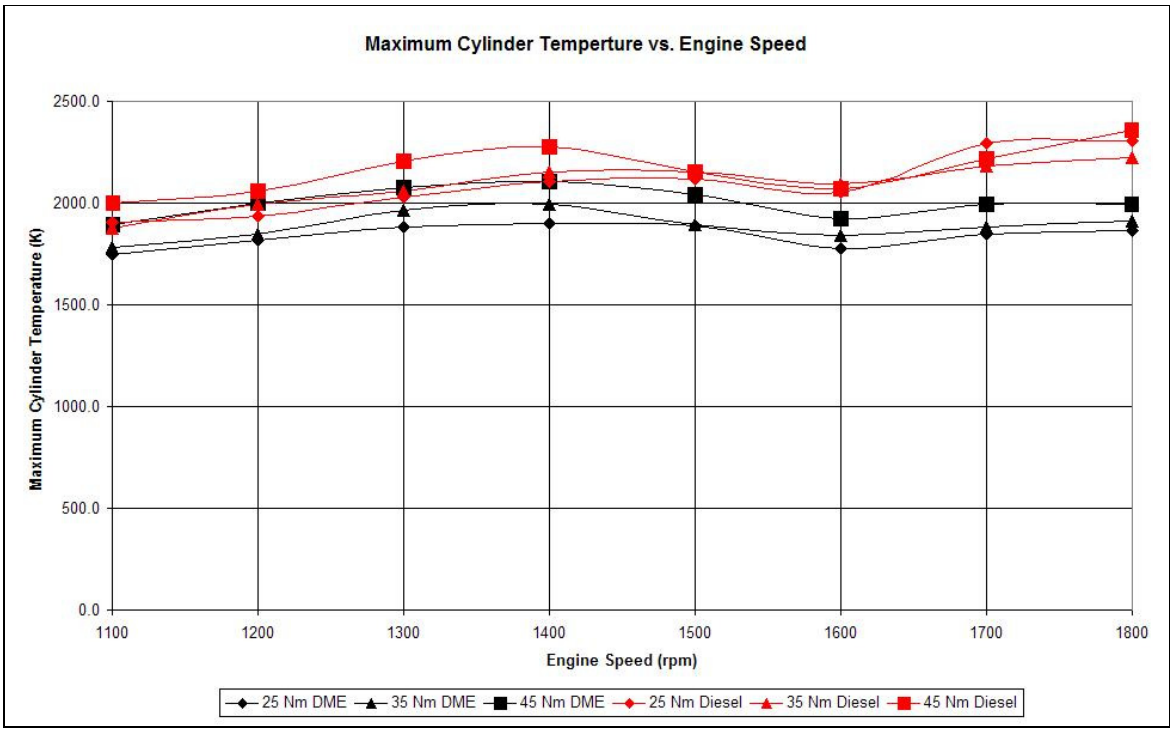

Figure 5.18 – Maximum cylinder temperature vs. engine speed

As expected due to the relationship between temperature and pressure, the plot of maximum cylinder temperature in Figure 5.18 follows the same trend as the maximum cylinder pressure, with the maximum cylinder temperature being consistently higher when the engine is fuelled with diesel, and increasing with both engine speed and engine load for both fuels.

5.3 Emissions Analysis

The combustion of diesel fuel in a compression ignition engine produces the following emissions, amongst others:

~ Oxides of Nitrogen (NO_x)

~ Carbon Monoxide (CO)

~ Carbon Dioxide (CO_2)

~ Total Unburned Hydrocarbons (THC)

The emissions testing was carried out concurrently with the engine performance tests as outlined in Section 4, with exhaust gases being diverted to the emissions analyser.

In analysing the emissions characteristics of the test engine when fuelled with diesel and dimethyl ether, particular attention was paid to the emissions of oxides of nitrogen. The emissions of carbon dioxide, carbon monoxide and unburned hydrocarbons were reviewed, and a summary of trends presented below.

5.3.1 Emissions of Oxides of Nitrogen (NO_x)

Of particular interest in this investigation are the emissions of nitric oxide (NO) and nitrogen dioxide (NO_2), collectively referred to as oxides of nitrogen (NO_x). The processes responsible for the production of these emissions are highly inter-related, and the proportions of each depend on the in-cylinder combustion conditions.

In both spark and compression ignition engines, the oxides of nitrogen are not a direct product of the combustion process, but products of a number of reactions that take place in the flame front, and postflame gases immediately behind the flame front during the combustion process. In compression ignition engines, NO_2

generally makes up between 10% and 30% of emissions of oxides of nitrogen [15].

Nitric oxide emissions are largely the result of the oxidation of atmospheric nitrogen (and to a lesser extent nitrogen in the fuel), and can be represented by a series of chemical processes known as the Zeldovich mechanism, as follows [15]:

$$O + N_2 = NO + N$$

$$N + O_2 = NO + O$$

$$N + OH = NO + H$$

These reactions occur predominantly in the high temperature burned postflame gases, and to a lesser extent in the flame front itself, with the third reaction above being more prevalent in rich fuel/air mixtures where the required OH is available [15].

These reactions are highly temperature dependent, with high temperatures and high oxygen concentrations resulting in increased NO formation rates.

The formation of NO_2 is a result of two interacting reactions that take place in the flame front and postflame gases:

$$NO + HO_2 \rightarrow NO_2 + OH$$

The NO_2 is subsequently converted back to NO by means of the following reaction:

$$NO_2 + O \rightarrow NO + O_2$$

unless the NO_2 is quenched by mixing with cooler fluid in the combustion chamber.

The degree to which this quenching takes place is dependent on combustion chamber design and engine operating conditions. Low load and speed conditions allow for more quenching due to lower in-cylinder temperatures, resulting in more NO_2 being produced [15].

Figure 5.19 and Figure 5.20 are plots of the NO_x and specific NO_x emissions respectively versus engine speed, fuelled by both diesel and dimethyl ether. Specific emissions are normalised with respect to brake power for purposes of meaningful comparison.

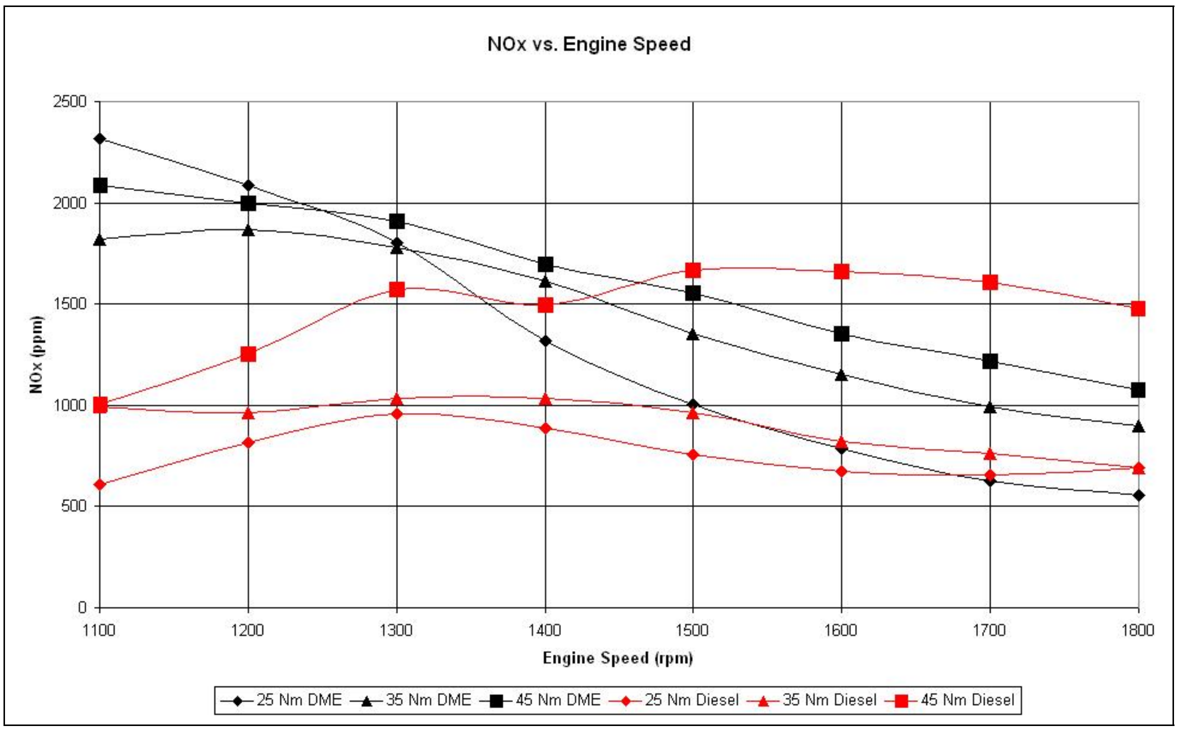

Figure 5.19 – NO_x emissions for diesel and dimethyl ether

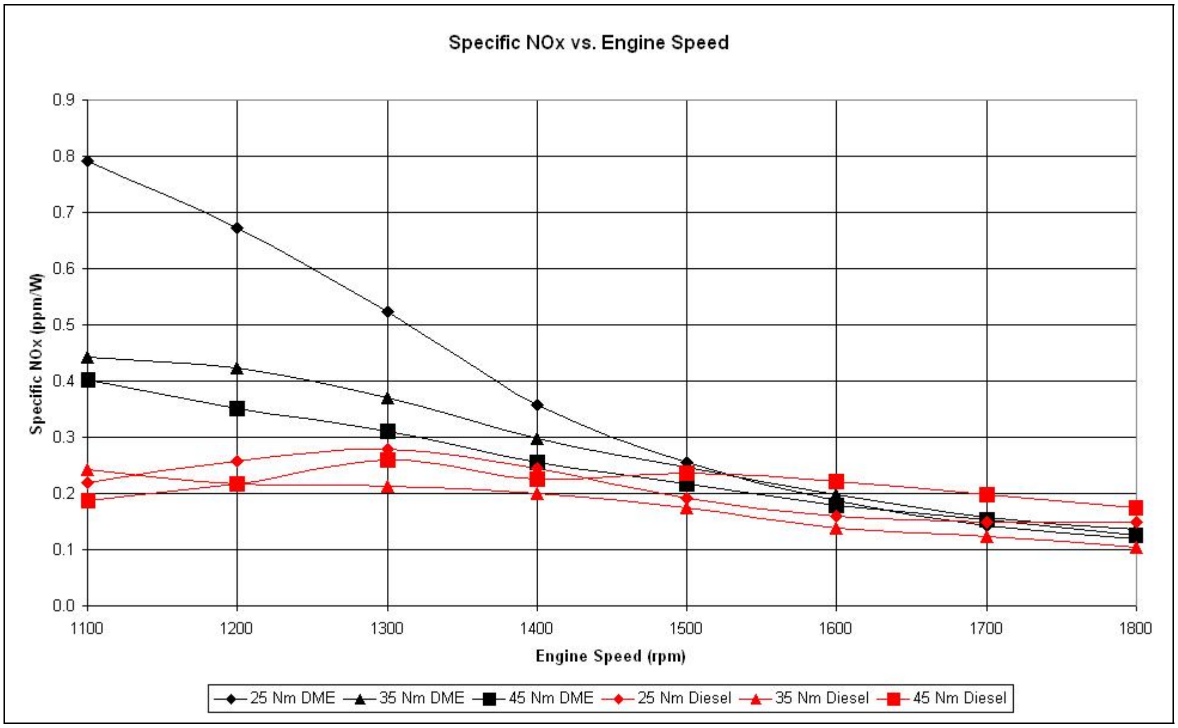

Figure 5.20 – Specific NO_x emissions for diesel and dimethyl ether

Figure 5.19 and Figure 5.20 clearly illustrate that the NO_x emissions at low engine speeds, for dimethyl ether are considerably higher than when fuelled by diesel, especially with respect to brake power. For instance at 1100rpm and 25Nm loading, the NO_x emissions of the dimethyl ether fuelled test are almost 4 times greater than when fuelled by diesel. Also evident is the fact that the NO_x emissions produced by the engine when powered by dimethyl ether decrease as engine speed and load increases. On the other hand, when fuelled by diesel, the specific NO_x emissions stay relatively constant.

The higher NO_x emissions produced with dimethyl ether fuelling can be partially explained by two factors relating to the presence of oxygen for the oxidation of nitrogen. The first is the fact that the engine is being fuelled leaner when fuelled with dimethyl ether than with diesel. The excess air available as a result of this, supplies more reactants for the oxidation of nitrogen required for the production of NO (and subsequently NO_2) as discussed above. However, the equivalence ratio is relatively constant as engine speed and load increases (see Figure 5.13), so this does not explain the reduction in NO_x emissions under these conditions. The second is the presence of oxygen in the chemical composition of the dimethyl ether itself. As with the lower equivalence ratio discussed above, this serves to partially explain the higher NO_x emissions when the engine is fuelled with dimethyl ether, but fails to explain why these emissions reduce as engine speed and load increase.

The reactions responsible for the production of NO_x emissions are highly temperature dependent. Although the maximum cylinder temperature when the engine is fuelled with diesel is consistently higher than when fuelled with dimethyl ether, as engine speed increases the difference becomes greater (see Figure 5.18). This may contribute to the reduction in NO_x production as engine speed and load increase, but contradicts the NO_x emissions from the dimethyl ether fuelled engine being higher than when fuelled with diesel. The higher temperature experienced when diesel is used needs to be considered in conjunction with the higher availability of oxygen when the engine is fuelled with dimethyl ether.

The extended injection duration, greater penetration depth, and wider spray angle characteristics of the dimethyl ether injection, as illustrated and discussed in Section 5.1, offer an explanation to the higher levels of NO_x emissions. When compared to the gradual build-up in penetration and spray angle of the diesel injection, the dimethyl ether injection has minimal ramp up to full strength. The dimethyl ether injection remains at a higher intensity for the duration of the injection, and has a greater penetration depth and spray angle, resulting in a wider dispersion of the air/fuel mixture. The diesel injection builds up uniformly and tapers down in a controlled fashion, covering a smaller area due to its smaller spray angle.

This visual analysis suggests that, when fuelled with dimethyl ether, the reactants have a longer residence time for the creation of NO_x. This is more pronounced under low engine speed and load conditions, when residence time is already extended, resulting in an decrease in NO_x emissions as engine speed and load increase, as can be seen in Figure 5.20.

Another factor that may explain the increased NO_x under low speed and load conditions is the level of swirl. Although particulate and CO emissions decrease with increased swirl due to increased fuel/air mixing rate, NO_x formation increases [15]. The turbulent nature of the dimethyl ether injection has the same effect, in increasing the fuel/air mixing rate, and therefore increasing NO_x emissions. This is more prevalent at low engine speeds and loads where reactant residence times are higher.

5.3.2 Summary of Other Emissions Characteristics

Although not the focus of this investigation, the emission characteristics of carbon dioxide, carbon monoxide and total unburned hydrocarbons were reviewed and are briefly discussed below.

Emissions of Carbon Monoxide (CO)

The engine operating characteristic that affects carbon monoxide (CO) emissions most is the equivalence ratio, with the levels of emissions increasing as the fuel/air mixture becomes richer, and amount of excess fuel increases [15].

Figure 5.21 is a plot of the specific CO emissions, for both diesel and dimethyl ether.

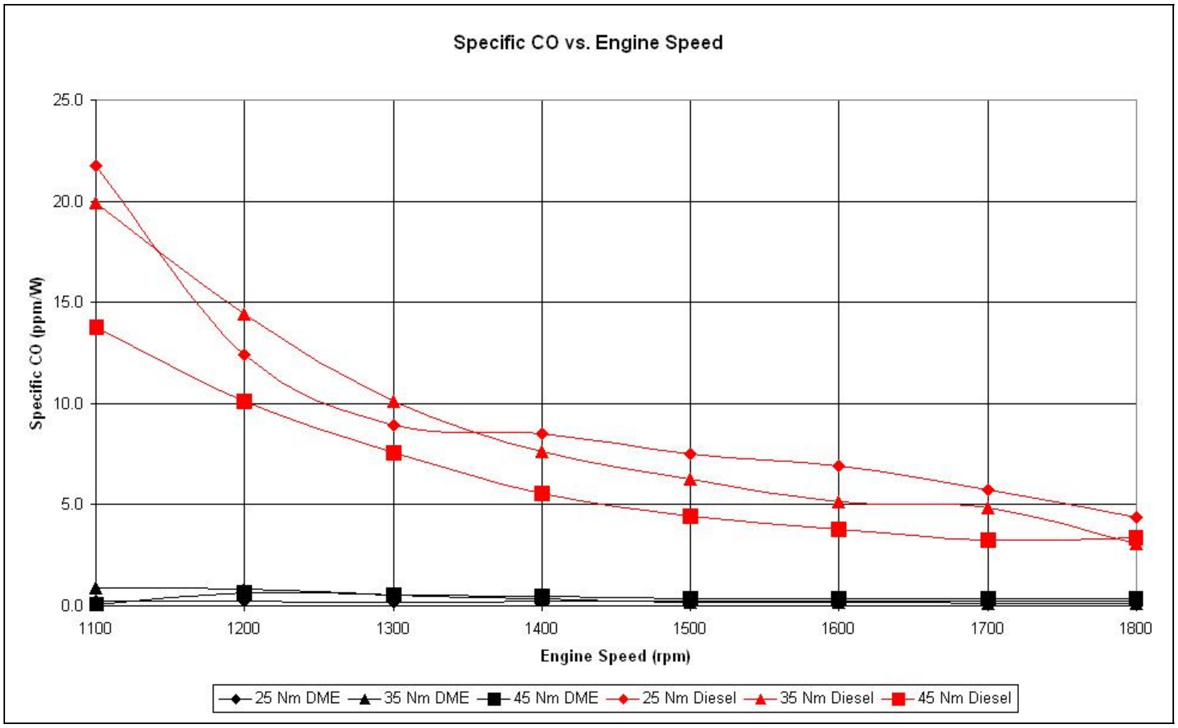

Figure 5.21 – Specific CO emissions for diesel and dimethyl ether

The CO emissions produced by the engine when fuelled by dimethyl ether are significantly lower than when fuelled with diesel, with emissions produced by the diesel tests declining as the engine speed increases.

The fact that the CO emissions produced when the engine is fuelled with diesel are higher than when fuelled with dimethyl ether can to a large extent be explained by the relative equivalence ratios during the two tests. As discussed in Section 5.2, the equivalence ratio experienced when fuelled with dimethyl ether is lower that experienced when fuelled with diesel, which explains the CO emissions being higher when the engine is fuelled with diesel.

Emissions of Carbon Dioxide (CO_2)

Carbon dioxide (CO_2) emissions are produced as a result of the oxidation of CO during the combustion process.

Figure 5.22 is a plot of the specific CO_2 emissions, for both diesel and dimethyl ether.

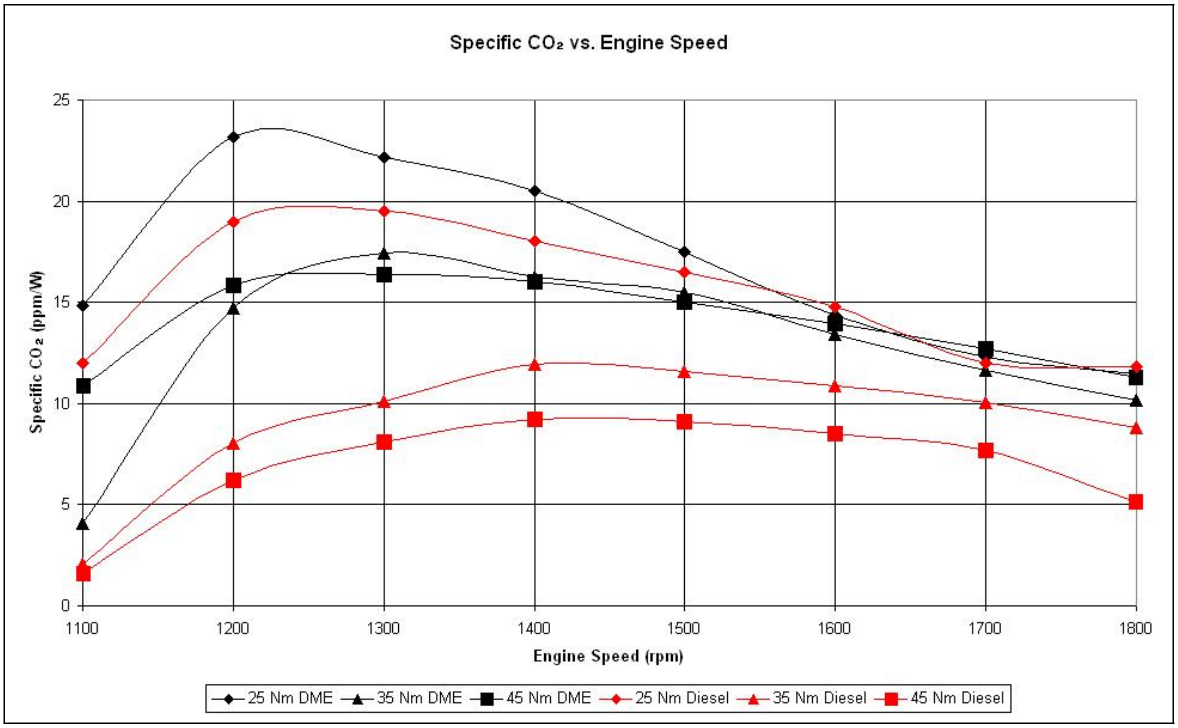

Figure 5.22 – Specific CO_2 emissions for diesel and dimethyl ether

Although CO_2 emission trends are similar for diesel and dimethyl ether, the CO_2 emissions are consistently higher when the engine is fuelled with dimethyl ether.

When fuelled with diesel, the CO_2 emissions decrease as engine load increases. Under 25Nm load conditions the CO_2 emissions peak at approximately 1250rpm, after which they decrease constantly as engine speed increases. At 35Nm and 45Nm engine load, they increase until approximately 1450rpm, and decrease constantly as engine load increases after that.

When fuelled with dimethyl ether, the CO_2 emissions increase until approximately 1250rpm when under 25Nm and 45Nm load conditions, and 1300rpm under 35Nm conditions, after which they decrease constantly as engine speed increases.

Emissions of Total Unburned Hydrocarbon (THC)

Emissions of hydrocarbons are largely the result of incomplete combustion of the fuel/air mixture in the combustion process. In compression ignition engines, this can either be a result of the fuel/air mixture being too lean for auto-ignition, or being too rich to support a flame [15].

Figure 5.23 is a plot of the specific THC emissions, for both diesel and dimethyl ether.

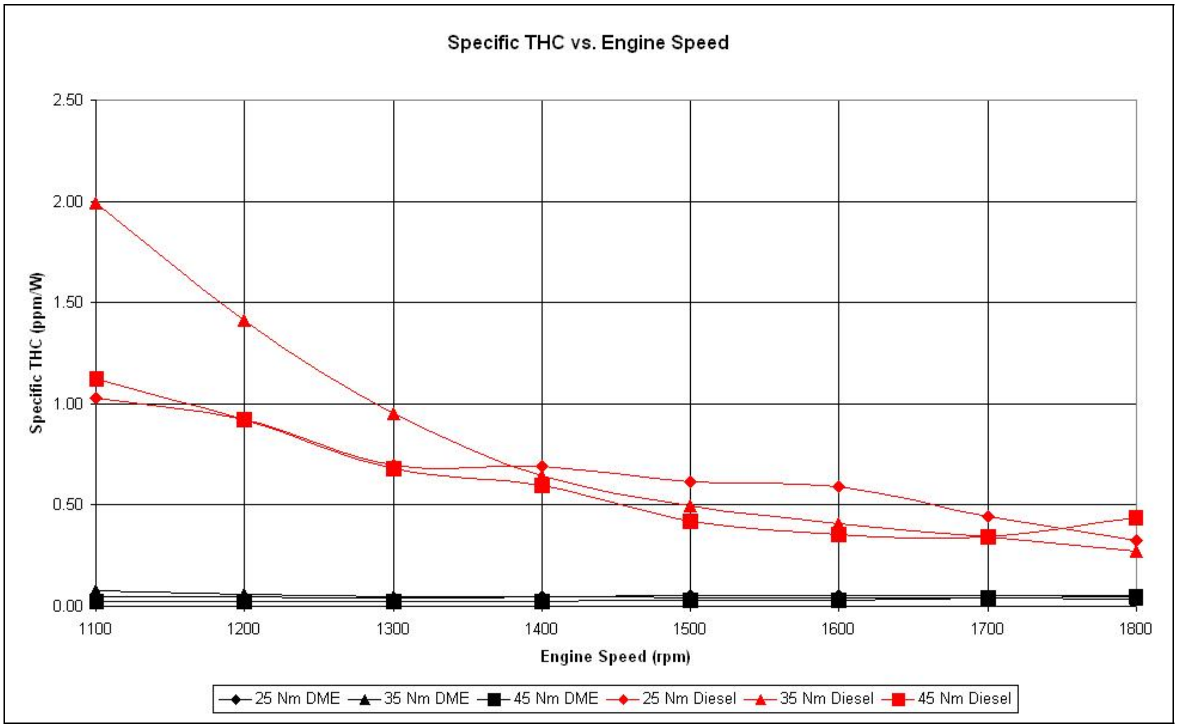

Figure 5.23 – Specific THC emissions for diesel and dimethyl ether

The levels of THC emissions are considerably lower when the engine is fuelled with dimethyl ether than when fuelled with diesel, and are not engine load dependent. The emissions resulting from the diesel tests are greatest at low engine speeds. The lower THC emissions produced when the engine is fuelled with dimethyl ether can be explained by both its chemical properties and injection characteristics. Dimethyl ether has a higher cetane number meaning that it is more susceptible to auto ignition than diesel, which reduces its dependency on fuel/air mixture conditions to achieve complete combustion.

The injection characteristics of dimethyl ether discussed in Section 5.1, such as larger spray angle and penetration depth, which result in higher degree of atomisation of the fuel, also produce combustion conditions less prone to incomplete combustion. This is supported by the higher fuel conversion efficiency of dimethyl ether compared to diesel as discussed in Section 5.2, with the dimethyl ether tests having a higher fuel conversion efficiency than diesel.

6 CONCLUSIONS

The injection characteristics of a compression ignition engine were analysed when fuelled with both diesel and dimethyl ether fuel. This analysis comprised a visual analysis, making use of high speed digital Schlieren videography, and an analysis of engine testing results from a performance and emissions perspective.

The results of the visual analysis proved to be highly repeatable, and clearly illustrated the differences in injection characteristics of diesel and dimethyl ether:

- pre-injection fuel leakage occurs when injecting dimethyl ether,
- the injection of diesel is uniform and ordered, whilst that of dimethyl ether is turbulent and of a higher intensity, with a higher level of atomisation,
- the spray angle resulting from the dimethyl ether injection is approximately double that of diesel – this correlates to theoretical analysis,
- the penetration depth of dimethyl ether is significantly longer than that of diesel – this correlates to theoretical analysis,
- the penetration speed of dimethyl ether is significantly faster than diesel,
- the injection duration of dimethyl ether is approximately 40% longer than that of diesel.

The engine testing results were analysed with respect to performance characteristics and emissions. The results of the performance data revealed the following characteristics:

- the main performance characteristics of the engine such as power, mean effective pressure and mechanical efficiency are comparable for the diesel and dimethyl ether tests,

- the equivalence ratio data illustrated the fact that the engine runs significantly leaner with dimethyl ether than diesel,

- the ignition delay is longer when the engine is fuelled with diesel than when fuelled with dimethyl ether,

- the maximum cylinder pressure and temperatures experienced in the engine were consistently higher when the engine was fuelled with diesel.

The emissions analysis was carried out in terms of emission concentrations, and specific emissions – emissions concentration/brake power - which allowed for direct comparisons to be made between the emissions produced when the engine was fuelled with diesel and dimethyl ether. Analysis of the emissions data revealed that:

- the NO_x emissions produced when the engine is fuelled with dimethyl ether are higher than when fuelled with diesel, especially at low engine speeds and engine load,

- the CO emissions produced when the engine is fuelled with dimethyl ether are substantially lower than when fuelled with diesel, with the emissions decreasing with engine speed when fuelled with diesel,

- the CO_2 emissions produced when the engine is fuelled with dimethyl ether are higher than when fuelled with diesel,

- the THC emissions produced when the engine is fuelled with dimethyl ether are substantially lower than when fuelled with diesel, with the emissions decreasing with engine speed when fuelled with diesel.

These differences between the test results when testing diesel and dimethyl ether can be attributed to the variations in physical and chemical properties of the two fuels, the physical geometry of the injection system itself, and the combustion environment that is created due to these variations

7 RECOMMENDATIONS

Although the techniques employed in the visual analysis allowed for a valuable analysis of the injection characteristics of diesel and dimethyl ether, certain limitations were imposed by the experimental set-up due to technical, financial and time constraints, and the scope of the project itself. A more realistic simulation of the in-cylinder conditions would be created by:

- pressurising the visualisation chamber,
- incorporating a cylindrical combustion chamber,
- inducing swirl into the chamber,
- introducing piston movement and change in combustion chamber volume,
- replacing the hand pump with reliable mechanised unit.

APPENDIX A

VISUALISATION CHAMBER DESIGN

A VISUALISATION CHAMBER DESIGN

The primary aim in the design of the injector visualisation chamber was to facilitate a well simulated and meaningful visual analysis of the injector behaviour, given the scope of the project, the financial limitations, and the technical restrictions dictated by the choice of Schlieren photography as a means of analysis.

Two visualisation chamber designs were considered – pressurised and non-pressurised.

A1 Pressurised Visualisation Chamber

To facilitate a thorough and meaningful analysis of the injector behaviour and jet characteristics, a 200mm x 200mm x 200mm pressure vessel was designed.

As discussed in Chapter 3, the use of Schlieren photography dictates that the visualisation chamber must have two parallel sides, of very high quality glass (BK70). The reason for this is that Schlieren photography relies on the deviation of light, and hence the light passing through the object plane needs to be parallel to allow for analysis of the deviations through the area under analysis.

High quality glass, with no inclusions or internal or surface irregularities, is necessary because these inclusions and irregularities would cause light deviation which would be magnified on the resulting Schlieren image.

The pressurised visualisation chamber was designed to withstand a pressure of 2.5MPa, in order to simulate the pressure characteristics in the cylinder at the point of injection.

The pressurised visualisation chamber is a simple cube design, gusseted for the extra strength required to withstand the internal pressure. This design is illustrated in Figure A1 and Figure A2, and the subsequent finite element analysis in Figure A3 to Figure A7.

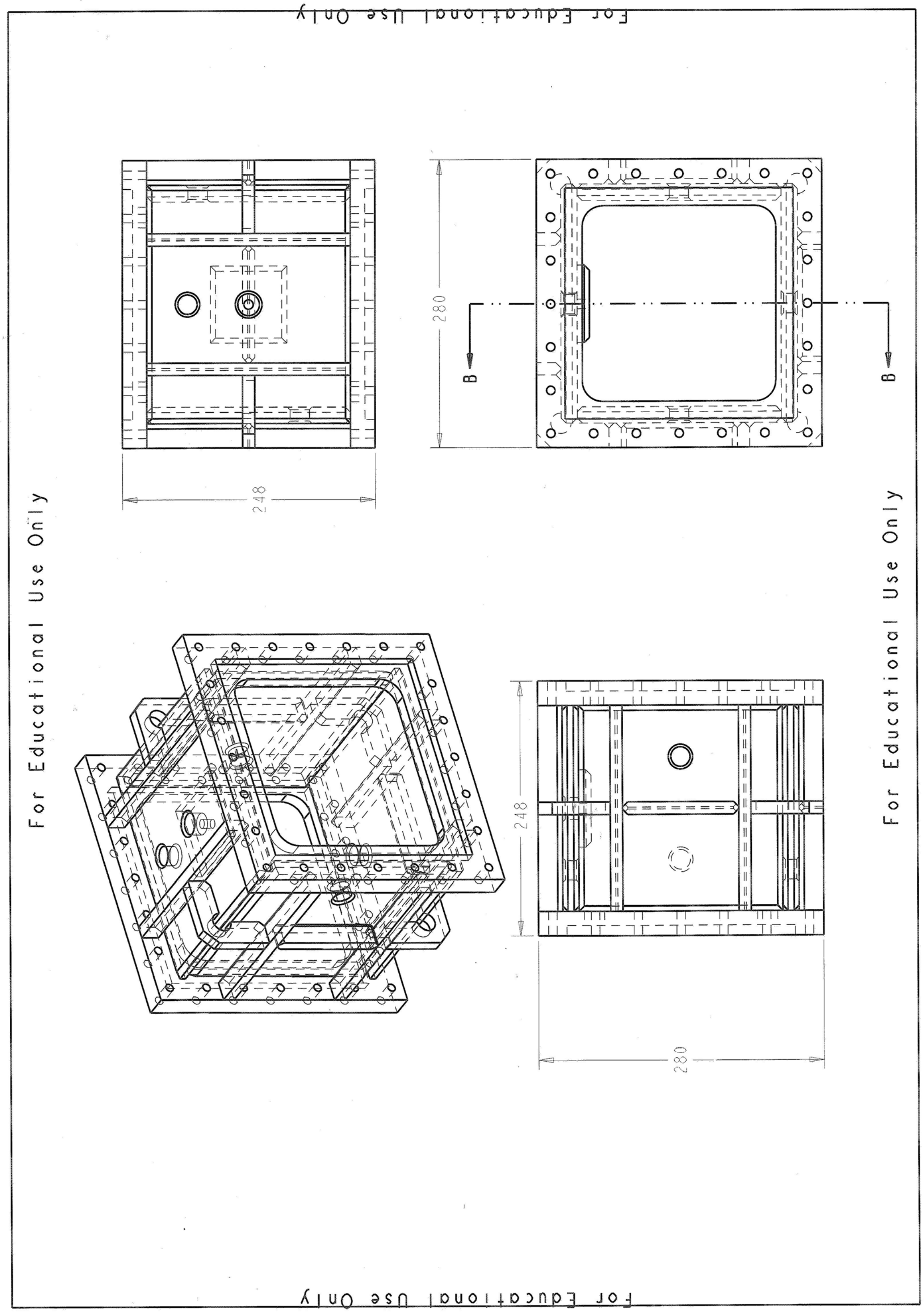

Figure A1 – Pressurised visualisation chamber, Drawing 1

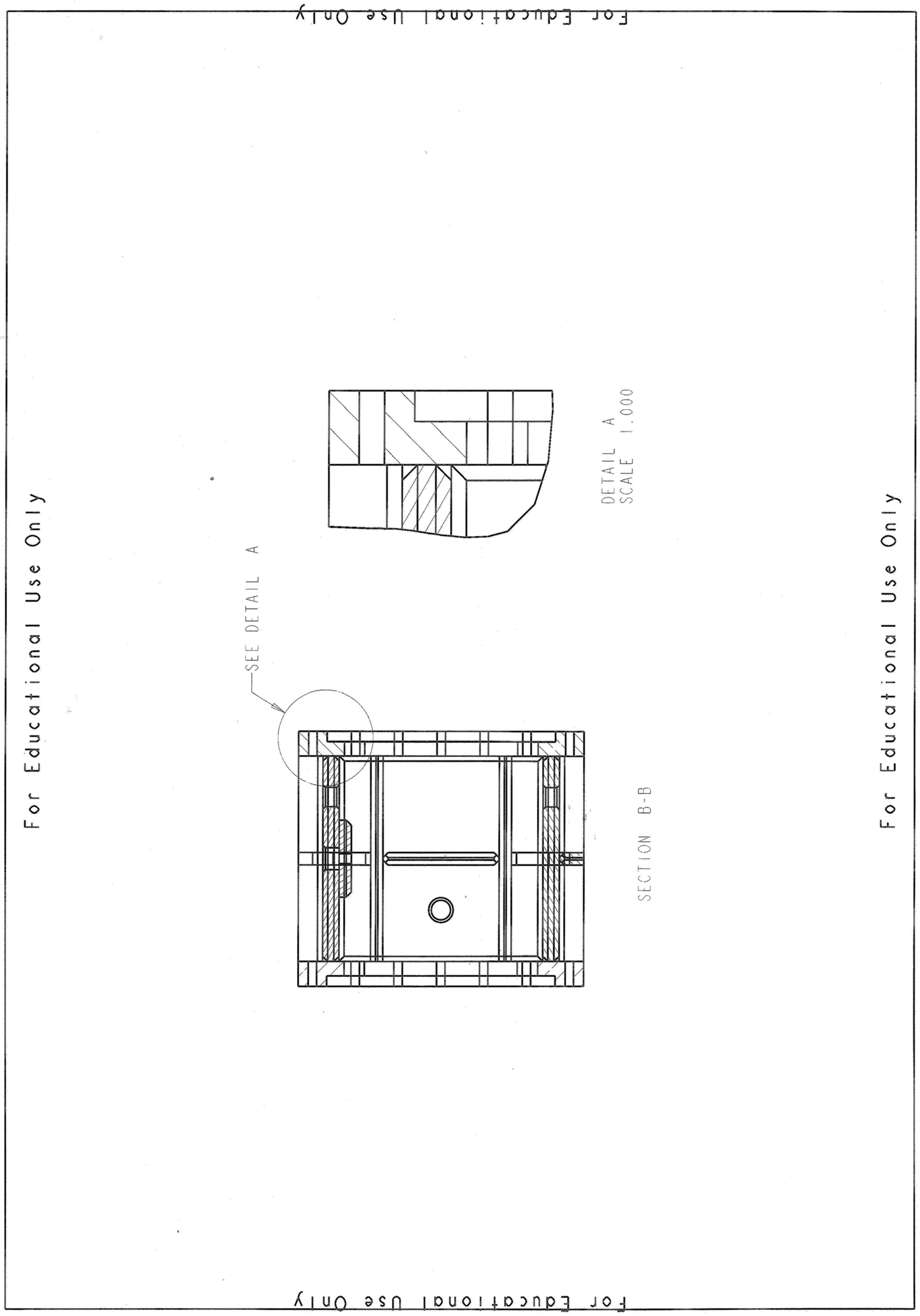

Figure A2 – Pressurised visualisation chamber, Drawing 2

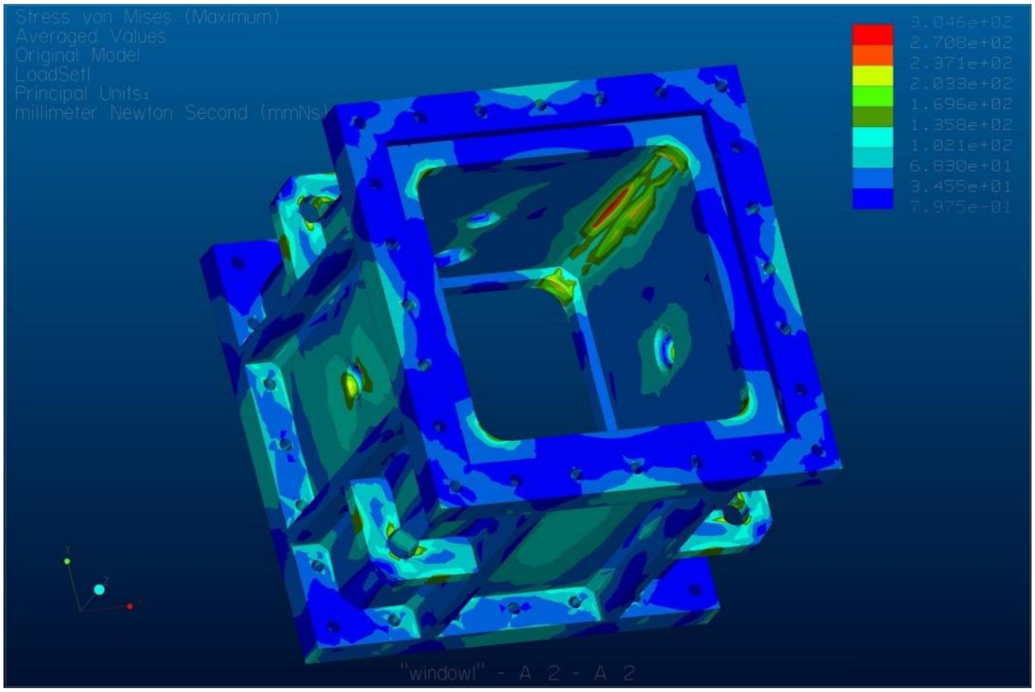

Figure A3 – Pressurised visualisation chamber, FEA 1

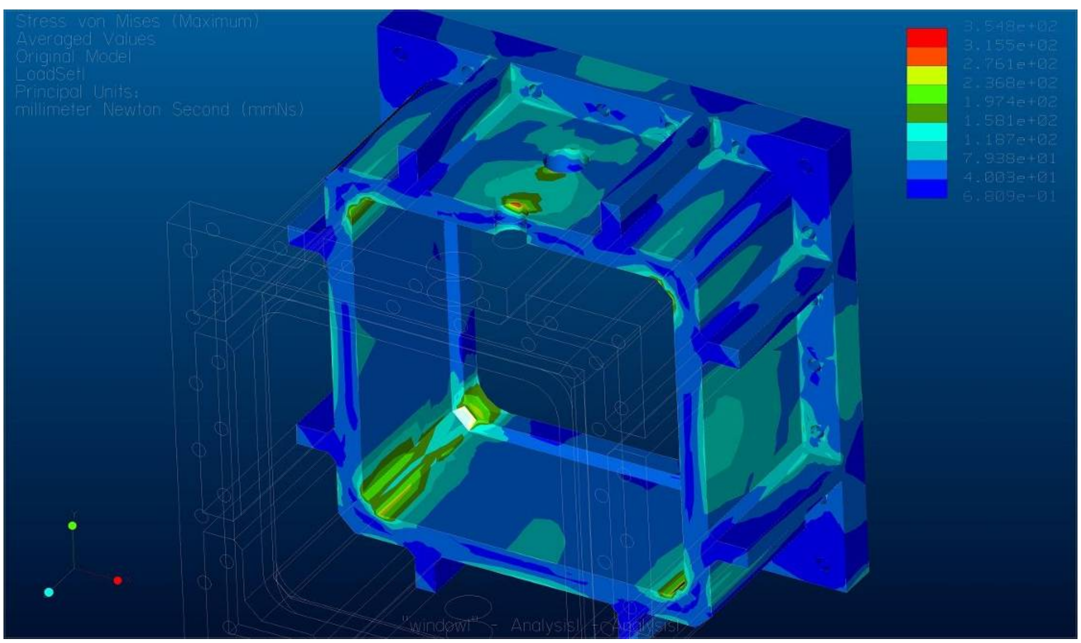

Figure A4 – Pressurised visualisation chamber, FEA 2

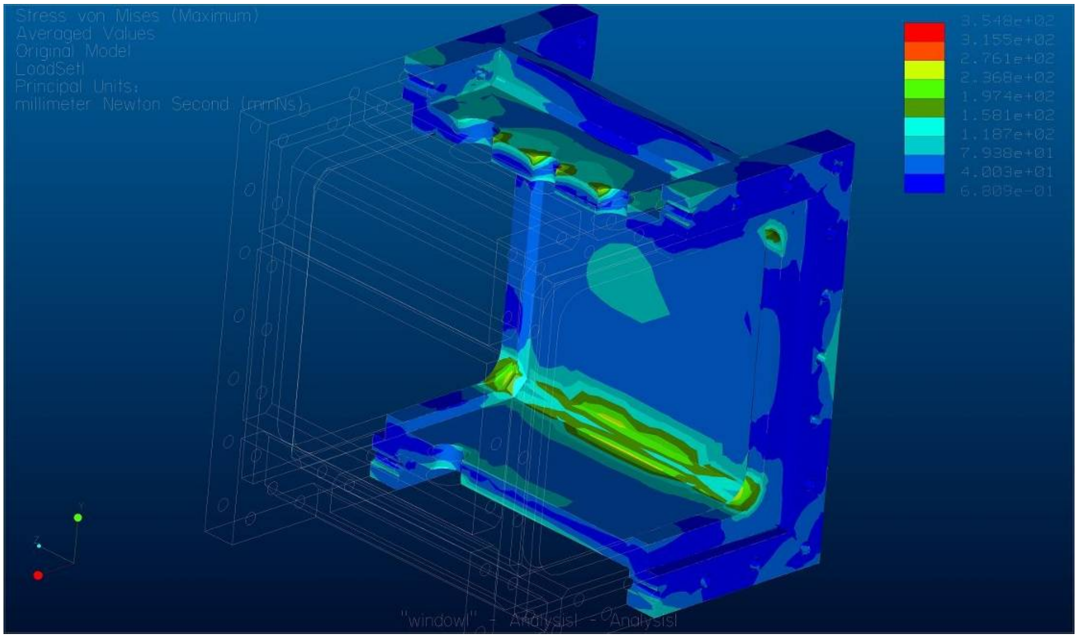

Figure A5 – Pressurised visualisation chamber, FEA 3

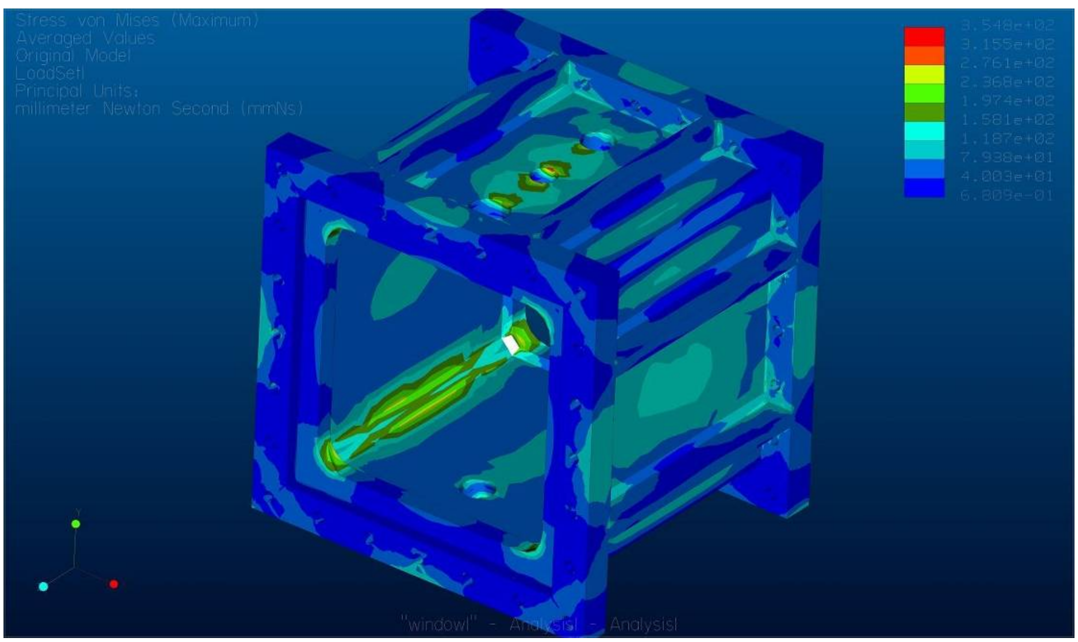

Figure A6 – Pressurised visualisation chamber, FEA 4

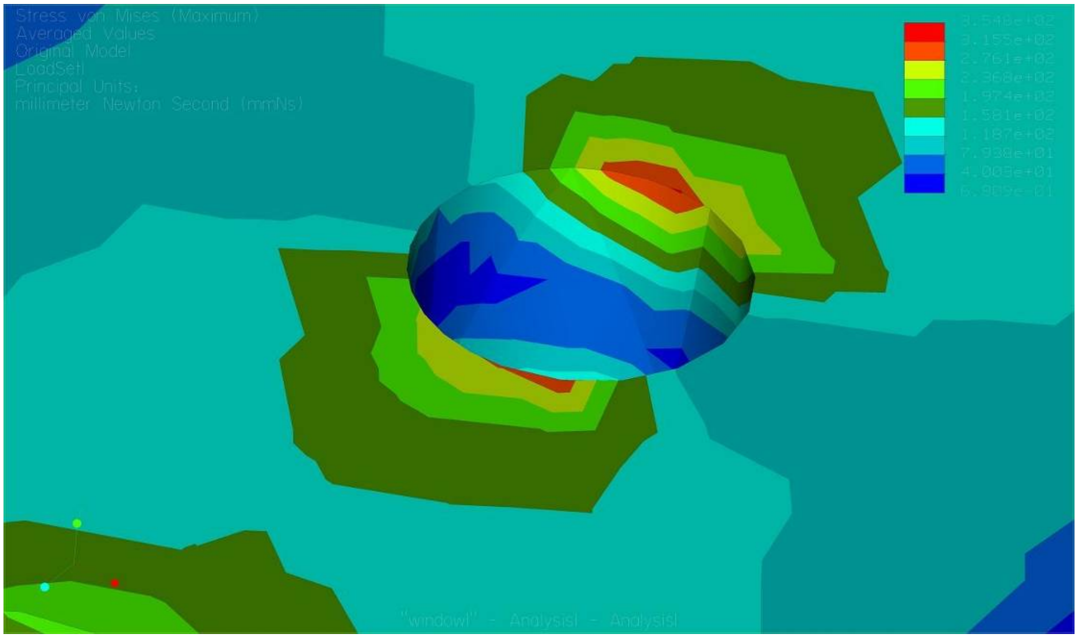

Figure A7 – Pressurised visualisation chamber, FEA 5

A2 Non-pressurised Visualisation Chamber

The principle behind the non-pressurised visualisation chamber is simply to facilitate effective and repeatable visualisation of the injected diesel and dimethyl ether. As in the case of the pressurised visualisation chamber design above, the use of Schlieren photography as a visualisation technique required parallel windows, and hence the square as opposed to circular shape. Due to the fact that the chamber was not going to be pressurised, no stress analysis was required. The lack of internal pressure also meant that a thinner glass thickness could be used, although it was still required to be of a very high quality to eliminate the amplification of impurities in the resulting images. The chamber design consisted of a 120mm x 90mm x 90mm structure, with two sides of 5mm thick BK70 quality glass. The injector was mounted to the top plate and there was a fluid drain in the bottom plate. The manufacturing drawings are shown in Figure A3.1 to Figure A3.9.

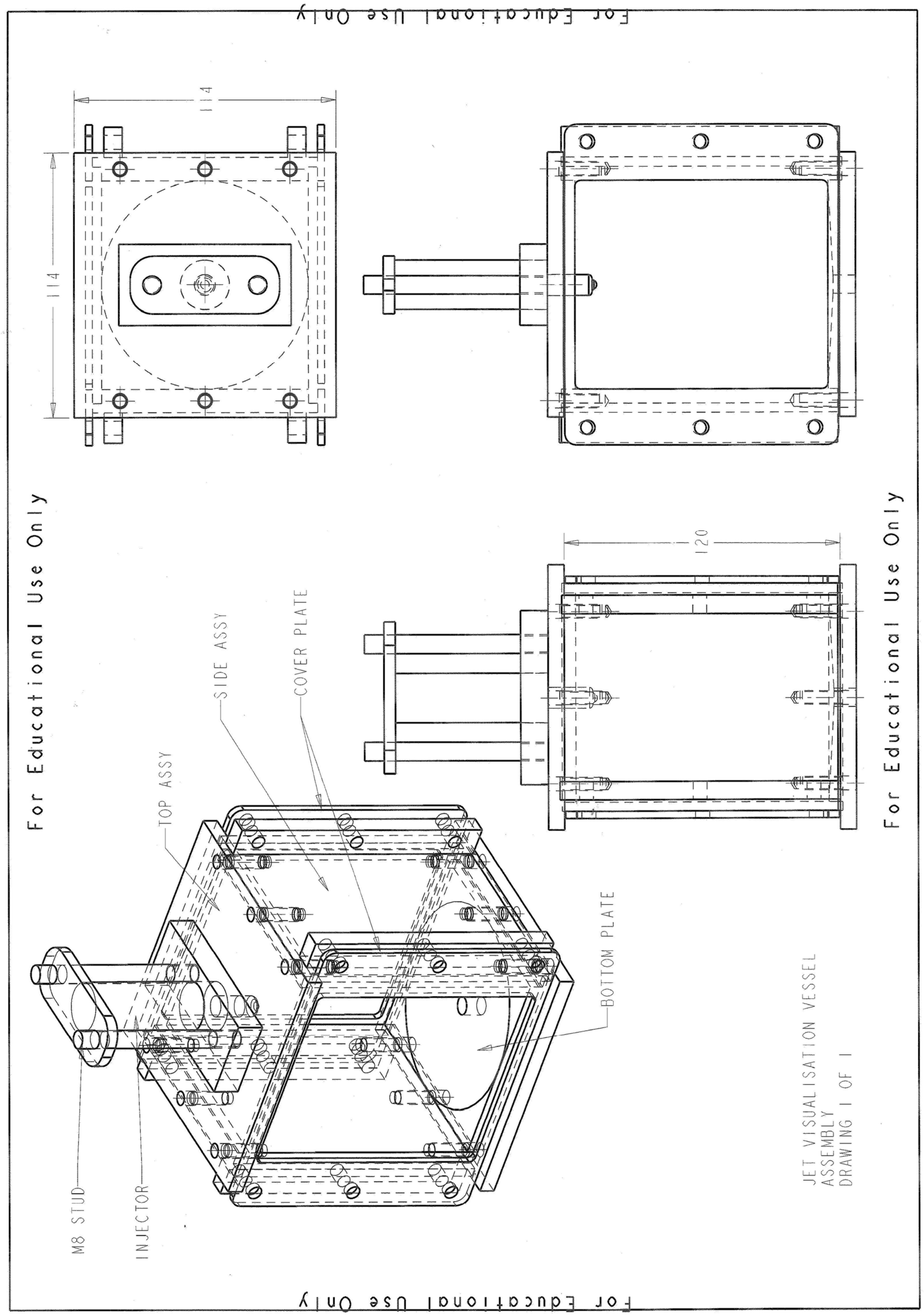

Figure A8 – Non-pressurised visualisation chamber, Drawing 1

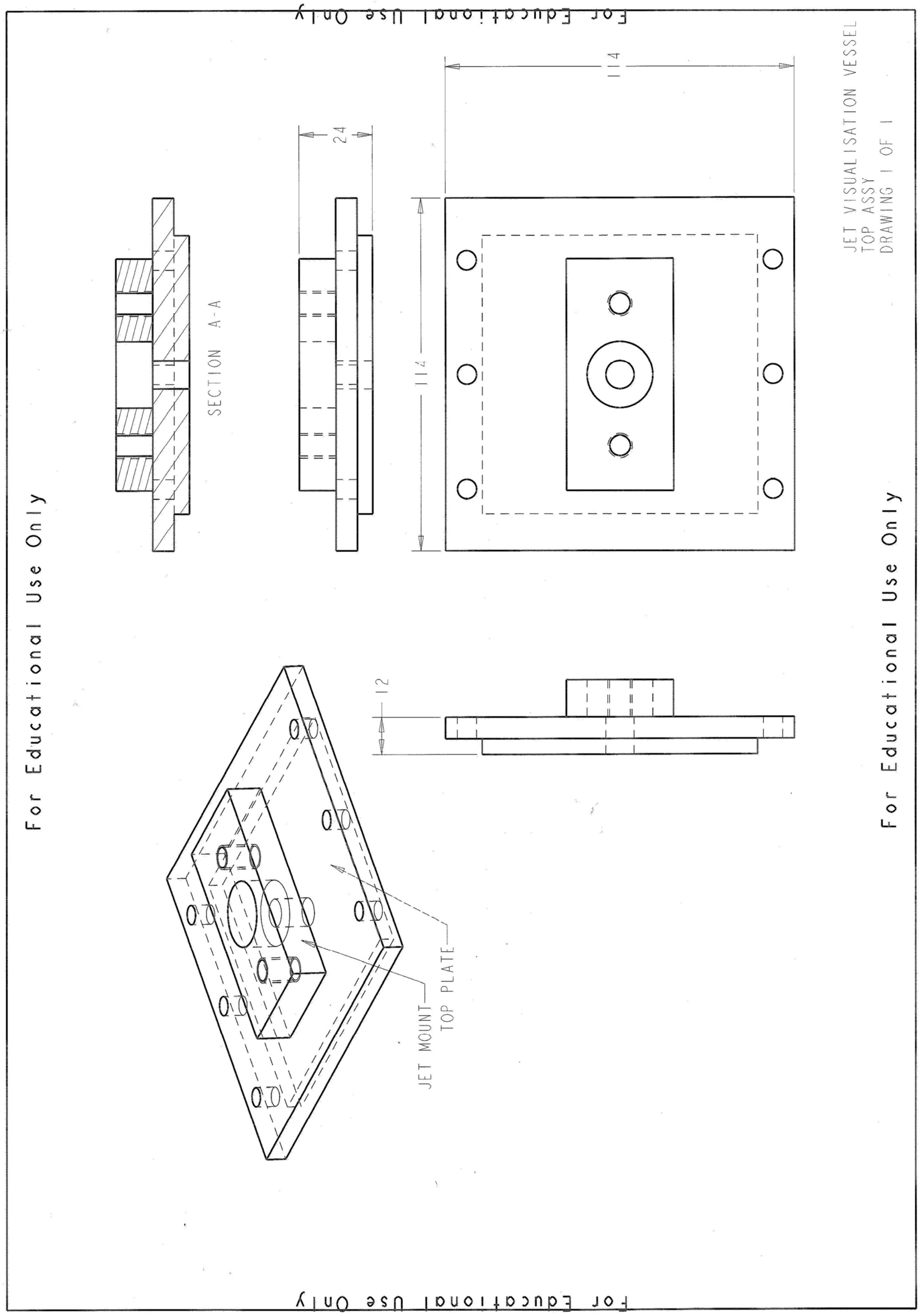

Figure A9 - Non-pressurised visualisation chamber, Drawing 2

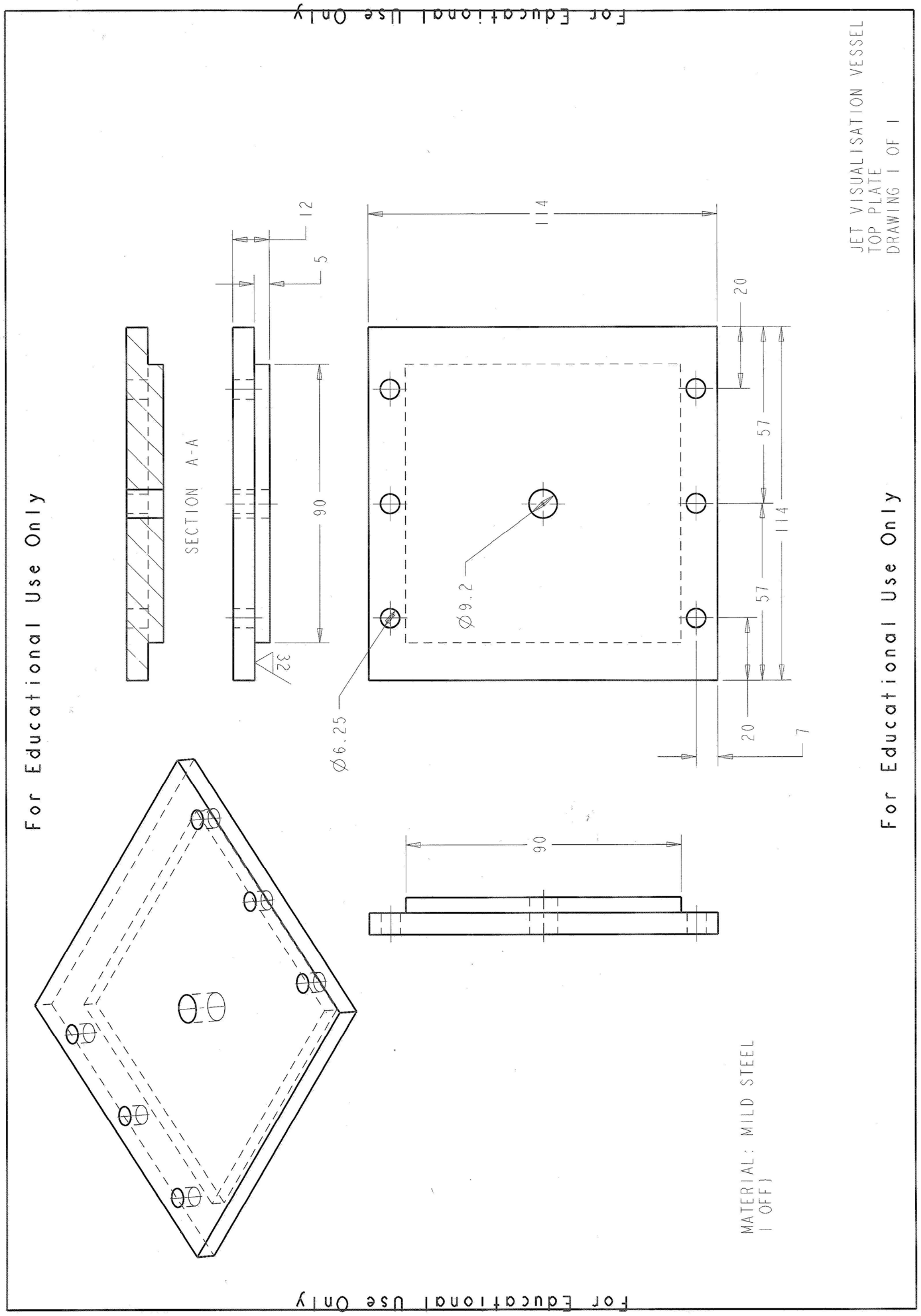

Figure A10 - Non-pressurised visualisation chamber, Drawing 3

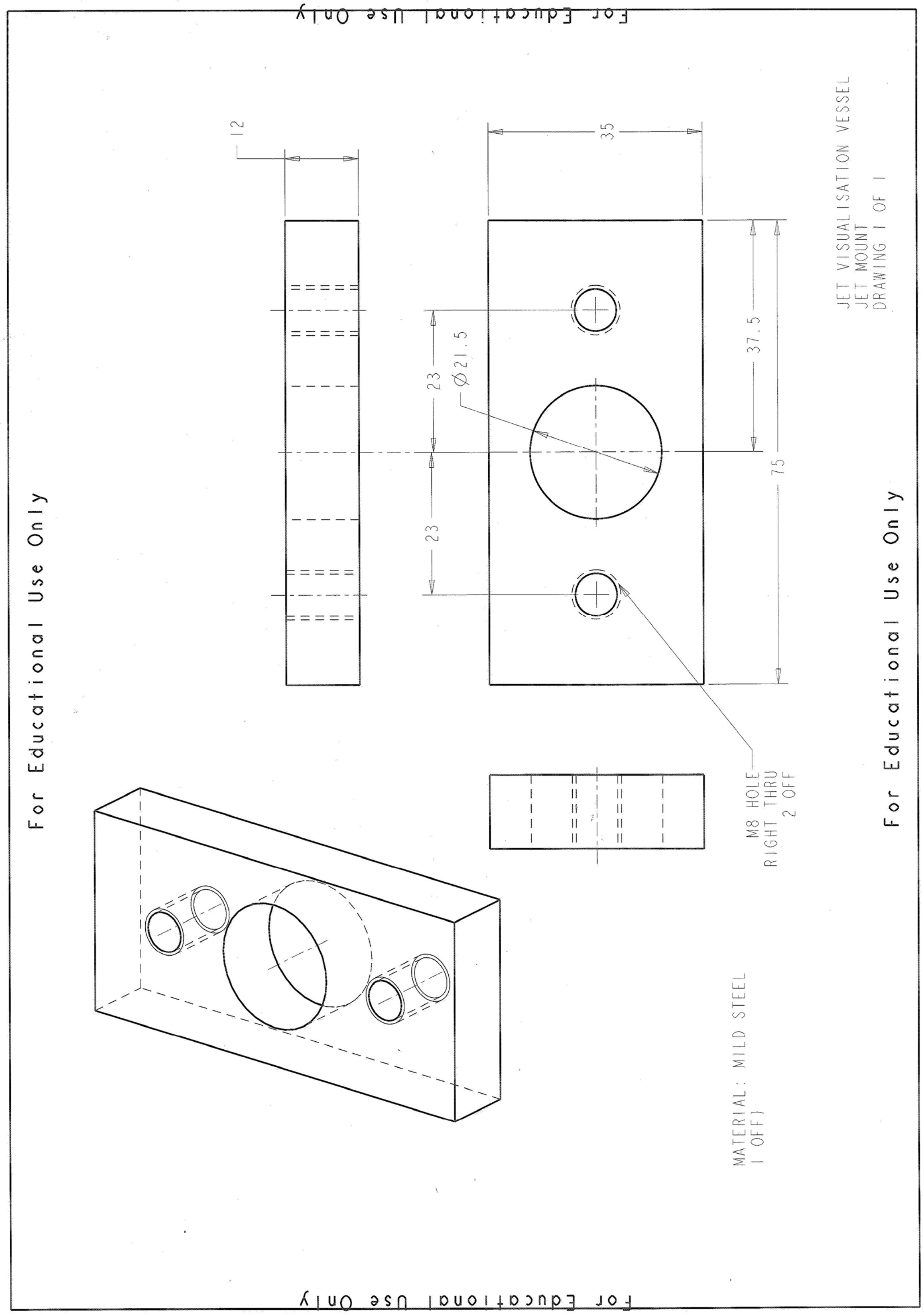

Figure A11 - Non-pressurised visualisation chamber, Drawing 4

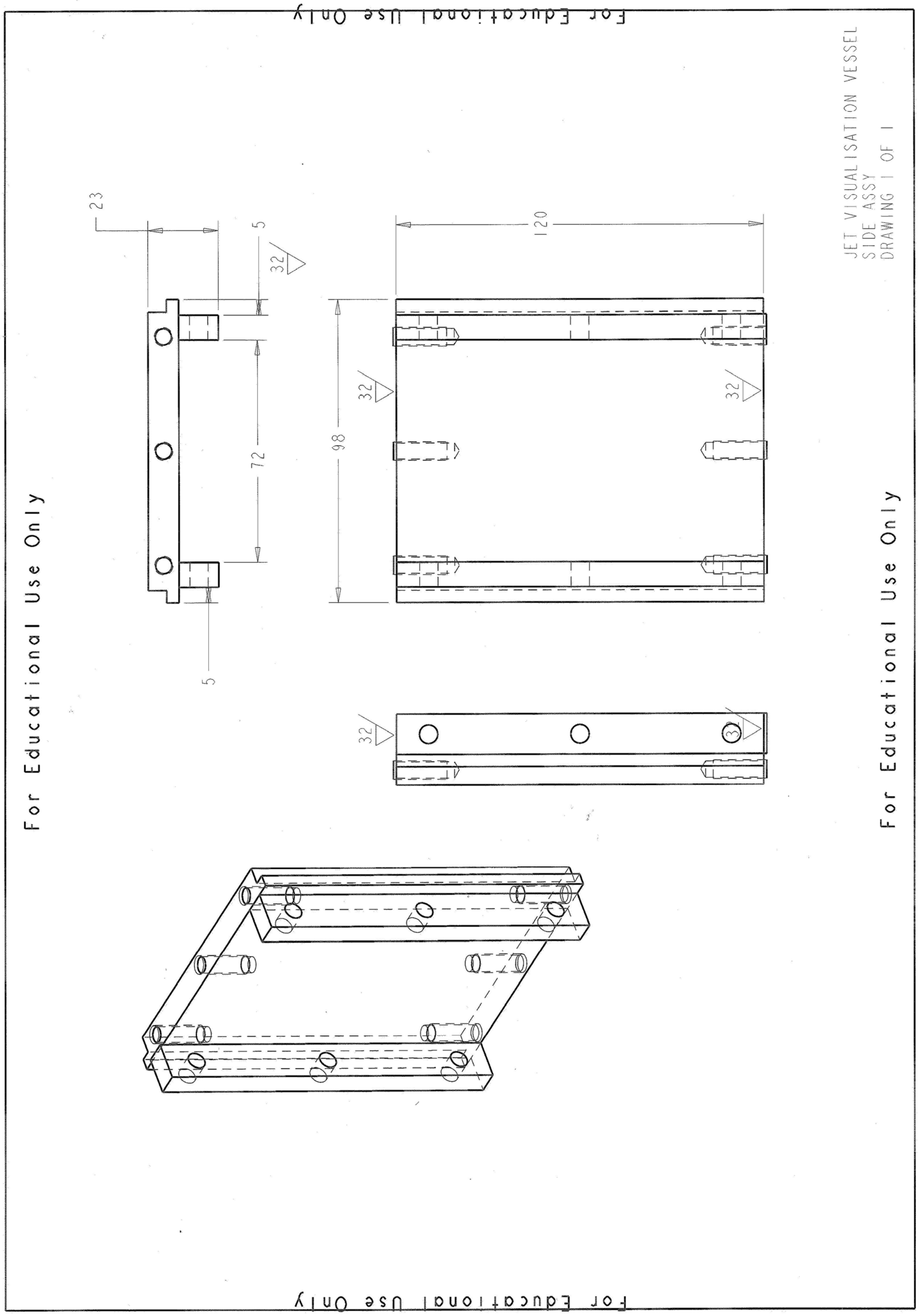

Figure A12 - Non-pressurised visualisation chamber, Drawing 5

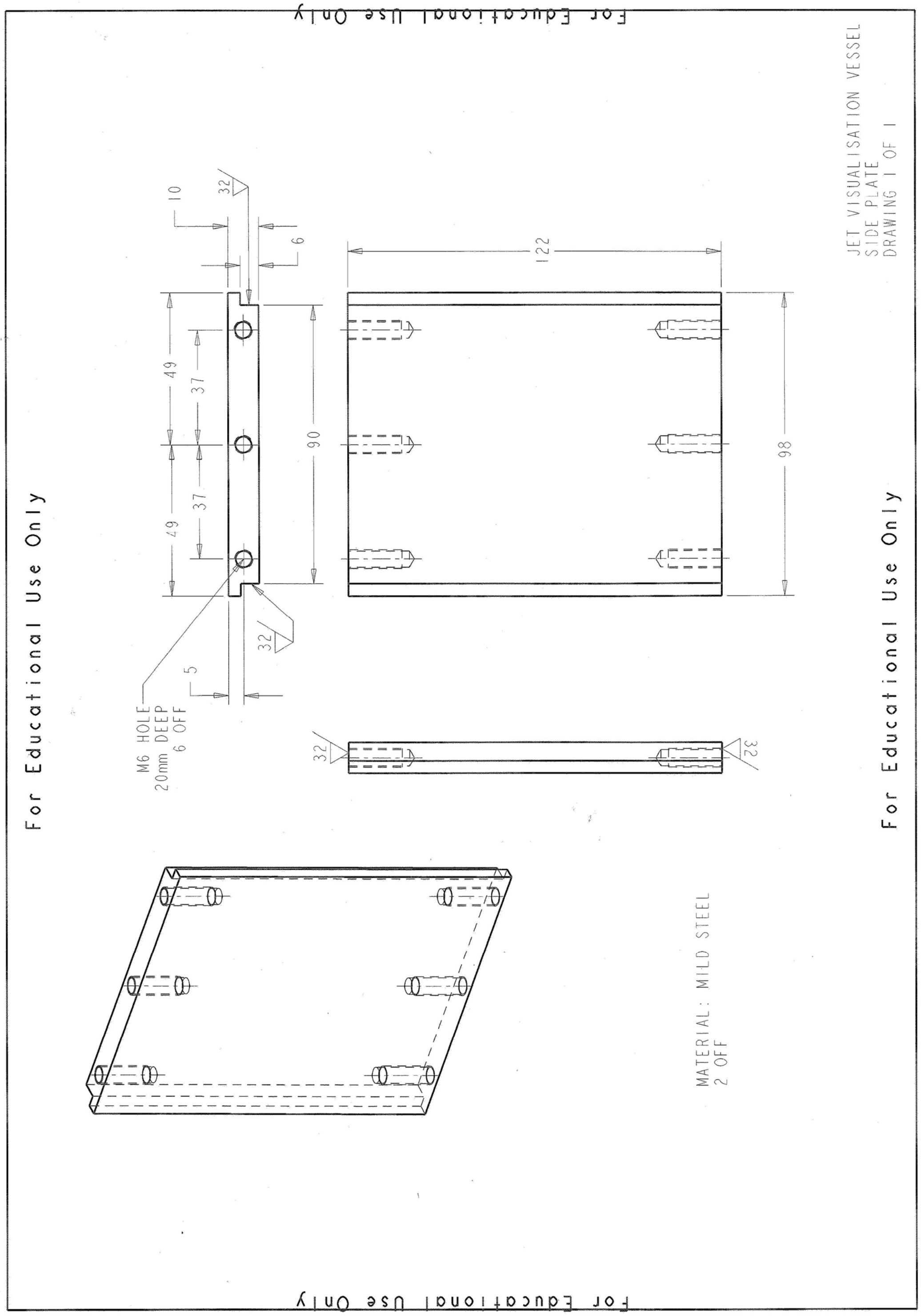

Figure A13 - Non-pressurised visualisation chamber, Drawing 6

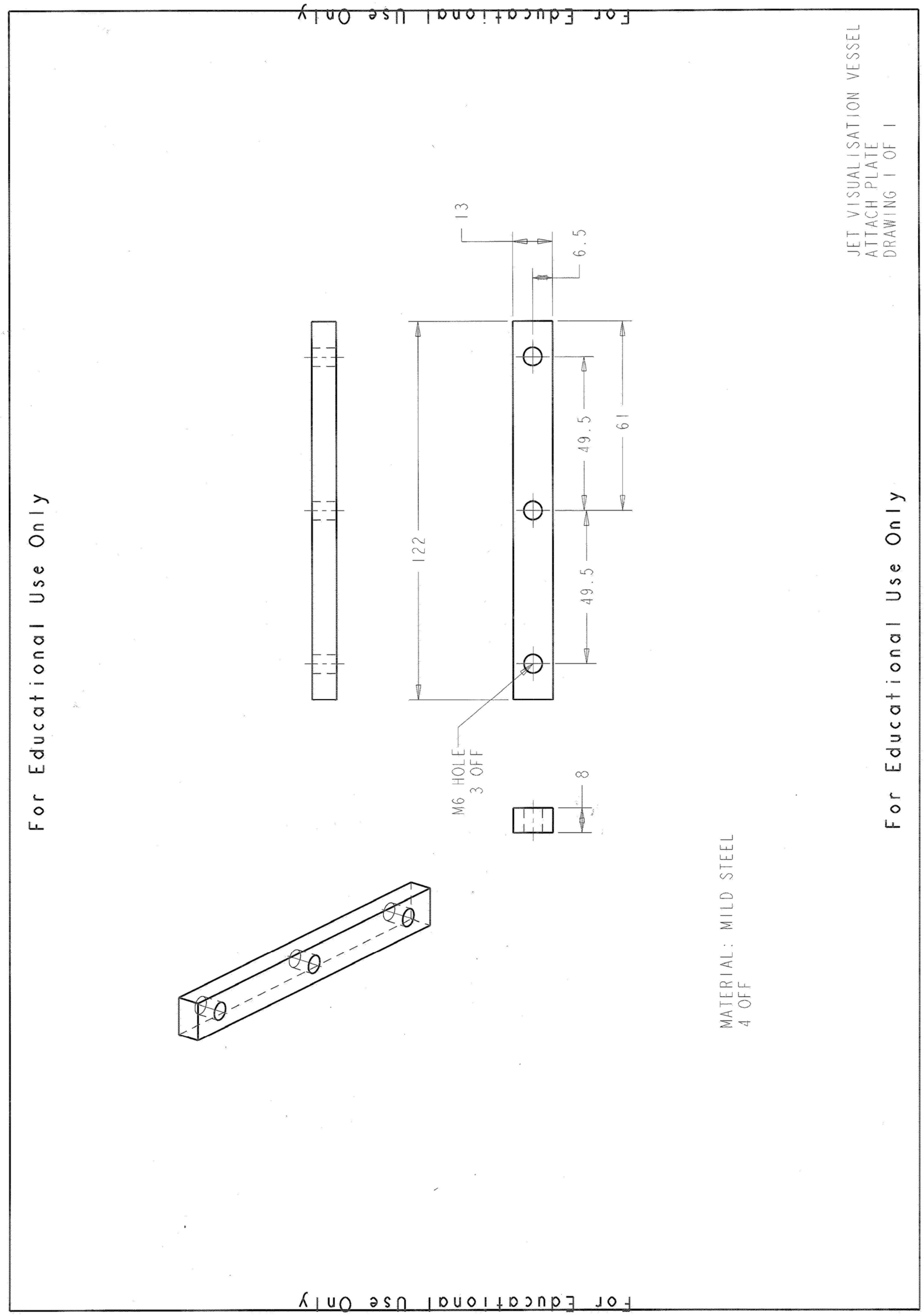

Figure A14 - Non-pressurised visualisation chamber, Drawing 7

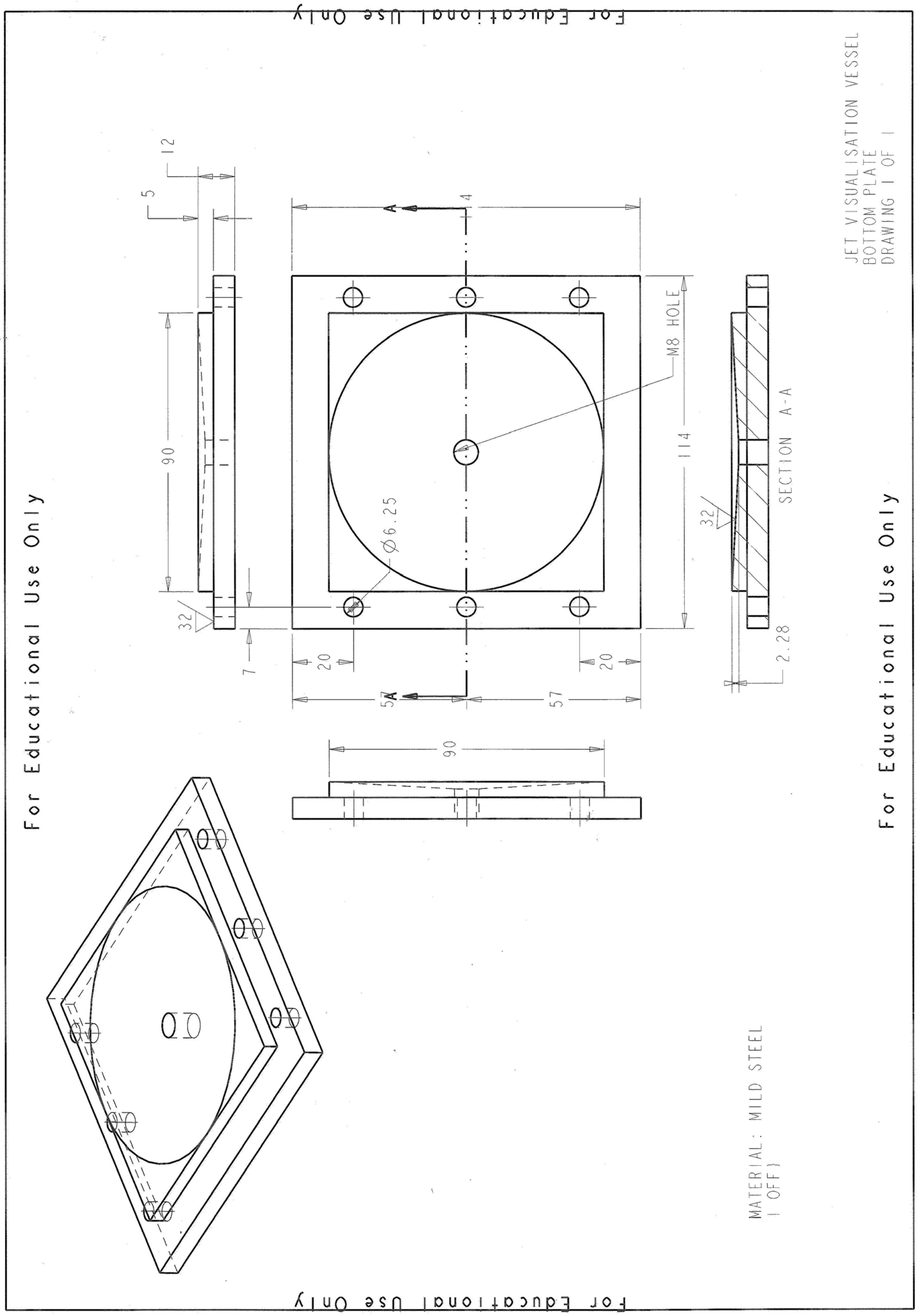

Figure A15 - Non-pressurised visualisation chamber, Drawing 8

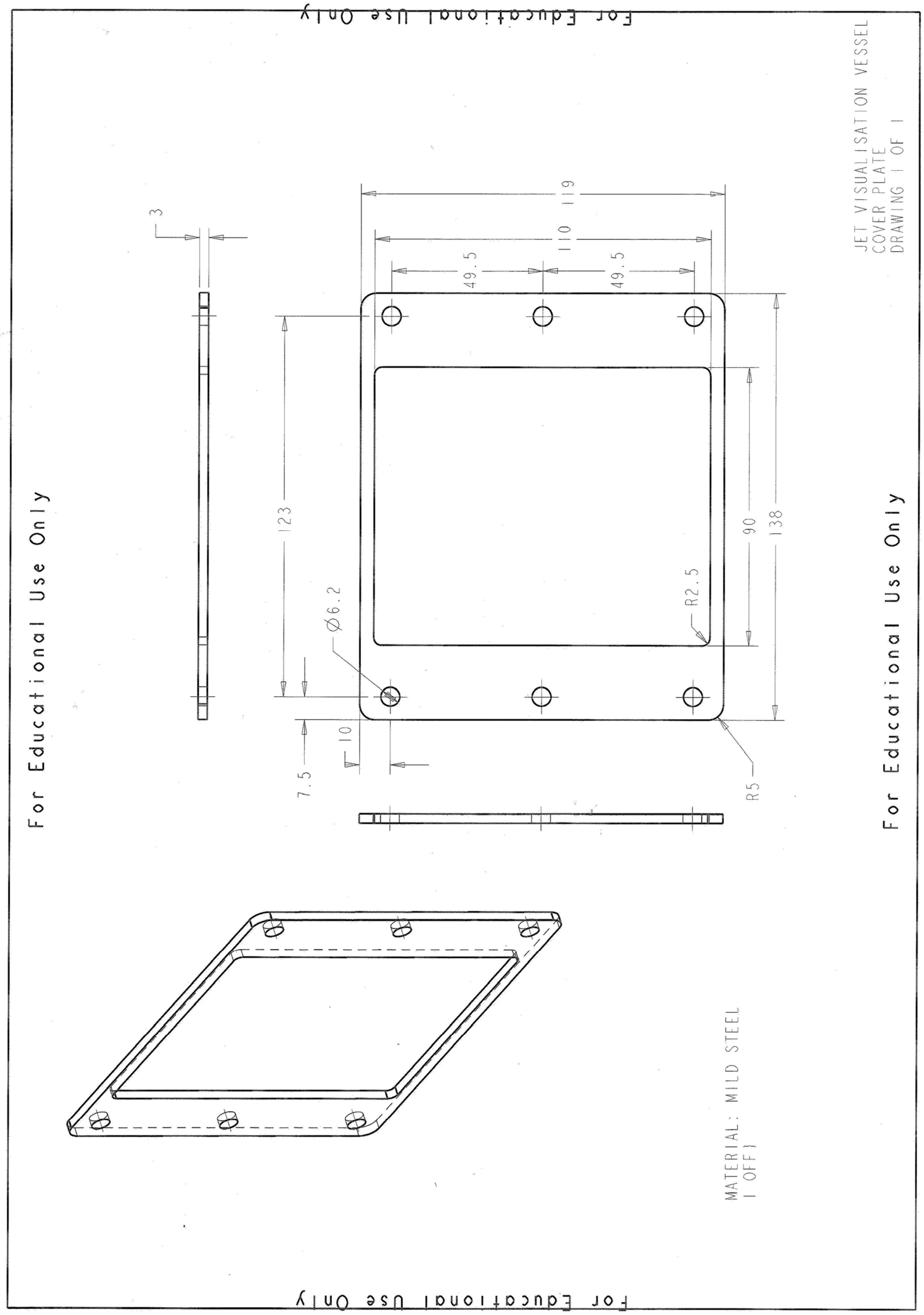

Figure A16 - Non-pressurised visualisation chamber, Drawing 9

APPENDIX B

SCHLIEREN PHOTOGRAPHY TEST LOGBOOK

Table B1 – Schlieren Photography Logbook

SCHLIEREN PHOTOGRAPHY TEST LOGBOOK					
TEST No.	FUEL TYPE	CAMERA SPEED	FRAME SIZE	INJECTOR TYPE	PRESSURE
[Date_Injector_Fuel_Pressure_Test No]		[frames/second]	[Pixels - Horiz. x Vert.]		[bar g]
20041204_3Hole_Diesel_210Bar_Test 1	Diesel	2000	1024x512	3 Hole	210
20041204_3Hole_Diesel_210Bar_Test 2	Diesel	4000	1024x512	3 Hole	210
20041204_3Hole_Diesel_210Bar_Test 3	Diesel	4000	512x512	3 Hole	210
20041204_3Hole_Diesel_210Bar_Test 4	Diesel	4000	512x512	3 Hole	210
20041204_3Hole_Diesel_210Bar_Test 5	Diesel	8000	1024x256	3 Hole	210
20041204_3Hole_Diesel_210Bar_Test 6	Diesel	8000	1024x256	3 Hole	210
20041209_3Hole_Diesel_210Bar_Test 7	Diesel	2000	1024x1024	3 Hole	210
20041209_3Hole_Diesel_210Bar_Test 8	Diesel	2000	1024x1024	3 Hole	210
20041209_3Hole_Diesel_210Bar_Test 9	Diesel	2000	1024x1024	3 Hole	210
20041209_3Hole_Diesel_210Bar_Test 10	Diesel	4000	1024x512	3 Hole	210
20041209_3Hole_Diesel_210Bar_Test 11	Diesel	4000	1024x512	3 Hole	210
20041209_3Hole_Diesel_210Bar_Test 12	Diesel	4000	512x512	3 Hole	210
20041209_3Hole_Diesel_210Bar_Test 13	Diesel	4000	512x512	3 Hole	210
20041209_3Hole_Diesel_210Bar_Test 14	Diesel	4000	512x512	3 Hole	210
20041209_3Hole_Diesel_210Bar_Test 15	Diesel	4000	1024x512	3 Hole	210
20041209_4Hole_Diesel_210Bar_Test 1	Diesel	4000	1024x512	4 Hole	210
20041209_4Hole_Diesel_210Bar_Test 2	Diesel	4000	1024x512	4 Hole	210
20041209_4Hole_Diesel_210Bar_Test 3	Diesel	4000	1024x512	4 Hole	210
20041209_4Hole_Diesel_210Bar_Test 4	Diesel	4000	1024x512	4 Hole	210
20041209_4Hole_Diesel_210Bar_Test 5	Diesel	4000	512x512	4 Hole	210
20041209_4Hole_Diesel_210Bar_Test 6	Diesel	4000	512x512	4 Hole	210
20041209_4Hole_Diesel_210Bar_Test 7	Diesel	4000	512x512	4 Hole	210
20041209_4Hole_DME_150Bar_Test 1	DME	4000	1024x512	4 Hole	150
20041209_4Hole_DME_150Bar_Test 2	DME	4000	1024x512	4 Hole	150
20041209_4Hole_DME_150Bar_Test 3	DME	4000	1024x512	4 Hole	150
20041209_4Hole_DME_150Bar_Test 4	DME	4000	1024x512	4 Hole	150
20041209_4Hole_DME_150Bar_Test 5	DME	4000	1024x512	4 Hole	150
20041210_4Hole_DME_150Bar_Test 6	DME	4000	1024x512	4 Hole	150
20041210_4Hole_DME_150Bar_Test 7	DME	4000	1024x512	4 Hole	150
20041209_3Hole_DME_150Bar_Test 1	DME	4000	1024x512	3 Hole	150
20041209_3Hole_DME_150Bar_Test 2	DME	4000	1024x512	3 Hole	150
20041209_3Hole_DME_150Bar_Test 3	DME	4000	1024x512	3 Hole	150
20041209_3Hole_DME_150Bar_Test 4	DME	4000	1024x512	3 Hole	150
20041210_3Hole_DME_150Bar_Test 5	DME	4000	1024x512	3 Hole	150
20041210_3Hole_DME_150Bar_Test 6	DME	4000	1024x512	3 Hole	150
20041210_4Hole_Diesel_150Bar_Test 8	Diesel	4000	1024x512	4 Hole	150
20041210_4Hole_Diesel_150Bar_Test 9	Diesel	4000	1024x512	4 Hole	150
20041210_3Hole_Diesel_150Bar_Test 10	Diesel	4000	1024x512	3 Hole	150
20041210_3Hole_Diesel_150Bar_Test 11	Diesel	4000	1024x512	3 Hole	150

APPENDIX C

ENGINE TESTING RESULTS

PERFORMANCE

C1 ENGINE TESTING RESULTS - DIESEL

Table C1 – Performance Results – Diesel – 25Nm Load

DIESEL		25 Nm							
		1100 rpm	1200 rpm	1300 rpm	1400 rpm	1500 rpm	1600 rpm	1700 rpm	1800 rpm
Speed	(rpm)	1100.3	1200.4	1305.4	1399.6	1503.6	1600.8	1701.8	1800.0
Load	(Nm)	25.1	24.6	25.0	24.7	25.0	25.2	24.9	24.8
Brake Power	(W)	2896.4	2895.1	3421.4	3620.7	3941.0	4218.5	4441.3	4677.0
Ind. work per Cycle	(J)	299.7	341.7	364.3	333.5	313.7	251.1	249.5	235.5
Indicated Power	(W)	4519.8	6836.6	7925.2	7778.1	7861.4	6698.6	7077.7	7063.8
imep	(kPa)	450.7	513.9	547.8	501.4	471.7	377.5	375.2	354.1
bmep	(kPa)	237.5	232.6	236.5	233.4	236.5	237.8	235.4	252.4
Equivalence Ratio	()	0.740	0.647	0.669	0.618	0.611	0.626	0.639	0.607
Air/fuel ratio	()	20.2	23.2	22.3	24.2	24.6	23.9	23.4	24.7
Air Flow	(g/s)	11.0	11.6	12.0	12.6	14.1	15.5	15.6	16.3
Fuel Flow	(g/s)	0.544	0.500	0.538	0.520	0.576	0.648	0.664	0.664
Additive Flow	(g/s)	0	0	0	0	0	0	0	0
Percentage DME	(%)	0	0	0	0	0	0	0	0
Fuel Conv. Eff.	(%)	12.20	14.20	14.58	15.92	15.74	14.98	15.32	16.20
isfc	(kg/J)	9.934E-08	7.314E-08	6.793E-08	6.318E-08	7.314E-08	9.699E-08	9.483E-08	9.434E-08
bsfcf	(kg/J)	1.881E-07	1.616E-07	1.573E-07	1.442E-07	1.457E-07	1.533E-07	1.497E-07	1.417E-07
Injection	(°CA)	350.8	346.5	346.5	346.8	347.1	346.5	347.4	347.8
Ignition	(°CA)	352.8	351.9	353.5	353.5	353.4	351.7	353.0	353.4
Ignition delay	(°CA)	2.0	5.4	7.0	6.7	6.3	5.3	5.6	5.6
Patm	(kPa)	82.6	82.6	82.6	83.1	83.1	83.0	83.0	83.0
Exhaust Temperature	(°C)	368.7	393.5	415.7	421.7	432.3	438.7	452.6	468.4
Pmax	(kPa)	7242.7	7020.1	6950.7	7205.2	7526.5	7660.2	8044.9	7925.8
Position of Pmax	(°CA)	363.9	365.0	365.3	364.3	364.7	363.6	364.8	365.0
Tmax	(K)	1904.1	1935.6	2029.4	2108.0	2119.7	2052.9	2295.2	2303.9
Position of Tmax	(°CA)	366.6	368.0	368.8	367.6	367.8	366.6	367.2	368.1
Mech Efficiency	(%)	52.9	45.3	43.2	46.6	50.2	63.2	63.3	66.7
ITE	(%)	23.1	31.4	33.8	34.2	31.4	23.8	24.4	24.4
BTE	(%)	12.2	14.2	14.6	15.9	15.7	15.0	15.3	16.2
Volumetric Efficiency	(%)	90.1	87.1	83.1	81.5	84.6	87.1	82.6	81.9

Table C2 – Performance Results – Diesel – 35Nm Load

DIESEL		35 Nm							
		1100 rpm	1200 rpm	1300 rpm	1400 rpm	1500 rpm	1600 rpm	1700 rpm	1800 rpm
Speed	(rpm)	1104.1	1201.3	1304.4	1401.5	1497.7	1600.8	1699.0	1800.0
Load	(Nm)	34.9	34.8	34.8	35.0	34.6	35.2	34.8	35.1
Brake Power	(W)	4031.0	4379.2	4748.2	5132.0	5421.3	5907.0	6188.3	6607.5
Ind. work per Cycle	(J)	366.6	356.2	426.8	420.0	396.9	507.4	495.0	494.5
Indicated Power	(W)	6745.2	7132.1	9278.7	9811.4	10057.9	13538.0	14014.8	14833.1
imep	(kPa)	551.2	535.7	641.8	631.6	605.9	763.0	744.3	743.5
bmep	(kPa)	329.4	328.9	328.4	330.4	326.6	332.9	328.6	331.2
Equivalence Ratio	()	0.950	0.860	0.800	0.815	0.820	0.774	0.749	0.743
Air/fuel ratio	()	15.7	17.5	18.9	18.4	18.3	19.3	20.0	20.1
Air Flow	(g/s)	11.3	11.6	12.3	12.6	13.7	15.7	15.6	16.4
Fuel Flow	(g/s)	0.718	0.670	0.650	0.683	0.754	0.813	0.784	0.814
Additive Flow	(g/s)	0	0	0	0	0	0	0	0
Percentage DME	(%)	0	0	0	0	0	0	0	0
Fuel Conv. Eff.	(%)	12.88	14.98	16.73	17.25	16.56	16.70	18.14	18.60
isfc	(kg/J)	1.065E-07	9.413E-08	7.015E-08	2.249E-07	7.474E-08	5.995E-08	5.600E-08	5.502E-08
bsfcf	(kg/J)	1.932E-06	2.407E-07	4.435E-07	1.330E-07	1.386E-07	1.373E-07	1.266E-07	1.233E-07
Injection	(°CA)	351.1	341.0	345.4	347.2	348.0	346.1	346.4	347.5
Ignition	(°CA)	351.2	341.7	352.4	353.7	352.7	353.3	352.4	355.5
Ignition delay	(°CA)	0.0	0.8	7.0	6.6	4.6	7.2	6.0	8.0
Patm	(kPa)	82.6	82.6	82.6	82.6	82.6	83.0	83.0	83.0
Exhaust Temperature	(°C)	385.8	402.7	413.8	435.9	455.2	460.3	478.1	496.6
Pmax	(kPa)	7383.4	7495.7	7161.4	7141.9	7353.1	7327.9	7228.5	7132.9
Position of Pmax	(°CA)	363.8	363.2	365.3	365.7	365.0	366.7	366.4	367.0
Tmax	(K)	1876.3	1996.7	2058.6	2150.4	2151.6	2091.7	2184.8	2221.8
Position of Tmax	(°CA)	368.4	367.0	370.6	370.6	369.9	374.8	374.4	374.9
Mech Efficiency	(%)	59.8	61.5	51.2	52.4	53.9	43.7	44.0	44.6
ITE	(%)	19.7	24.5	32.8	33.0	30.7	38.4	41.1	41.7
BTE	(%)	12.9	15.0	16.7	17.3	16.6	16.7	18.1	18.6
Volumetric Efficiency	(%)	92.3	87.4	84.8	80.9	82.7	88.3	83.1	82.2

Table C3 – Performance Results – Diesel – 45Nm Load

DIESEL		45 Nm							
		1100 rpm	1200 rpm	1300 rpm	1400 rpm	1500 rpm	1600 rpm	1700 rpm	1800 rpm
Speed	(rpm)	1104.1	1202.3	1299.5	1400.6	1503.6	1602.7	1702.8	1801.0
Load	(Nm)	46.2	45.6	44.5	45.4	44.7	44.8	45.2	44.7
Brake Power	(W)	5344.2	5744.1	6056.8	6659.4	7042.3	7520.3	8067.5	8430.1
Ind. work per Cycle	(J)	447.3	426.8	469.0	472.2	431.7	421.9	409.5	345.7
Indicated Power	(W)	8231.3	8552.4	10158.1	11021.2	10819.6	11271.6	11620.1	10374.8
imep	(kPa)	672.6	641.8	705.3	710.0	649.2	634.5	615.7	519.8
bmep	(kPa)	436.7	431.0	420.5	429.0	422.6	423.3	427.5	422.3
Equivalence Ratio	()	0.969	1.063	0.893	0.946	0.891	0.848	0.953	0.971
Air/fuel ratio	()	15.4	14.1	16.8	15.8	16.8	17.6	15.7	15.4
Air Flow	(g/s)	11.1	11.4	11.9	12.4	13.6	15.2	15.1	16.0
Fuel Flow	(g/s)	0.722	0.814	0.708	0.786	0.810	0.860	0.958	1.040
Additive Flow	(g/s)	0	0	0	0	0	0	0	0
Percentage DME	(%)	0	0	0	0	0	0	0	0
Fuel Conv. Eff.	(%)	16.96	16.26	19.58	19.44	19.96	20.04	19.28	18.60
isfc	(kg/J)	8.796E-08	9.522E-08	7.004E-08	7.143E-08	7.480E-08	7.637E-08	8.268E-08	1.004E-07
bsfcf	(kg/J)	1.354E-07	1.416E-07	1.172E-07	1.181E-07	1.149E-07	1.144E-07	1.189E-07	1.232E-07
Injection	(°CA)	351.2	351.8	345.5	347.9	345.9	346.2	346.5	346.9
Ignition	(°CA)	351.3	351.8	352.6	352.6	352.5	352.5	352.3	353.8
Ignition delay	(°CA)	0.1	0.0	7.1	4.8	6.6	6.3	5.8	6.8
Patm	(kPa)	83.2	83.2	83.1	83.1	83.1	83.1	83.1	83.1
Exhaust Temperature	(°C)	445.3	467.1	476.1	472.7	486.1	491.1	515.7	501.3
Pmax	(kPa)	7616.4	7400.5	7473.8	7459.1	7162.2	7282.4	7443.4	8097.7
Position of Pmax	(°CA)	364.2	364.2	364.8	365.4	365.6	364.5	364.6	363.6
Tmax	(K)	2000.1	2061.4	2205.4	2276.1	2151.9	2068.1	2215.4	2357.0
Position of Tmax	(°CA)	371.0	369.9	371.6	372.2	372.6	372.1	372.2	366.5
Mech Efficiency	(%)	65.0	67.3	59.7	60.5	65.1	66.7	69.5	81.5
ITE	(%)	26.1	24.3	32.8	32.2	30.7	30.1	27.8	22.9
BTE	(%)	17.0	16.3	19.6	19.4	20.0	20.0	19.3	18.6
Volumetric Efficiency	(%)	91.1	85.8	82.7	80.1	81.4	85.3	79.8	80.1

C2 ENGINE TESTING RESULTS – DIMETHYL ETHER

Table C4 – Performance Results – Dimethyl Ether – 25Nm Load

DME		25 Nm							
		1100 rpm	1200 rpm	1300 rpm	1400 rpm	1500 rpm	1600 rpm	1700 rpm	1800 rpm
Speed	(rpm)	1105.1	1198.5	1301.5	1399.6	1499.9	1598.8	1702.8	1802.9
Load	(Nm)	25.3	24.7	25.3	25.2	25.2	25.2	24.7	24.7
Brake Power	(W)	2925.0	3107.1	3444.5	3688.4	3956.0	4213.4	4405.1	4664.1
Ind. work per Cycle	(J)	376.2	381.5	377.9	375.0	400.8	398.0	384.9	376.3
Indicated Power	(W)	6929.8	7620.3	8197.4	8747.3	10020.9	10606.1	10924.4	11306.9
imep	(kPa)	565.8	573.7	568.3	563.9	602.8	598.5	578.9	565.8
bmep	(kPa)	238.8	233.9	238.8	237.8	238.0	237.8	233.4	233.4
Equivalence Ratio	()	0.480	0.474	0.476	0.465	0.477	0.438	0.473	0.449
Air/fuel ratio	()	20.4	20.7	20.7	21.2	20.7	22.6	20.9	22.1
Air Flow	(g/s)	11.4	11.8	12.3	12.7	14.0	15.9	15.8	16.6
Fuel Flow	(g/s)	0.560	0.570	0.590	0.600	0.680	0.700	0.760	0.752
Additive Flow	(g/s)	0	0	0	0	0	0	0	0
Percentage DME	(%)	0	0	0	0	0	0	0	0
Fuel Conv. Eff.	(%)	18.34	19.10	20.42	21.62	20.55	21.06	20.50	21.88
isfc	(kg/J)	8.092E-08	7.540E-08	7.240E-08	6.868E-08	6.765E-08	6.638E-08	6.952E-08	6.630E-08
bsfcf	(kg/J)	1.916E-07	1.842E-07	1.724E-07	1.626E-07	1.713E-07	1.670E-07	1.718E-07	1.606E-07
Injection	(°CA)	351.8	334.7	353.3	354.5	355.2	355.4	355.0	356.2
Ignition	(°CA)	353.3	335.4	355.0	355.6	357.2	357.5	359.0	359.0
Ignition delay	(°CA)	1.4	0.7	1.8	1.1	2.1	2.2	4.0	2.8
Patm	(kPa)	82.9	82.9	82.9	82.9	82.8	82.8	82.8	82.8
Exhaust Temperature	(°C)	335.8	334.8	335.3	343.8	351.0	355.4	350.4	371.6
Pmax	(kPa)	6679.6	6552.6	6370.9	6082.9	6021.6	5779.1	5559.4	5407.0
Position of Pmax	(°CA)	366.0	366.9	367.3	368.4	368.9	370.0	370.6	370.7
Tmax	(K)	1748.3	1814.8	1880.1	1900.6	1886.2	1777.2	1846.4	1864.0
Position of Tmax	(°CA)	371.7	372.0	372.8	374.9	376.1	378.3	378.6	379.7
Mech Efficiency	(%)	42.2	40.9	42.0	42.2	39.5	39.7	40.5	41.3
ITE	(%)	43.5	46.9	48.6	51.2	52.0	53.0	50.9	53.1
BTE	(%)	18.3	19.1	20.4	21.6	20.6	21.1	20.5	21.9
Volumetric Efficiency	(%)	93.4	89.0	85.0	82.1	84.5	89.7	83.7	83.0

Table C5 – Performance Results – Dimethyl Ether – 35Nm Load

DME		35 Nm							
		1100 rpm	1200 rpm	1300 rpm	1400 rpm	1500 rpm	1600 rpm	1700 rpm	1800 rpm
Speed	(rpm)	1103.2	1202.3	1299.5	1396.7	1503.6	1600.8	1701.6	1803.9
Load	(Nm)	35.7	35.0	35.3	37.0	34.9	34.8	35.1	34.8
Brake Power	(W)	4121.8	4410.1	4807.3	5409.1	5489.5	5839.8	6260.9	6580.7
Ind. work per Cycle	(J)	418.9	409.5	427.6	427.3	413.0	432.6	438.9	420.9
Indicated Power	(W)	7702.5	8205.4	9260.5	9947.7	10350.2	11541.4	12447.9	12654.5
imep	(kPa)	630.0	615.8	643.0	642.6	621.1	650.5	660.1	632.9
bmep	(kPa)	337.1	330.9	333.8	349.4	329.4	329.1	332.0	329.2
Equivalence Ratio	()	0.607	0.534	0.560	0.578	0.593	0.574	0.591	0.624
Air/fuel ratio	()	15.9	18.2	17.3	17.3	16.3	16.9	16.5	15.4
Air Flow	(g/s)	11.3	11.6	12.0	12.6	14.1	15.5	15.6	16.3
Fuel Flow	(g/s)	0.710	0.640	0.700	0.750	0.860	0.920	0.950	1.060
Additive Flow	(g/s)	0	0	0	0	0	0	0	0
Percentage DME	(%)	0	0	0	0	0	0	0	0
Fuel Conv. Eff.	(%)	20.28	24.22	24.32	25.36	22.38	22.32	23.28	21.82
isfc	(kg/J)	9.286E-08	7.810E-08	7.516E-08	7.579E-08	8.358E-08	7.980E-08	7.615E-08	8.400E-08
bsfcf	(kg/J)	1.734E-07	1.451E-07	1.447E-07	1.390E-07	1.573E-07	1.576E-07	1.513E-07	1.613E-07
Injection	(°CA)	354.3	353.8	353.6	355.5	355.9	356.7	331.3	357.1
Ignition	(°CA)	354.6	354.0	353.6	356.0	356.1	357.4	333.4	359.7
Ignition delay	(°CA)	0.3	0.2	0.0	0.5	0.3	0.6	2.2	2.5
Patm	(kPa)	83.3	83.3	83.3	83.3	83.3	83.3	83.3	83.3
Exhaust Temperature	(°C)	417.9	435.3	435.5	446.6	431.8	444.9	466.3	480.0
Pmax	(kPa)	6522.8	6430.0	6488.6	6229.8	6002.5	5911.5	5687.6	5539.3
Position of Pmax	(°CA)	367.7	367.2	366.8	368.4	369.0	370.0	370.1	370.9
Tmax	(K)	1783.1	1849.1	1967.5	1996.8	1893.4	1839.1	1883.2	1911.9
Position of Tmax	(°CA)	373.7	373.6	374.0	375.4	375.5	376.9	380.0	379.2
Mech Efficiency	(%)	53.6	53.8	51.9	54.5	53.1	50.4	50.4	52.1
ITE	(%)	37.9	45.1	46.9	46.6	42.1	44.1	46.2	42.0
BTE	(%)	20.3	24.2	24.3	25.4	22.4	22.3	23.3	21.8
Volumetric Efficiency	(%)	92.7	87.4	83.4	81.2	81.9	87.5	82.6	81.7

Table C6 – Performance Results – Dimethyl Ether – 45Nm Load

DME		45 Nm							
		1100 rpm	1200 rpm	1300 rpm	1400 rpm	1500 rpm	1600 rpm	1700 rpm	1800 rpm
Speed	(rpm)	1104.1	1200.4	1299.5	1399.6	1502.6	1600.8	1705.3	1800.0
Load	(Nm)	46.6	45.1	45.2	45.2	45.3	45.0	44.4	45.4
Brake Power	(W)	5174.6	5673.4	6152.9	6626.3	7127.5	7544.0	7923.8	8553.5
Ind. work per Cycle	(J)	449.0	464.9	467.9	484.2	500.2	498.7	484.6	487.0
Indicated Power	(W)	8262.5	9301.0	10133.4	11294.4	12526.3	13304.1	13771.0	14608.6
imep	(kPa)	675.2	699.1	703.6	728.1	752.2	749.9	728.6	732.2
bmep	(kPa)	422.9	426.4	427.2	427.2	428.0	425.4	419.3	428.7
Equivalence Ratio	()	0.567	0.610	0.590	0.610	0.599	0.547	0.441	0.572
Air/fuel ratio	()	17.1	15.7	16.3	15.8	16.1	17.8	17.1	17.0
Air Flow	(g/s)	10.9	11.3	11.6	12.2	13.5	15.2	15.2	16.1
Fuel Flow	(g/s)	0.640	0.720	0.710	0.780	0.840	0.856	0.890	0.940
Additive Flow	(g/s)	0	0	0	0	0	0	0	0
Percentage DME	(%)	0	0	0	0	0	0	0	0
Fuel Conv. Eff.	(%)	28.44	27.82	30.48	29.98	29.82	31.10	31.33	31.90
isfc	(kg/J)	7.724E-08	7.717E-08	7.009E-08	6.889E-08	6.722E-08	6.420E-08	6.468E-08	6.475E-08
bsfcf	(kg/J)	1.237E-07	1.265E-07	1.154E-07	1.173E-07	1.180E-07	1.130E-07	3.617E-07	1.103E-07
Injection	(°CA)	351.6	351.8	353.9	354.5	356.9	358.3	358.4	360.6
Ignition	(°CA)	351.8	351.8	355.0	355.3	358.5	360.4	358.9	362.1
Ignition delay	(°CA)	0.2	0.0	1.1	0.7	1.6	2.1	0.5	1.5
Patm	(kPa)	83.2	83.2	83.2	83.2	83.1	83.1	83.1	83.0
Exhaust Temperature	(°C)	491.9	516.1	530.2	537.0	556.4	548.2	563.5	599.9
Pmax	(kPa)	6778.5	6773.6	6469.9	6369.3	5985.5	5710.0	5520.1	5273.4
Position of Pmax	(°CA)	366.6	366.9	367.3	367.4	369.4	370.7	370.6	371.6
Tmax	(K)	1893.5	2000.9	2078.6	2105.3	2040.9	1921.1	1993.9	1992.9
Position of Tmax	(°CA)	373.0	373.2	374.9	376.4	379.6	381.6	382.8	386.3
Mech Efficiency	(%)	62.7	61.0	60.8	58.7	57.0	56.7	57.6	58.7
ITE	(%)	45.4	45.6	50.2	51.1	52.4	54.9	54.4	54.5
BTE	(%)	28.4	27.8	30.5	30.0	29.8	31.1	31.3	31.9
Volumetric Efficiency	(%)	89.2	84.9	80.5	78.9	81.1	85.4	80.4	80.4

APPENDIX D

ENGINE TESTING RESULTS

EMISSIONS

D1 ENGINE TESTING EMISSIONS RESULTS - DIESEL

Table D1 – Emissions Results – Diesel – 25Nm Load

DIESEL		25 Nm							
		1100 rpm	1200 rpm	1300 rpm	1400 rpm	1500 rpm	1600 rpm	1700 rpm	1800 rpm
CO	(ppm)	60370.0	39445.3	30686.0	30878.3	29565.5	25440.3	20339.0	25440.3
CO2	(ppm)	35000.0	60000.0	66000.0	65000.0	65000.0	62000.0	52500.0	53500.0
THC	(ppm)	2853.0	2930.0	2403.0	2499.0	2428.0	2501.8	1977.0	1511.5
NOx	(ppm)	608.3	818.3	960.0	884.8	755.5	676.0	658.0	693.5
O2	(ppm)	5.1	6.0	6.8	7.8	9.0	10.2	11.0	11.3
Specific CO	(ppm/W)	21.770	12.400	8.930	8.528	7.502	6.943	5.729	4.349
Specific CO2	(ppm/W)	12.000	19.000	19.500	18.000	16.500	14.800	12.000	11.800
Specific THC	(ppm/W)	1.029	0.921	0.699	0.690	0.616	0.593	0.445	0.323
Specific NOx	(ppm/W)	0.219	0.257	0.279	0.244	0.192	0.160	0.148	0.148
Specific O2	(ppm/W)	0.00184	0.00189	0.00198	0.00215	0.00228	0.00242	0.00248	0.00242

Table D2 – Emissions Results – Diesel – 35Nm Load

DIESEL		35 Nm							
		1100 rpm	1200 rpm	1300 rpm	1400 rpm	1500 rpm	1600 rpm	1700 rpm	1800 rpm
CO	(ppm)	20339.0	63652.0	49088.0	39218.8	34576.3	30395.7	27097.3	20337.0
CO2	(ppm)	8389.7	35578.4	49112.0	61251.5	64077.0	63903.0	62066.0	57929.6
THC	(ppm)	8170.1	6235.0	4611.8	3310.5	2734.7	2414.5	2113.2	1776.1
NOx	(ppm)	993.2	962.4	1036.1	1031.7	962.6	818.8	761.4	690.3
O2	(ppm)	6.1	5.2	6.3	7.8	9.1	10.2	10.8	11.1
Specific CO	(ppm/W)	19.940	14.400	10.130	7.635	6.265	5.160	4.838	3.086
Specific CO2	(ppm/W)	2.047	8.049	10.130	11.920	11.610	10.850	10.040	8.789
Specific THC	(ppm/W)	1.993	1.411	0.951	0.644	0.496	0.410	0.342	0.270
Specific NOx	(ppm/W)	0.242	0.218	0.214	0.201	0.174	0.139	0.123	0.105
Specific O2	(ppm/W)	0.00149	0.00118	0.00130	0.00152	0.00165	0.00173	0.00175	0.00168

Table D3 – Emissions Results – Diesel – 45Nm Load

DIESEL		45 Nm							
		1100 rpm	1200 rpm	1300 rpm	1400 rpm	1500 rpm	1600 rpm	1700 rpm	1800 rpm
CO	(ppm)	73653.4	58126.4	45780.4	37172.3	31215.8	28415.6	26207.2	28342.2
CO2	(ppm)	8389.7	35578.4	49112.0	61251.5	64077.0	63903.0	62066.0	43156.8
THC	(ppm)	5999.6	5296.8	4100.3	3956.8	2941.8	2659.8	2742.6	3712.0
NOx	(ppm)	1005.5	1251.0	1569.8	1497.3	1665.0	1658.8	1604.8	1476.2
O2	(ppm)	3.0	3.6	5.6	6.9	8.0	8.2	9.4	10.3
Specific CO	(ppm/W)	13.780	10.120	7.558	5.582	4.433	3.779	3.249	3.362
Specific CO2	(ppm/W)	1.570	6.194	8.108	9.198	9.099	8.498	7.694	5.119
Specific THC	(ppm/W)	1.123	0.922	0.677	0.594	0.418	0.354	0.340	0.440
Specific NOx	(ppm/W)	0.188	0.218	0.259	0.225	0.236	0.221	0.199	0.175
Specific O2	(ppm/W)	0.00056	0.00063	0.00093	0.00104	0.00114	0.00109	0.00117	0.00122

D2 ENGINE TESTING EMISSIONS RESULTS – DIMETHYL ETHER

Table D4 – Emissions Results – Dimethyl Ether – 25Nm Load

DME		25 Nm							
		1100 rpm	1200 rpm	1300 rpm	1400 rpm	1500 rpm	1600 rpm	1700 rpm	1800 rpm
CO	(ppm)	640.2	760.5	689.5	788.5	990.2	1079.4	1136.0	1207.2
CO2	(ppm)	43314.0	71893.5	76309.0	75697.0	69309.2	60617.6	54039.5	53402.8
THC	(ppm)	137.8	143.3	147.0	164.3	199.0	218.4	238.0	247.8
NOx	(ppm)	2317.6	2088.3	1801.3	1319.0	1007.0	785.6	624.3	555.6
O2	(ppm)	9.5	10.3	11.0	12.6	14.0	15.1	15.6	15.5
Specific CO	(ppm/W)	0.219	0.245	0.200	0.214	0.250	0.256	0.258	0.259
Specific CO2	(ppm/W)	14.810	23.140	22.150	20.530	17.520	14.390	12.270	11.450
Specific THC	(ppm/W)	0.047	0.046	0.043	0.045	0.050	0.052	0.054	0.053
Specific NOx	(ppm/W)	0.792	0.672	0.523	0.358	0.255	0.187	0.142	0.119
Specific O2	(ppm/W)	0.00325	0.00332	0.00319	0.00342	0.00354	0.00358	0.00354	0.00332

Table D5 – Emissions Results – Dimethyl Ether – 35Nm Load

DME		35 Nm							
		1100 rpm	1200 rpm	1300 rpm	1400 rpm	1500 rpm	1600 rpm	1700 rpm	1800 rpm
CO	(ppm)	3746.9	3682.0	2536.0	2074.8	965.4	871.9	880.8	930.5
CO2	(ppm)	16800.9	64891.3	83954.0	87897.0	85051.0	78213.0	72919.5	66952.2
THC	(ppm)	309.4	269.0	233.1	240.1	233.3	243.3	250.0	251.9
NOx	(ppm)	1821.3	1869.2	1776.3	1614.5	1353.8	1150.3	992.3	897.7
O2	(ppm)	10.6	6.8	7.7	8.6	10.7	11.8	12.9	13.2
Specific CO	(ppm/W)	0.909	0.835	0.528	0.364	0.176	0.149	0.141	0.141
Specific CO2	(ppm/W)	4.076	14.710	17.460	16.250	15.490	13.390	11.650	10.170
Specific THC	(ppm/W)	0.075	0.061	0.048	0.044	0.042	0.042	0.040	0.038
Specific NOx	(ppm/W)	0.442	0.424	0.370	0.299	0.247	0.197	0.159	0.136
Specific O2	(ppm/W)	0.00257	0.00154	0.00160	0.00159	0.00195	0.00202	0.00206	0.00201

Table D6 – Emissions Results – Dimethyl Ether – 45Nm Load

DME		45 Nm							
		1100 rpm	1200 rpm	1300 rpm	1400 rpm	1500 rpm	1600 rpm	1700 rpm	1800 rpm
CO	(ppm)	3589.0	3652.8	3143.0	3041.0	2722.5	2625.3	2910.7	2998.7
CO2	(ppm)	56197.8	89831.5	100670.0	105964.7	107165.5	105393.7	100508.0	96723.3
THC	(ppm)	125.0	131.3	141.7	167.3	218.0	234.3	338.5	381.0
NOx	(ppm)	2085.5	1996.3	1910.7	1697.0	1551.5	1355.3	1217.7	1076.3
O2	(ppm)	5.1	6.0	6.8	7.8	9.0	10.2	11.0	11.3
Specific CO	(ppm/W)	0.069	0.644	0.511	0.459	0.382	0.348	0.367	0.351
Specific CO2	(ppm/W)	10.860	15.830	16.360	15.990	15.040	13.970	12.680	11.310
Specific THC	(ppm/W)	0.024	0.023	0.023	0.025	0.031	0.031	0.043	0.045
Specific NOx	(ppm/W)	0.403	0.352	0.311	0.256	0.218	0.180	0.154	0.126
Specific O2	(ppm/W)	0.00099	0.00110	0.00110	0.00120	0.00130	0.00140	0.00140	0.00130

REFERENCES

1 Ofner, H. and Gill, D.W., Dimethyl Ether as Fuel for CI Engines – A New Technology and its Environmental Potential, SAE Technical Paper 981158, 1998

2 http://yosemite.epa.gov/oar/globalwarming.nsf/content/climate.html, Environmental Protection Agency of United States of America, 2005

3 Intergovernmental Panel on Climate Change, Special Report on Emissions Scenarios, 2001.

4 www.ncdc.noaa.gov/oa/climate/globalwarming.html, National Climate Data Centre, United States Department of Commerce, 2005

5 http://www.sierraclub.org/globalwarming/suvreport/suvthreat.asp, 2005

6 Naparstek, A., The Coming Energy Crunch, New York Press 01/06/2004, www.nypress.com/print.cfm?content_id=10329, 2004

7 OPEC Annual Statistical Bulletin 2007, www.opec.org, 2008

8 Mouawad, J., With it's vast reserves of oil, OPEC has a promising future, New York Times, 2004

9 Sato, Y. and Noda, A., Effects of Fuel Injection Characteristics on Heat Release and Emissions in a DI Diesel Engine Operated on Dimethyl Ether, SAE Technical Paper 2001-01-3634, 2001

10 MacLean, H.L. and Lave, L.B., Evaluating Automobile Fuel/Propsulsion System Technologies, Progress in Energy and Combustion Science Journal, 2003

11 Song, J., Huang, Z., Qiao, X. and Wang W., Performance of controllable premixed combustion engine fuelled with dimethyl ether, Energy Conversion and Management Journal, 2003

12 http://www.oilnergy.com/1obrent.htm, 2008

13 http://nj.gov/health/eoh/rtkweb/documents/fs/0758.pdf, Hazardous Substance Fact Sheet, New Jersey Department of Health, 2002

14 http://www.acts.co.za/haz_sub/index.htm, Hazardous Substance Act, 1973. Republic of South Africa., 1973

15 Heywood, J.B., Internal Combustion Engine Fundamentals, McGraw Hill International, 1988

16 South African National Standard, Automotive Diesel Fuel, SANS342:2003, 2003

17 Sato, Y. and Noda, A., An Experimental Study of Spray Characteristics and Evaporation Processes in a High Pressure Chamber, SAE Technical Paper 2001-01-3635, 2001

18 Heywood, J., Automotive Engines and Fuels: A Review of Future Options, Progress in Energy and Combustion Science Paper, 1981

19 Ogden, J., Wlilliams, R., and Larson, E., Societal Lifecycle Costs of Cars with Alternative Fuels/Engines, Energy Policy Journal, 2002

20 Joskow, P., Energy Policies and their Consequences after 25 years, The Energy Journal, 2003

21 MacLean, H. and Lave, L., Evaluating Automobile Fuel/Propulsion System Technologies, Progress in Energy and Combustion Science Paper, 2002

22 Sorenson, S.C., Glensvig, M., and Abata, D.L., Dimethyl Ether in Diesel Fuel Injection Systems, SAE Technical Paper 981159, 1998

23 Sidu, X., Mingfa, Y., and Junfeng, X., An Experimental Investigation on the Spray Characteristics of Dimethyl Ether, SAE Technical Paper 2001-01-0142, 2001

24 Jun, L., Sato, Y. and Noda, A., An Experimental Study on DME Spray Characteristics and Evaporation Processes in a High Pressure Chamber, SAE Paper 2001-01-3635, 2001

25 Merzkirch, W., Flow Visualisation, 1987

26 Bjorkquist, D.C. and Fingerson, L.M., Particle Image Velocimetry, TSI Incorporated, Progress in Visualization, Vol 1, Atlas of Visualization, Pergamon Press, 1998

27 Westerweel, J., What is PIV?, Delft University of Technology, 1997

28 Engel, C.E., Photography for Scientists, Academic Press, London and New York, 1968

29 Roebl, A., High Speed Video for Flow Visualisation, TSS Technology Technical Note 2002-12-07, 2002

30 Engel, C., Photography for the Scientist, Academic Press London and New York, 1968

31 Hentschel, W. and Stoffregen, B., Flow Visualisation with Laser Light Sheet Techniques in Automotive Research, Volkswagen AG, Research and Development Division, 1988

32 Strong, C., The Amateur Scientist – An air flash lamp advances colour Schlieren Photography, Scientific American Paper, 1974

33 Schlieren Photography: Kodak Scientific and Technical Data, 1960

34 Bjorkquist, D. and Fingerson, L., Particle Image Velocimetry, TSI Incorporated, 1992

35 Reznicek, R., Photoelectric Schlieren Method used to study the properties of diesel engine injection, Flow Visualisation IV, 1986

36 Green, A.B. and Lucas, G.G., The Testing of Internal Combustion Engines, 2nd Edition, The English University Press Ltd., 1969

BIBLIOGRAPHY

1 International Dimethyl Ether Association website, www.vs.ag, 2001

2 Heisler, H., Vehicle and Engine Technology, 2nd Edition, Arnold Publishers, London, 1999

3 Plint, M. and Martyr, A., Engine Testing-Theory and Practice, 2nd.Edition, Butterworth-Heinemann, 1999

4 Obert, E.F., Internal Combustion Engines, Second Edition, International Textbook Company, 1950

5 Horlock, J.H. and Winterbone,D.E., The Thermodynamics and Gas Dynamics of Internal-Combustion Engines Volume 2, Claredon Press, Oxford, 1986

6 www.aboutdimethyl ether.org, 2005

7 George Monbiot, Loosing the Battle with Entropy, 08/06/2004, www.monbiot.com, 2004

8 George Monbiot, Living with the Age of Entropy, 23/08/2004, www.monbiot.com, 2004

9 George Monbiot, The Bottom of the Barrel, 02/12/2003, www.monbiot.com, 2004

10 www.odac-info.org, The Oil Depletion Analysis Centre, 2005

11 www.naparstek.com, 2005

12 Yao, M., Zheng, Z., Xu, S. and Fu, M., Experimental Study of the Combustion Process of Dimethyl Ether, SAE Technical Paper 2003-01-3194, 2003

13 Yang, S. and Kim, Y., Studies on the Optimisations with regard to relationships between performance and emissions characteristics in Dimethyl Ether fuelled engines using common rail fuel injection systems, SAE Technical Paper 2003-01-1927, 2003

14 Kinoshita, K., Oguma, O. and Goto, S., Effects of Fuel Injection Conditions on Driving Performance of a DME Diesel Vehicle, SAE Technical Paper 2003-01-3193, 2003

15 Taylor, C.F., The Internal Combustion Engine in Theory and Practice, Vol 1, The Technology Press, MIT and John Wiley and Sons, New York and London, 1960

16 OPEC Annual Statistical Bulletin 2002, www.opec.org, 2003

17 OPEC Annual Statistical Bulletin 2005, www.opec.org, 2006